DISSERTATION

ORGANOMETALLIC COMPOUNDS AS ANTI-CANCER AGENTS: INTERACTION WITH DNA AND MIGRATION IN CELLS

SPECIALTY: PHYSICS AND PHYSICAL CHEMISTRY

SUBMITTED BY

MARCELINA JOANNA KLAJNER

IN PARTIAL FULFILLMENT OF THE REQUIREMENTS

FOR THE DEGREE OF DOCTEUR OF THE UNIVERSITY OF STRASBOURG, FRANCE

AND

FOR THE DEGREE OF DOKTOR OF THE WROCŁAW UNIVERSITY OF TECHNOLOGY, POLAND

DEFENDED JANUARY 28TH, 2011

IN FRONT OF THE COMMITTEE:

DIDIER CHATENAY	EXTERNAL REFEREE
ANDRZEJ RADOSZ	EXTERNAL REFEREE
THIERRY CHARITAT	EXAMINER
JAN MISIEWICZ	ADVISOR
CHRISTIAN GAIDDON	INVITED MEMBER
PASCAL HÉBRAUD	EXAMINER
CLAUDE SIRLIN	INVITED MEMBER
SÉBASTIEN HARLEPP	INVITED MEMBER

Ms Marcelina Klajner was a member of the European Doctoral College of the University of Strasbourg during the preparation of her PhD, from 2007 to 2011, class name Marco Polo. She has benefited from specific financial supports offered by the College and, along with her mainstream research, has followed a special course on topics of general European interests presented by international experts. This PhD research project has been led with the collaboration of two universities: the Wrocław University of Technology, Poland, and the University of Strasbourg, France.

Acknowledgements

Professor Jean-Pierre Münch and Professor Jan Misiewicz for giving me the opportunity of doing a joint-supervision PhD,

Region of Lower Silesia, Region of Alsace and CNRS for providing the financial support,

European Doctoral College for broadening my horizons,

The Polish society which helped me to survive in the foreign country,

Dr. Sébastien Harlepp for his management of all of the experiments which were performed and his involvement in the project,

Dr. Pascal Hébraud for never-ending help, organization and his extensive influence on the final appearance of this thesis,

My Parents and my brothers, Adrian and Bernard, for the support which only a perfect family can give,

And at last but not least my husband, Piotr, for everything,

Thank you.

Contents

Chapter 1

Introduction

1.1 The cell

All of the living organisms consist of cells, and these units of living matter all share the same machinery for their most basic functions. Human body includes more than 10^{13} cells and the whole organism has been generated by cell divisions from a single cell. Living things, though infinitely varied when viewed from the outside, are fundamentally similar inside.

Cell consists of the components adapted or specialized for carrying out the vital functions (Figure 1.1) [81]. They are called organelles and they are immersed in the cytosol—the intracellular liquid providing the optimal environment for all the physiological processes.

The protein filaments (microfilaments, microtubules, intermediate filaments) compose the cytoskeleton which organizes and maintains the cell's shape. It also keep organelles in their place and takes part in cell's uptake (endocytosis).

Nucleus is a headquarters of the cell. This spherical, enclosed by double-layer membrane, organelle, stores all of the genetic information of the organism in chromosomal DNA. Moreover, nearly all of the DNA replication and RNA transcription takes place inside the nucleus.

Nucleus is surrounded by the network of tubules and vesicles called Endoplasmic Reticulum (ER). Two ER conformations coexist: the smooth one, where lipids and steroids synthesis takes place and the rough one which synthesizes proteins. Rough ER is studded by ribosomes, small formations which make proteins from amino-acids. They are built from RNA and proteins. Proteins synthesized on the rough ER first move to the Golgi complex, where they are processed and sorted for transport to the cell surface or other destination

Inside the nucleus there is a non-membrane structure where ribosomal RNA is assembled and stored: the nucleolus. Built from proteins and condensed DNA (chromatin), nucleolus disappears during cell division. All of the chromatin present inside the nucleus is being condensed then.

All of the energy utilized by the cell is generated in mitochondria. They generate the energy by phosphorylation of ATP using oxygen obtained by a reduction of glucose. Cell's respiration takes place in mitochondria. Mitochondria contain their own genetic material in the DNA form. They have a highly permeable outer double-layer membrane and a protein-enriched inner membrane that is extensively folded.

Peroxisomes are small organelles containing enzymes that oxidize various organic compounds without the production of ATP. By-products of oxidation are used in biosynthetic reactions. Lysosomes have an acidic interior and contain various hydrolases that degrade worn-out or unneeded cellular components and some ingested materials. Endosomes internalize plasma-membrane proteins and soluble materials from the extracellular medium, and they sort them back to the membranes or to lysosomes for degradation.

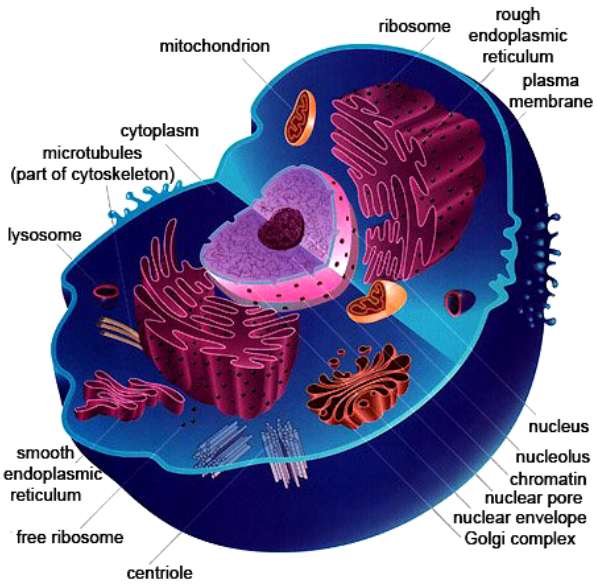

Figure 1.1: Scheme of a typical animal (eukaryotic) cell, showing subcellular components (organelles). [81]

1.2 Deoxyribonucleic acid (DNA)

All living cells on Earth, without any known exception, store their hereditary information in the universal language of DNA sequences [81]. These monomers are strung together in a long linear sequence that encodes the genetic information.

1.2.1 Chemical structure

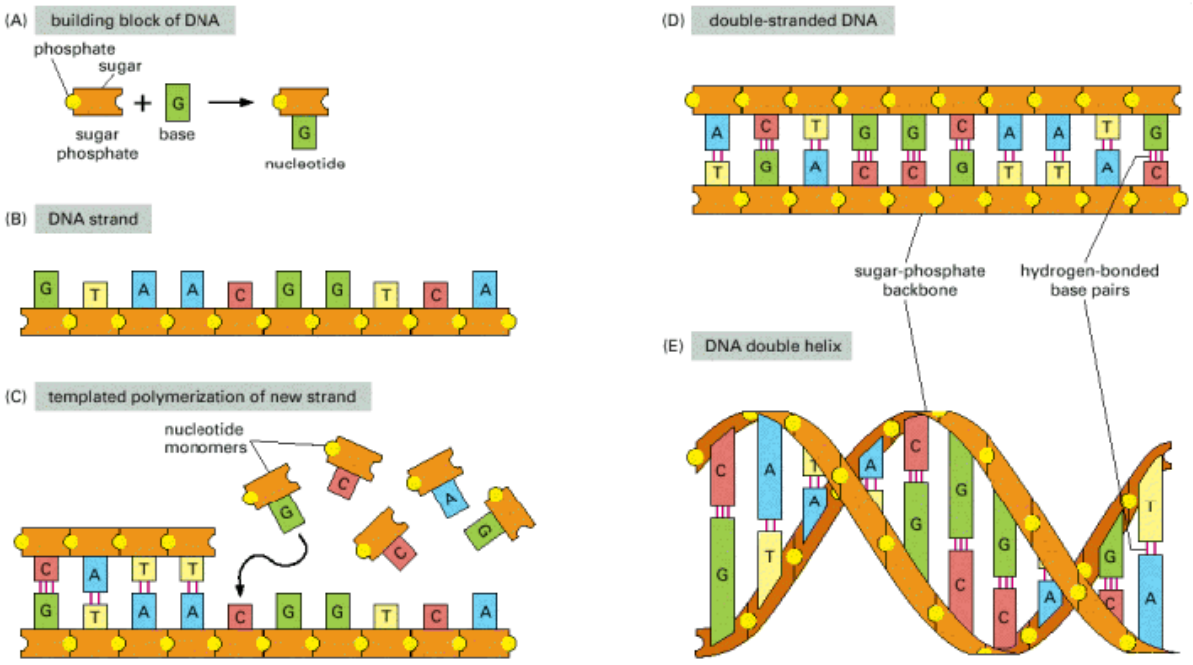

Figure 1.2: **(A)** Building block of DNA. **(B)** DNA strand. **(C)** Templated polymerisation of new strand. **(D)** Double-stranded DNA. **(E)** DNA double helix.

DNA is made from simple subunits, called *nucleotides* (Figures 1.2A and 1.3), each consisting of a sugar-phosphate molecule with a nitrogen-containing sidegroup, called base, attached to it [86]. The bases are of four types (adenine, guanine, cytosine, and thymine), corresponding to four distinct nucleotides, labeled A, G, C, and T. A single strand of DNA consists of nucleotides joined together by sugar-phosphate linkages (Figure 1.2B). Note that the individual sugar-phosphate units are asymmetric, giving the backbone of the strand a definite directionality, or polarity. The backbone has two important features: it is highly flexible and is highly charged (in water, at room temperature). The negative charge of the backbone is due to the fact that the phosphate groups in water or under physiological pH are fully dissociated. Through templated

polymerization (Figure 1.2C), the sequence of nucleotides in an existing DNA strand controls the sequence in which nucleotides are joined together in a new DNA strand; T in one strand pairs with A in the other, and G in one strand with C in the other. The new strand has a nucleotide sequence complementary to that of the old strand, and a backbone with opposite directionality, i.e. GTAA. . . of the original strand, and . . . TTAC in complementary one. Normally DNA molecule consists of two complementary strands (Figure 1.2D). The nucleotides within each strand are linked by strong (covalent) chemical bonds; the complementary nucleotides on opposite strands are held together more weakly, by hydrogen bonds. The two strands twist around each other forming a double helix (Figure 1.2E)—a strong structure that can accommodate any sequence of nucleotides without changing its basic structure. The bases can pair in this way only if the two polynucleotide chains that contain them are antiparallel to each other.

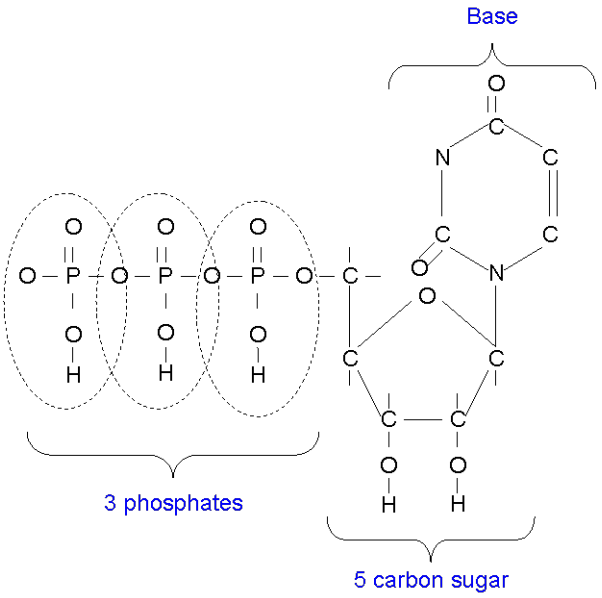

Figure 1.3: DNA consists of nucleotides. Single nucleotide is a sugar-phosphate molecule with attached nitrogen-containing base[81]. Here, thymine is presented.

In different types of cells, process of DNA replication occurs at different rates, with different controls to start it or stop it, and different auxiliary molecules to help it along.

The information in genes is copied and transmitted from cell to daughter cell millions of times during the life of a multicellular organism, and it survives the process essentially unchanged.

The genetic information stored in an organism's DNA contains the instructions for

all the proteins the organism will ever synthesize.

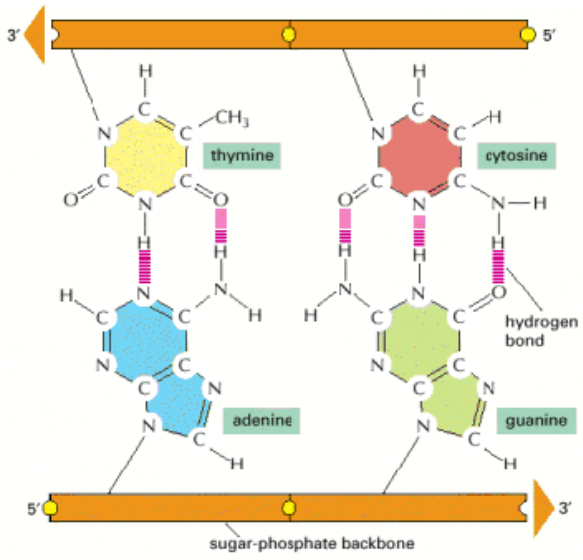

Figure 1.4: Complementary base pairs in the DNA double helix [81]

The shapes and chemical structure of the bases allow hydrogen bonds to form efficiently only between A and T and between G and C, where atoms that are able to form hydrogen bonds can be brought close together without distorting the double helix (Figure 1.4) [81].

1.2.2 Physical properties

The physical structure of double-stranded DNA is determined by the fact that its character is amphiphilic [76]. That means that one part of DNA chain (the phosphate backbone) is hydrophilic and another one (bases) is hydrophobic. Along with the flexibility of backbone, this amphiphilic character is a cause of double-helical structure of DNA. Double-stranded DNA occurs as a ladder which is twisted around its axis right-handed. The diameter of such twisted double-helix is 2.37 nm [76]. The twisting angle between adjacent base pairs is $34,6°$ and the distance between two neighbor nucleotides is 0.33 nm. Number of base pairs coincided with the full twist (360°) of DNA double-helix is $\simeq 10.4$ [76]. That full twist repeats itself in every 3.4 nm (Figure 1.5). Between two molecules of deoxyribose attached to complementary base pairs, there is a space creating grooves, which go along the whole DNA chain. Both of the N-glycosidic bonds connecting deoxyribose with base pairs are on the same side of double helix. Therefore the size of the grooves is not identical. They are 0.22 nm or 0.12 nm wide and are called major and minor groove, respectively [74].

DNA in solution is not rigid but is continually changing its conformation due to thermal fluctuations. Therefore, the bending stiffness of DNA is measured by the persistence length. It is defined as the distance over which the direction of a polymer segment persists, in the time or ensemble average, owing to limited flexibility of the polymer. It means the length of the DNA along which a thermally excited bend of 1 radian typically occurs (the DNA is essentially straight over shorter distances). For DNA the persistence length is $\simeq$ 50 nm, ($\simeq$ 150 bp). This value is larger than the persistence length of synthesized polymers: DNA is referred to as semi-flexible. The flexibility of DNA is due to fact that the covalent P-O (phosphate-oxygen) bonds can freely rotate around, so adjacent PO^-, and deoxyribose rings can rotate freely. DNA chain may be described with the Worm-Like Chain model (WLC) [84].

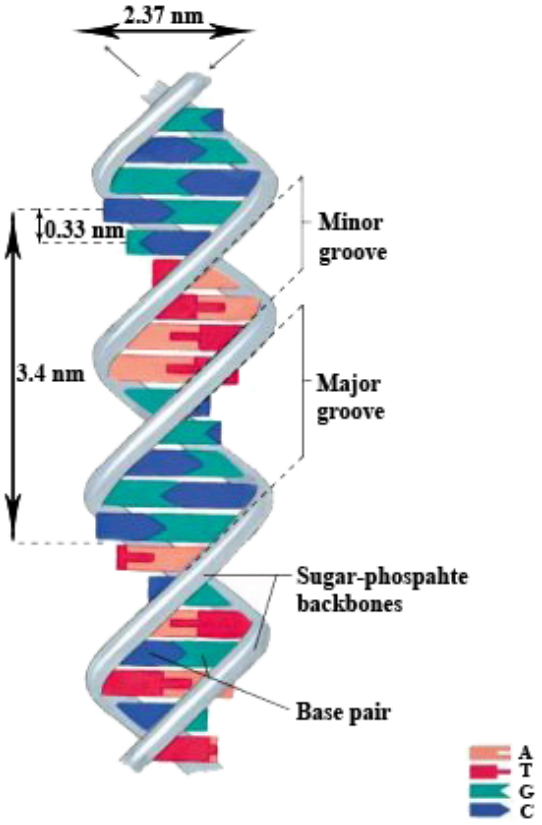

Figure 1.5: Physical structure of DNA

1.3 Cancer and its therapies

1.3.1 Mechanisms of cancer evolution

The term of cancer refers to a huge number of diseases. Nowadays 20 million people live with cancer all over the world. More than 100 types of cancer are listed at the moment, all have in common the abnormal growth of cells that invade and destroy normal tissues. An organism becomes cancerous in 3 steps: initiation, promotion and progression [81, 92].

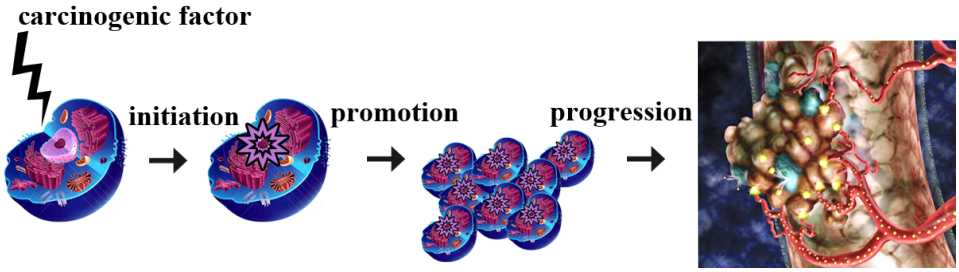

Figure 1.6: Evolution pathway of cancer

The cancer origins underlie in some carcinogenic factors which cause changes in the DNA structure. These changes (damages) are called mutations. Initiation of cancer corresponds to a particular mutation in the DNA that usually occurs many years before symptoms can be detected (Figure 1.6). Many mutations affecting DNA segments that encode for any gene often have no biological impact. The cell possesses an entire enzymatic material for repairing damages. Some repair mechanisms of DNA damage have been elucidated through advances in molecular biology. When DNA repair is not possible, the cell may program its suicide (apoptosis) to prevent the spread of this mutation. In the case of cancer, regulatory genes are frequently broken. For example, a mutation of the p53 gene (tumor suppressor genes, indicator of mutagens) is observed in more than 50% of human cancers. Moreover changes do not develop systematically. It is necessary that the affected cells acquire new properties. Among others, cell must be able to overcome the control of cell division's growth factors, and modify membrane factors to be able to displace itself and acquire invasiveness remotely.

The promotion is controlled by proliferation of initiated mutated cells. This is the beginning of tumor formation (Figure 1.6). Over cell division, accumulation of errors in several genes provides special features of the group of cancer cells. They become more aggressive in their environment and gradually resist any defense mechanism. Under the effect of carcinogens or promoters often acting over long periods (several years) many uncontrolled divisions occur. The origin of them is uncertain, but nutrition, hormones

contribution, toxic chemicals or genetics, have all factors of promotion. A significant number of mitosis leads to cell death by apoptosis. However due to the high number of cell divisions, some cells acquire enough independence to proliferate much faster than die. A number of these cells will develop the ability to self-reproduce without control of the body, cloning themselves. It is difficult to establish a formal boundary between benign and malignant tumors. The growth rate of cells, their invasiveness, their boundaries and their diversification from the tissue of origin (e.g.: presence of cells of irregular size, stacking layers of cells) are some criteria used in diagnosis.

The last step of becoming cancerous is the progression or invasion of tumor cells (Figure 1.6). Additionally to its never-ending proliferation, the cell undergoes more profound changes. The basement membrane proteins are modified, causing the loss of order and cohesion of the tissue that holds the cells. Thus cancer cells gain the ability to invade neighboring tissue. Breaking and crossing these tissues is a formal criterion to distinguish invasive cancer from carcinoma *in situ*. Gradually healthy tissue is replaced by tumor formation, blurring the boundaries between tissues in the body. In solid organ (brain, liver, kidney etc.), the proliferation forms a single rounded mass (tumor), whereas in a hollow organ (digestive tract) the tumor invades successively in-depth structural plans of the body (mucous membranes, submucosal etc.). Then the blood requirements can be met by formation of new blood vessels around the tumor (angiogenesis). These branches will contribute to the oxygen and nutrients needed for rapid growth and uncontrolled cell invasion. Formed vessels are often fragile and bleed easily, leading to hemorrhages indicative of this step. Angiogenesis is sometimes not sufficient to meet the metabolic needs of the tumor, which causes the onset of necrosis (natural death of cells) generally located at the center of the tumor. Lymphatic vessels (valvular structures that transport nutrients and detritus of a majority of tissue) draining waste from normal tissue will be achieved. The tumor cells are removed by lymphatic flow and reach the lymph nodes. If they survive, they can reach the lymph node without effect or bind with or without the appearance of inflammatory reactions, or move and invade the lymph node relays to win the following. The lymph node shows the first sign of metastasis and microscopic diffuse (Figure 1.7). After their spread along the lymph vessels cancer cells are often localized in a lymph node above the left clavicule (Troisier node), the last relay before the generalization of cancer within the organism [93]. Tumor cells can then invade other organs. They disassociate themselves from the primary tumor escaping from the cohesion of the tissue upon the achievement of proteins. They are also resistant to the immune system and turbulence of blood flow. When these changes are sustained, the tumor cells may cause the metastasis, which means that they appear

and start the tumor formation at a distance [78]. Metastatic preferential localization was observed for certain tumors. For example, a tumor of the prostate has an affinity for the development of metastases in the bone [81].

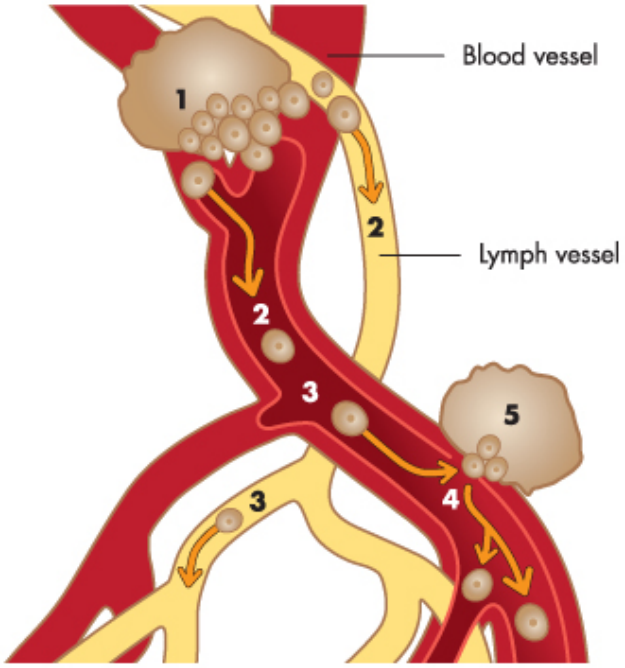

1 Cells grow locally as a tumour

2 Cells break away from tumour and enter the bloodstream or lymphatic system

3 Cells travel via the blood or lymph vessels to other parts of the body

4 Cells escape from the blood or lymph vessels into local tissues

5 Cells grow and divide in new location, producing secondary tumour elsewhere in the body

Figure 1.7: Scheme of metastasis process

A chronology of metastasis (metastasis revealing) exists and is indicative of progress in the carcinogenesis of a patient. It is especially important for certain types of cancers that develop only very little locally and metastasize quickly. The types of cancers are named according to the origin of the tissue initially injured. More generally we can distinguish three major types of malignancies identified by the nomenclature: lymphomas, sarcomas and carcinomas [94]. Lymphomas include cancer cells that reach lymphocytes. Unlike leukemia cancer cells invade the bloodstream but not particularly affect the lymph nodes. Sarcomas comprise the family of malignant tumors that develop from connective tissue cells. The latter consists of cells that form the frame (support and filling) of a

body whose elements cooperate with each other. They represent about 10% of cancers. Carcinomas are derived from cells of an epithelium. They are by far the most abundant (85%). The tumors are often described as "solid tumors" because they form a cluster of cells more or less dense, in contrast to leukemic cells. Leukemia includes blood tissue cancers that can affect other tissues such as the myeloid or lymphoid. The cells move freely in the blood. Cancer is a widespread disease. The three forms of cancer the most lethal (lung cancer, stomach and liver) are also the most common worldwide (17.8%, 10.4% and 8.8% of all cancer deaths). However, there are effective treatments against several cancers which are now briefly described.

1.3.2 Different treatment of cancer

There are several types of treatments to cure the cancer. Cancer treatment generally involves a combination of several treatment methods [79, 95].

Surgery is a treatment option that often allows to remove the tumor. It is very effective, but this intervention may be dangerous (e.g. glioblastoma) or severely debilitating (removal of the colon or gall bladder).

Radiation therapy involves the administration of Ionizing Radiation (IR) to induce high energy mainly irreparable breaks in DNA of cancer cells. IR beams are directed with great precision on the tumor to avoid damaging healthy tissue.

Hormone therapy is an important form of therapy in treating cancers usually dependent gonadotropic hormones (steroids). In some cancer cells from hormone-dependent, hormone receptors may remain functional. Their level of expression was studied to establish a possible hormonal treatment.

Immunotherapy [96] involves antibodies, proteins of the immune system that defend the body from invasive agents. The antibodies can also destroy cancer cells bearing tumor antigens (proteins produced by specific mutated cancer cells) although the expression of the latter is rarely observed in cancer patients.

Chemotherapy refers to a therapy based on drug products. In most cases, chemotherapy is administered by injection (e.g. intravenous infusion, a series of injections, etc.) and also consists in a combination of several compounds. Thus all cells of the body are affected including those that divide rapidly (roots of the hair, lining of the intestine, stomach etc.).It may be observed (respectively, loss of hair, nausea and diarrhea among other examples). A chemotherapeutic agent must be as effective for the cancer and as non-toxic for healthy tissues as possible, minimizing side effects. Because of the variety and multitude of products, many mechanisms of action are observed according

to the chemicals used. However the ability of cancer cells to divide rapidly compared to a normal cell is exploited by most chemotherapeutic agents. They are often cytostatic effects (arrest of proliferation or cell growth) and thereby induce cell death. The choice of drugs depends on the tumor cells since some are more susceptible to a type of compounds. Depending on different functional groups, anti-cancer drugs reveal various ways of action. For example Glivec, Topotecan and Paclitaxel are enzymes' inhibitors, so they are targeted at proteins. They do not contain any core around which active groups are oriented. In case of Fluorouracil there is non-metallic fluorine core, which increases its efficiency in comparison to the previous ones. But the most efficient drugs are organo-metallic compounds, which contain a metal core which organic ligands are bound to. Many groups of organo-metallic compounds have been invented. The most efficient are those based on gold, gallium, iron, ruthenium and platinum.

1.3.2.1 Chemotheraphy/Cisplatin

The platinum complexes are, among the others, the most effective and widely used anticancer drug despite their known side effects. The discovery of anti-tumor properties of platinum was made by chance. In 1965 Rosenberg was performing a growth inhibition of *Escherichia coli* when the culture medium, containing ammonium chloride, was subjected to an electric current between two electrodes made of platinum [50]. He showed that the inhibitory effect was not due to the current but to the formation of a complex between platinum and molecules released ammonia and chloride bath (formation of cis-platinum-dichlorodiamine, cisplatin (Figure 1.8)). This observation led Rosenberg to study cisplatin and other complex derivatives [51]. He exposed their antineoplasmic effects in animals and humans. As far, the efficiency of cisplatin was quickly proven and widely confirmed. The mechanism of action of cisplatin *in vivo* is far from completely understood, for example, its transport inside the cell is unresolved. However many studies conducted *in vitro* and *in vivo*, revealed many features of the cisplatin mode of action. DNA is a target of this complex. Among others, this macromolecule causes the DNA damage and the main problem of its utilization is its cytotoxicity.

1.3.2.1.1 Mode of action

After injection of this compound into the bloodstream, the presence of a high chlorides' concentration (90 mM) prevents hydrolysis of the complex which provides and maintains its integrity in its neutral form. Nevertheless, it is likely to face interaction throughout the many proteins present in the medium. Once inside the cell, where the ion concen-

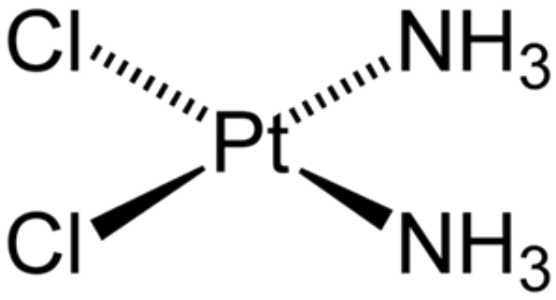

Figure 1.8: Cisplatin compound contains two chlorides and two ammonia groups in cis-orientation.

tration is lower (15 mM), the complex loses its ligands and chlorides are transferred into the cell nucleus. The obtained aquo complex $[Pt(NH_3)(H_2O)_2]^{2+}$ is more reactive than cisplatin and causes the formation of numerous adducts with DNA (monofunctional and bifunctional intrastrand, Figure 1.9). Adducts formed locally change the conformation of the double helix and if the lesion is not repaired, it will prevent replication of DNA and result in cell death. The complex with the DNA is formed by binding to two adjacent guanines via their nitrogen atoms (N7) covalently (1,2-GG intrastrand). The presence of an NH group (within the amine) also seems necessary for the activity of the complex as it stabilizes the adduct by forming hydrogen bond with a phosphate group (5') of nucleotide [52]. Nevertheless, the inhibition of DNA synthesis caused by these lesions does not fully explain the anti-cancer properties of cisplatin as for example, DNA lesions other than the majority (1,2-GG intrastrand) are repaired by cell (mainly via the NER: Nucleotide Excision Repair). Another hypothesis about the mechanism of action of this anti-cancer complex is widely accepted. It is based on the fact that there are proteins with increased affinity for DNA modified by cisplatin. The active sites of these enzymes recognize cisplatin-DNA adducts, which may directly or indirectly cause a disruption in the fundamental processes of the cell, including replication and transcription of DNA. Enzymes that recognize such adducts, are DNA-damage repairing proteins. Recognition by such proteins of damaged DNA directly interferes with its normal operation and therefore inhibits the transcription of DNA. This mechanism is more responsible for the anti-cancer activity of platinum adducts, than cisplatin-DNA adduct itself. Other proteins that are involved in the formation of cisplatin-DNA adducts have been elucidated [69]. The role of proteins also occurs before such adducts appear, during transport and incorporation of cisplatin into the cell. Proteins present in the bloodstream or inside the cell may interact with cisplatin or with one of its derivatives after hydrolysis. These

interactions are modulated by the strength of the bond between platinum and the atoms of the protein [53].

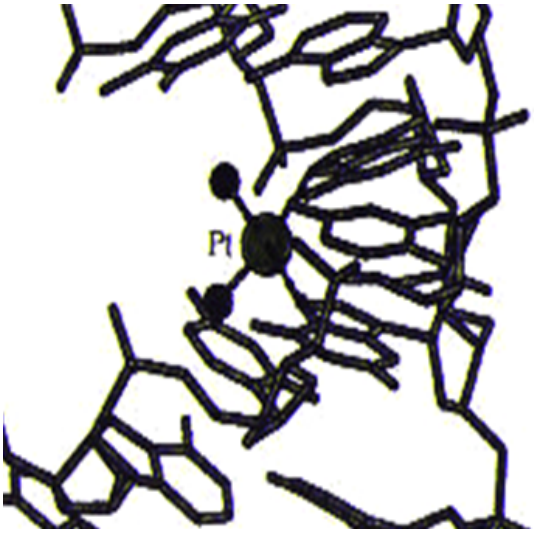

Figure 1.9: Cisplatin mode of action. Cisplatin loses its chlorides ions and as a positively charged molecule it is attracted to negatively charged DNA, binding to two guanines. This Cisplatin adduction changes DNA conformation.

1.3.2.1.2 Resistance

Resistance is a phenomenon defined as an absence or decrease of the effectiveness of a compound within an organism. There are many mechanisms that contribute to this resistance, some are general (e.g. cross-resistance) and others are specific to a type of drug or toxicity. In addition there are two modes of resistance: a lack of sensitivity to the natural effects of drugs (natural resistance) or a decrease of its activity after treatment with effective doses over time (acquired resistance). Acquired resistance is a common feature of cancer cells. Their high genetic instability and plasticity allow them to resist external aggression and result in a resistant cell. Acquired resistance of cisplatin is governed by three major processes: the accumulation of the complex, the production of thiols that modulate its toxicity and the ability to augment repair of damages caused to DNA. Its accumulation is governed by the influx or efflux from the cell. Even in the case of high degree of resistance, a moderate decrease in the intracellular accumulation of cisplatin is observed. An increase in glutathione levels was observed in some resistant cases. Glutathione protects the cell at first from interception of platinum compounds before they reach the DNA, but then also participates in the repair of damaged DNA. Cisplatin-glutathione adducts are formed and are quickly expelled from the cell through

ATP-dependent pumps [54]. Finally in regard to repairs of DNA damaged by cisplatin, studies have shown an improvement in the repairs of resistant strains, apart from the majority of intra-strand adducts. A description of the mechanisms of cisplatin resistance has recently been summarized in [55].

1.3.2.1.3 Side effects

Cisplatin treatment generally consists of a series of intravenous doses of 50–120 mg/m^2 for 3–4 weeks [11]. Cisplatin is a neoplasm inhibitor (inhibitor of tumor growth) active in the treatment of testicular or ovarian cancer in adults and in the treatment of solid tumors (osteosarcoma, neuroblastoma, hepatoblastoma) in children. In combination with other compounds, it is also used to treat bladder tumors and lungs. However it is responsible for limiting its adverse by causing side effects of dose treatment. Among them we can mention vomiting, aplastic anemia, a central nervous system toxicity and peripheral, and therefore kidney toxicity (nephrotoxicity), the hearing (ototoxicity) or eye disorders more or less significant (decrease in visual acuity to a temporary blindness) [97]. The disease is particularly important with cisplatin. To reduce this effect diuresis is enforced by adding sodium chloride. The water solubility of cisplatin is still quite low (1mg/ml), thus increasing volumes of intravenous therapy is required. That is the reason of side effects augmentation. The symptoms of neuropathy can occur after treatment with cisplatin which makes it difficult to use [56]. All these side effects are of course modulated among others by doses and treatment time. Some of them may be fully or partially reversible, which is in the case for many neuropathies. For ototoxicity, irreversible deafness in high number of patients is observed.

For these side effects and reasons for resistance, in addition to elucidating new insights into the mechanisms that lead to cancer, there is a need for new anti-cancer agents. Following the success of the anti-cancer activity of cisplatin, the search for chemotherapeutic agents based on metals has been widely developed, the primary aim of reducing toxic effects of this compound [57].

1.3.2.2 Ruthenium compounds

1.3.2.2.1 Chemical properties

New concepts (e.g. new membrane or intracellular receptors) have rapidly been developed in the study of cancer that allowed to understand the progress of cancer at the molecular level. The chemotherapeutic agents could then be designed differently, especially among the growing number of metal compounds to follow cisplatin in way of

action [57]. Ruthenium complexes have recently contributed to the design of new anti-cancer agents [58]. The DNA has been shown to be a typical target for many anti-cancer drugs. But other targets have been elucidated showing the complexity of mechanisms in oncogenesis and cancer treatment. Many new compounds including metal have demonstrated anti-cancer properties which gives a hope for a big advance in cancer therapy. An important parameter of the success of a drug is its cytotoxicity. Two different behaviors are observed: drugs having both a strong cytotoxicity and anti-tumor activity, and those which have little or no cytotoxic and have yet anti-tumor activity. The first case involves a lot of different cancer drugs and the most famous example is cisplatin. The representative of the second group is NAMI-A (Figure 1.10), a complex of ruthenium(III), currently being studied for the cure of metastasis [59].

The chemical synthesis of ruthenium-based complexes is well developed in various fields (catalysis, electrochemistry or applications in medicine), especially with ligands containing one or more nitrogen or based on phosphorus. Metals are naturally present in the human body (Fe, Cu, Zn) in large quantities (4–5 g of iron, which is essential for the respiratory system) [60]. Since cisplatin has been discovered, the use of metals, including ruthenium, has been more intensely developed and directed towards the medical field. In addition to the widespread idea, suggesting that ruthenium complexes are generally less toxic than other transition metals (due to their ability to mimic the iron binding sites in metallo-proteins [61]), the main reason for using ruthenium in the design of anti-cancer drugs, is due to its chemical properties. The chemistry of ruthenium allows to access to complexes of different geometries: octahedral geometry of ruthenium(II) is more malleable than the square planar geometry of platinum(II). It also allows to introduce ligands such as bidentate ligands, tridentate and different atoms bond to the centrally oriented metal. These ligands have been developed so that the redox potential of ruthenium compounds is high enough to induce oxidative damage possesses to the cell: the complexes of Ru(II), (III) and (IV) have been invented [58]. These properties prove to be interesting for the use of ruthenium for biological purposes. Many research teams are interested in these ruthenium complexes, which resulted in products which are made in clinical trials (phases I and II) complexes of Ru(III) appointed NAMI-A and KP-1019 (phase I)(Figure 1.10) in the early 2000s [62].

Further research on ruthenium complexes led to new idea of complex of ruthenium(II) structure which differ from these coordination complexes by the presence of a metallocyclic ligand (containing a ruthenium-carbon covalent bond) [63]. Some of these complexes have already shown *in vitro* anti-proliferative properties against cancer cells, therefore it seemed to be interesting to study their anti-cancer properties and improve

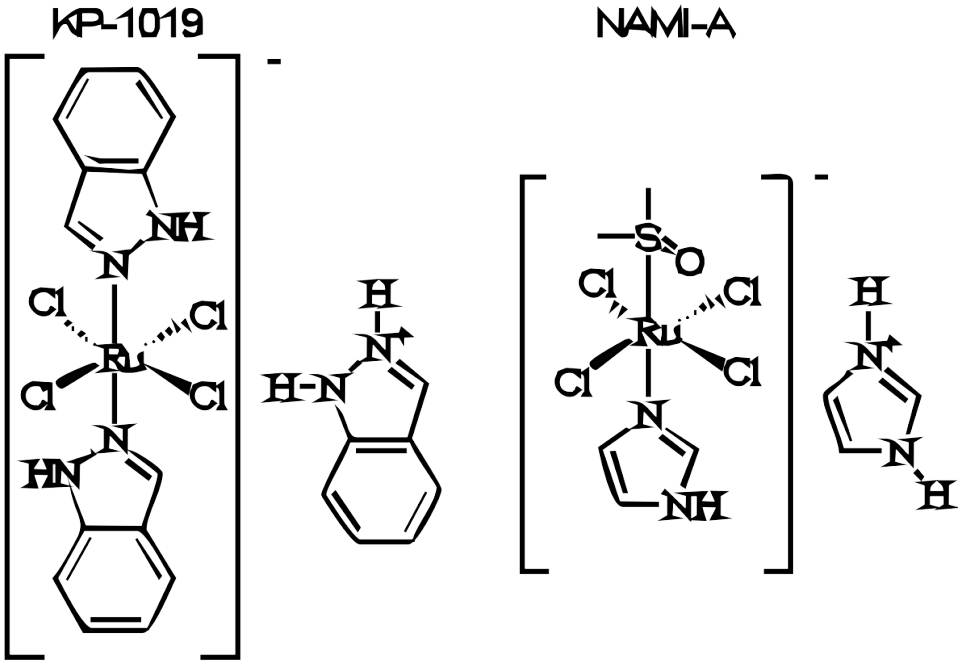

Figure 1.10: NAMI-A and KP-1019 chemical formula

their structure in that direction.

Some of the compounds of ruthenium(II) which biological activity has recently been demonstrated are organometallic Ruthenium Derived Compounds (RDC). They may present interesting interactions with biological macromolecules depending on modifications introduced in their structures. These compounds are called metallocyclic because they are characterized by the existence of a metallocycle which is composed of metal (ruthenium(II)) and a ligand bound to the metal by both covalent σ (C-M) or coordination (Y-M) bond [63].

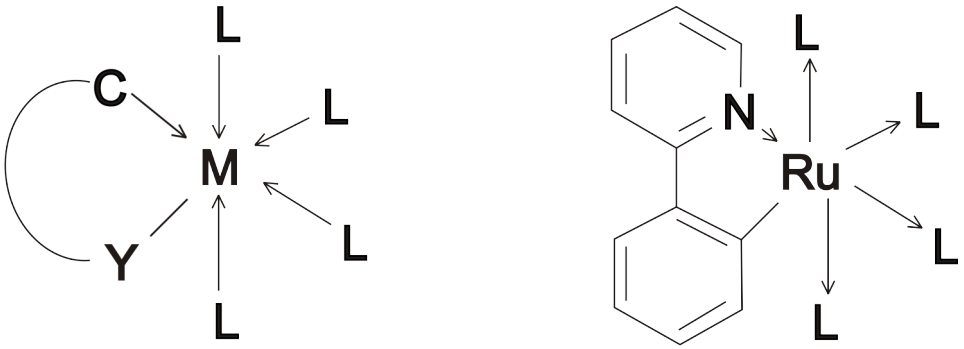

Figure 1.11: Metallocyclic unit, Ruthenocycle complex

In these compounds the carbon atom is aliphatic or aromatic, the atom Y may be

nitrogen, oxygen or other heteroatom. The metal coordination sphere is completed by monodentate ligands (L in Figure 1.11) or bidentate (e.g. phenylpyridine in the compound in Figure 1.11) or solvent molecules such as acetonitrile ($L = CH_3CN$) [75].

Complexes containing a Ru-C bond display a stability [75]. Generally a balance between efficiency, physicochemical properties and metabolism of toxic through pharmacokinetic data, is required for a candidate the selection of a drug. The stability of RDC complexes allows one to test a drug that remains unchanged in various solvents or media used for treatment. However although new RDCs are stable in solution, they probably change their internal structure within the organization to achieve the active species that interacts with biomolecules.

1.3.2.2.2 DNA as a target for Ruthenium Derived Compounds

One of the newly invented RDC has been examined by a group of biologists [3, 75]. They discovered a significant impact of the compound on the mice infected by the tumor. Its anti-tumoral efficiency was comparable to the one displayed by cisplatin. Acute-, chronic- and neuro-toxicity were also examined. Although RDC occurred to be toxic, its toxicity is not as high as cisplatin. These results are very promising. As mentioned above DNA is a target of cisplatin and of already invented ruthenium-containing compounds. For further investigation of differences and similarities between RDC and cisplatin we wondered if the new generation of Ruthenium Derived Compounds (RDCs) interacts with DNA. Biologists thus treated cells with RDC and cisplatin *in vitro* and followed the induction of DNA damages using as a marker the phosphorylation of histone pH2AX at serine 137. pH2AX is a histone, indicator of DNA damage. Treatment with cisplatin induces the phosphorylation of pH2AX after 12 hours and with RDC after 24 hours (Figure 1.12). The main goal of this thesis is to study quantitatively affinity of RDC to DNA, its dependence on RDC structure. We wish also to identify the structure of the DNA-RDC complex.

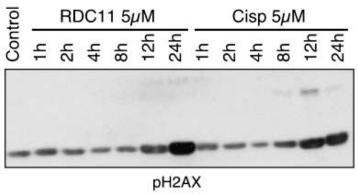

Figure 1.12: Western blots of pH2AX [3]

Outline of the manuscript

In chapter 2 we report RDC-DNA interaction. In section 2.2 we describe the use of Förster Resonant Energy Transfer (FRET) to determine the affinity constant K_a, number of base pairs occupied by one RDC molecule and dependence of K_a on ionic strength.

But understanding the molecular mechanisms of RDC-DNA interaction requires the resolution of their complex structure. To achieve this goal we performed force-extension experiments presented in section 2.3. The mechanical response of RDC-DNA complex, obtained by Optical trap, allows us to distinguish different kinds of interactions (e.g. intercalation and groove-binding (Figure 1.14)). We then show that depending on the specific ligands bound to Ruthenium atom, RDC may either intercalate between base pairs or binds to the groove (Figure 1.13).

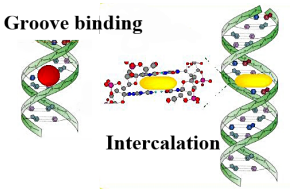

Figure 1.13: Groove binding and intercalation

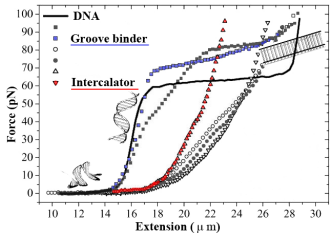

Figure 1.14: Force-extension curves: Intercalation and groove binding

These measurements were performed in solutions and indeed showed that RDC displays strong affinity to DNA. Nevertheless the presence of RDC-DNA complexes in cells have not yet been observed. Thus in chapter 3 we refer two kinds of experiments allowing us to recognize behavior of RDC with cells. We measure the kinetics of uptake RDC by cell to recognize whether the transport across the cellular membrane is passive or involves some energy (active) (Figure 1.15) in section 3.2. In section 3.3 we localize RDC inside the cell.

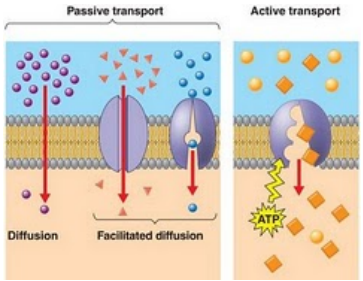

Figure 1.15: Passive and active way of transport across the cellular membrane

Chapter 2

DNA-RDC interactions

2.1 Introduction

From the large library of RDCs produced by chemists, only RDC11, RDC34, RDC44 have been chosen (Figure 2.1). RDC11 has been reported in previous studies as an efficient anti-tumor agent, as active as cisplatin, but with lower side effects [2, 75]. RDC34 is a modified RDC11 with an exchange of the two methyl groups by a phenanthroline one. This structure is supposed to exhibit higher hydrophobicity and therefore higher reactivity. RDC44 derives from RDC34 with the addition of a spermine tail on a C,N-(2-phenyl-pyridine) group to render this compound water-soluble and to increase its acceptance in physiological environment. Anti-cancer activity of RDC34 and RDC44 is under study these days but the results have not been published yet.

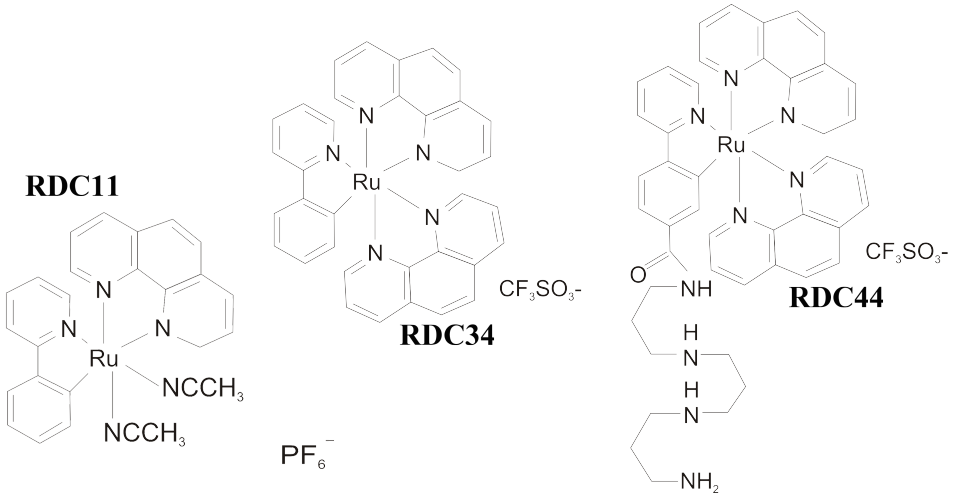

Figure 2.1: The three structurally different Ruthenium Derived Compounds (RDCs) studied in this thesis.

The goal of these structural modifications is to improve their anti-cancer activity [4]. Many comparative experiments between RDC and cisplatin were performed [2]. In comparison to other RDCs and cisplatin, RDC11 exhibits stronger effects on various cell lines and its biological reactivity does not extinguish over time *in vitro* [2, 3]. Moreover RDC11 is less sensitive to some of the resistance mechanisms limiting cisplatin or other RDCs' activity [2]. As opposed to them, RDC11 induces Bax and p21 activation—growth arrest and apoptosis factors, respectively [2].

Experiments performed *in vivo* let one observe that RDC11 reduces the growth of tumors implanted in mice with less cytotoxicity in comparison to cisplatin. Furthermore it was shown that RDC11 is uptaken by the cell, then interacts with DNA and induces DNA damage. This last interaction is the main cause of p53 protein activation and leads to cell apoptosis. Additionally there is another apoptotic pathway found—endoplasmic reticulum (ER) stress [3]. Activation of the transcription factor CHOP, a crucial mediator of ER stress apoptosis, was observed in tumors treated with RDC11 [3].

It was clearly demonstrated in former studies that RDC11 causes DNA damage, however it remains important to clearly identify how RDC induces them. To further understand the RDC-DNA interaction, we decide to determine their affinity.

People are highly interested in techniques that give the most relevant information about the molecular interactions. From the variety of different methods we focus on these that give the highest resolution at the molecular level.

X-ray crystalography can provide detailed structural information for the ligand-DNA complex [35]. It is probably the only method allowing a three-dimensional structure recognition at very high resolution (few Å) on high molecular weight complexes. Nevertheless this method needs a crystal [36], and the cristallisation of these structures is complicated—an extensive knowlegde and experience is needed. A second high resolution method commonly used is Nuclear Magnetic Resonance (NMR) spectroscopy. Sample preparation and handling is much easier and allows to perform experiments in a wide variety of conditions. One reason why this technique is not widely used in biophysics is due to a molecular weight limitation (the size of 50 kDa is a limit for obtaining good structure resolution) [35].

Although these methods are very precise and allow one to obtain very detailed results, the sample preparation and the acquisition time as well as the time needed for the interpretation [82, 83] of the results lower our interest in these techniques.

2.1.1 FRET

Optical measurements based on the fluorescent properties of a sample are very efficient as the absorption cross-section of fluorescent molecules is large and leads to high signal to noise ratio with a relatively short acquisition time. The fluorophores may be selected in such a manner that several compounds labeled with fluorescent molecules may be separated by their excitation and emission spectra.

Förster Resonant Energy Transfer (FRET) observation has become widely used in biology and biotechnology [8]. This process occurs between two coupled fluorescent molecules and strongly depends on the distance between them. The energy is transfered from the molecule in an excited electronic state called the donor (D) to another molecular chromophore called the acceptor (A), typically in a range of 0.5–10 nm. This process is non-radiative (Figure 2.2), which means that the energy is not emitted or absorbed as photons, but as Coulomb's charges [8].

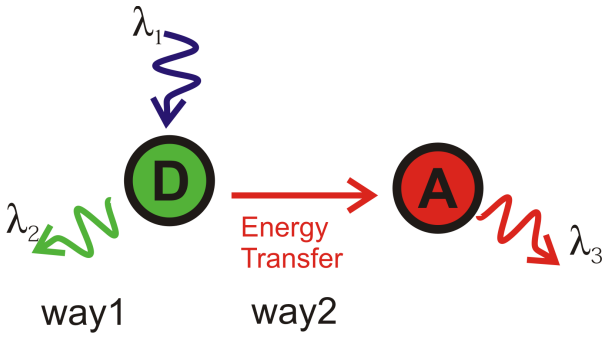

Figure 2.2: Two ways of de-excitation of a donor. D—donor, A—acceptor, λ_1—wavelength of the light exciting the donor, λ_2—wavelength of the light emitted by the donor, λ_3—wavelength of the light emitted by the acceptor.

The efficiency of energy transfer E_{FRET} is the fraction of photons absorbed by the donor and transferred in the form of charges to the acceptor and can be calculated from the following equation:

$$E_{FRET} = \frac{I_A}{I_A + I_D} \tag{2.1}$$

where I_A represents the intensity collected from the acceptor emission, and I_D is the intensity collected from the donor emission when the donor is illuminated at its absorption wavelength.

This efficiency is highly dependent on the distance between the donor and the accep-

tor (R^{-6}) so that any variation of E_{FRET} can be attributed to changes in the distance due to the dipolar coupling mechanism (Figure 2.3).

$$E_{FRET} = \frac{1}{1 + (\frac{R}{R_0})^6} \tag{2.2}$$

where R is the D-A distance and R_0 is the characteristic Förster distance, given for every chromophores pair at which E_{FRET} is equal to 50%. It is dependent on spectroscopic properties of fluorophores in the used environment:

$$R_0 = \frac{0.529 \cdot \kappa^2 \cdot \Phi_D \cdot J(\lambda)}{N \cdot n^4} \tag{2.3}$$

where Φ_D is the quantum yield of donor, N is the Avogadro number, n is the environment refractive index and κ^2 describes the relative orientation of the donor emission dipole moment and the acceptor absorption dipole moment. $\kappa^2 = \frac{2}{3}$ is often assumed, obtained when both fluorophores freely rotate and can be considered to be isotropically oriented during the excited state lifetime. $J(\lambda)$ is the spectral overlap integral shown as:

$$J(\lambda) = \frac{\int_0^\infty \phi_D(\lambda) \cdot \varepsilon_A(\lambda) \cdot \lambda^4 d\lambda}{\int_0^\infty \phi_D(\lambda) d\lambda} \tag{2.4}$$

where ϕ_D is the donor emission spectrum and ε_A is the acceptor spectrum of excitation expressed in $\mathrm{M^{-1}cm^{-1}}$ units.

We then modify the two extremities of a short double-stranded DNA (dsDNA) with two fluorophores, and measure the variation of the amount of energy transfer between them, as RDC is added to the solution, and forms a complex with DNA. We choose Alexa Fluor 488 as a donor and Alexa Fluor 568 as an acceptor, attached to the 3' and 5' ends, respectively, of a 15 bp (51 Å) long dsDNA (Figure 2.4), so that FRET efficiency is 76%. For this pair of fluorophores $R_0 = 62$ Å. Volumes required to perform the FRET examination are very low (around 10 µl). Number of DNA base pairs is limited by the range over which the energy transfer can take place, that is approximately 10 nm (100 Å). The sequence of DNA we study has been previously used to study cisplatin's activity [11]. It was observed that cisplatin prefers to bind to GG and AG base pairs. Therefore we decide to use a sequence rich in GG and AG regions (see Appendix A.2).

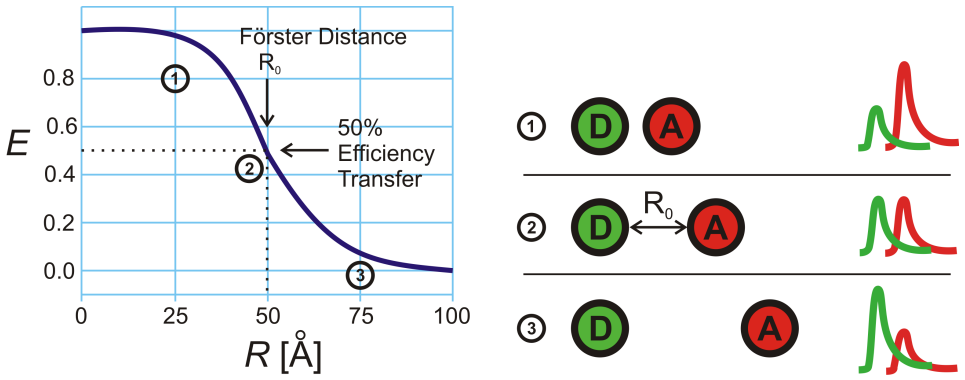

Figure 2.3: Distances between the donor and the acceptor and intensities of emission (left), relationship between efficiency and distance (right), corresponding regions marked with numbers 1–3 in circles.

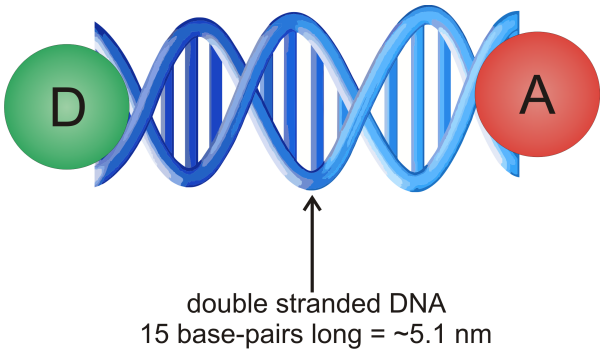

Figure 2.4: Sketch of DNA 2-stranded 2-labelled, 15 base-pair long with Alexa 488 donor (D) and Alexa 568 acceptor (A).

We know that depending on interaction, changes in DNA length appear. That is why it became essential for us to observe and measure DNA length variation as a function of the RDC amount added. Small variations in DNA conformation, by adding RDC, cause changes in the donor-acceptor coupling and consequently on the efficiency of FRET measurements. These changes are then translated into a change in length. We perform bulk experiments where orientation is averaged over all the equiprobable conformations and the only remaining parameter in this system is the distance separating the donor from the acceptor [8–10].

We vary the RDC concentration and measure the fluorescence intensity of two coupled fluorophores. We then calculate the FRET efficiency and its change depending on amount of RDC added. From these variation, which are in fact variations of DNA length, we can obtain the affinity of RDC-DNA complex. That means that FRET method allows us to measure the value of affinity constant K_a by changing RDC concentration.

2.1.2 Optical trap

We study the mechanical properties of DNA/RDC complex using an optical trap to pull the complex. The apparatus is described in Appendix B.2. The mechanical measurements related to the underlying structure of the complex are needed to infer the way RDC binds to DNA.

We decide to use optical trap as a complementary tool, well described and precise, willing to go into details about the structure changes and different kind of interactions appeared. The results obtained from experiments performed by this method are plenty of information about the mechanical properties of DNA [15] and their changes induced by interacting compounds [12]. We choose this method because it seems to be perfect in such precise manipulation. Optical trap enables us to apply forces of pN order and to stretch single DNA molecule precisely. It exhibits a strong stability and feedback. Not without significance is the low cost of its setup's design and use [77].

As mentioned before DNA exists in various conformations (ssDNA, dsDNA). These forms exhibit different mechanical properties which are significant in DNA/compound interaction understanding. Double-stranded DNA can be considered as a linear chain polymer built of nucleotides [90].

The most common form of DNA (dsDNA) takes the form of a double helix, which mechanical properties are these of spring. At longer scales, the double helix forms a random coil, which elasticity is of entropic origin [15].

When an external force applied, the mechanical response of a DNA molecule has two regimes: entropic and enthalpic [41]. The entropic response comes from thermal fluctuations and the enthalpic response from changes in base pairs interactions [41]. The use of optical trap leads to this response by manipulation of DNA.

We stretch a single molecule of dsDNA. In contrast to ssDNA pulling dsDNA reveals more information about its mechanical properties. At low stretching forces dsDNA reveals an entropic elastic response. As the force increases, enthalpic stretching of the base pairs takes place and results in a much stiffer response [28]. Then a transition between the double helix (B form) and a ladder (S form) occurs that happens at a constant force and results in an increase of the length of DNA [29]. A plateau is thus observed in the force-extension curve (Figure 2.5) which height (62pN) is characteristic of the transition [24].

When compounds are bound to DNA, there are many kinds of possible interactions. These interactions are ligand-dependent in the case of RDC and usually non-covalent [40]. It is known that ligand binding to DNA involve electrostatic interaction, intercalation of hydrophobic ligands between pairs and groove binding [21, 22, 40].

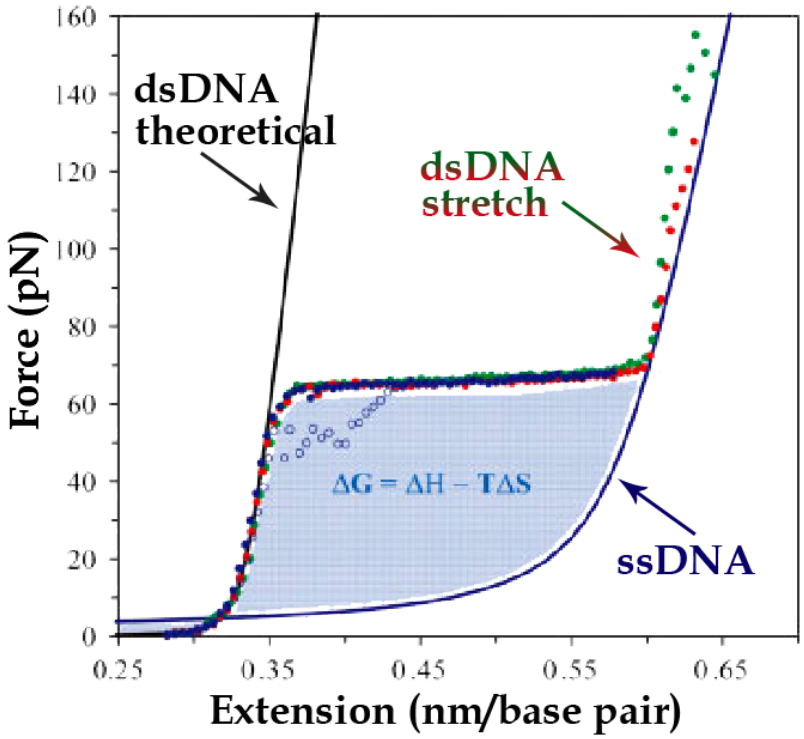

Figure 2.5: Under external force applied dsDNA reveals an entropic elastic response [90]. Force-extension curves for single molecules of dsDNA (red and green dots) and ssDNA (right navy blue line). A theoretical curve for dsDNA is shown as the left black line.

Minor groove binders do not exhibit a significant effect on the molecular length of the dsDNA. Applying the force causes a slightly increased value of contour length. In contrast to the results for the free dsDNA, the overstretching transition is shifted to higher force values and a drastic decrease in the persistence length can be observed [12]. Non-covalent binding of the groove binder is characterized by a combination of electrostatic, van der Waals, and bifurcated hydrogen bonds with a strong preference for AT-rich regions [30], which stabilizes the double strands and resists the force-induced melting.

The force-extension curve of dsDNA complexed with the major groove binder [31, 32] displays a transition between the elastic stretching of B-DNA at low forces and the overstretching transition at higher ones. Similar to the minor-groove binder, the force extension curve exhibits a merging of the overstretching transition into the nonequilibrium melting transition. The molecule length and the contour length is slightly increased. This observation can be associated with an electrostatic binding along with

a compensation of the negatively charged DNA backbone by the guanidine groups of the peptide [31], which neutralizes the intrinsic charge and extends the flexibility of the complexed dsDNA.

For all intercalators it was found that the plateau totally disappeared, the DNA length increased, and its persistence length was reduced compared to free dsDNA. Intercalation is additionally stabilized by ionic interaction between a positively charged group of the intercalator and the DNA backbone charged negatively. This unspecific electrostatic binding of the intercalators reduces the net charge and extends the flexibility of the DNA, which explains the decrease of the persistence length [12].

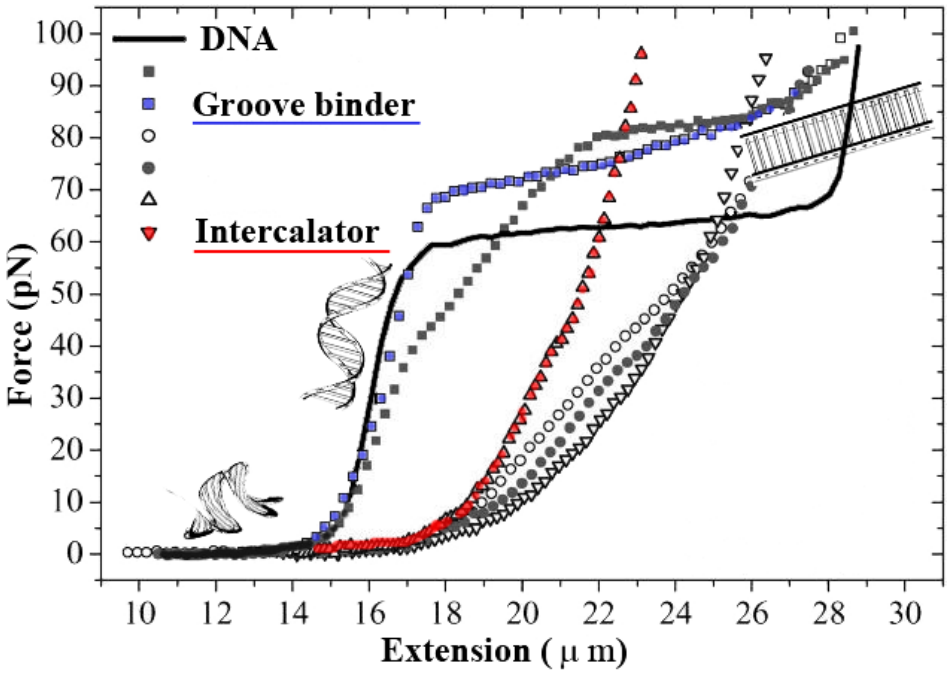

Figure 2.6: Untreated dsDNA molecule (black line) and complexed with a groove-binder (blue and grey squares), or intercalator (red and open triangles, circles), exhibit different elasticity curves indicating individual mechanical properties. [12]

As it is shown above the optical trap method allows us to extract directly the mechanical parameters of the DNA. We can suspect that interaction with RDC modifies the DNA structure and changes them significantly. Therefore mechanical measurements are a useful way to examine these changes caused by RDC addition [17].

2.2 FRET experiment

2.2.1 Low salinity

FRET experiments have been performed in low salinity environments (around 1 mM of NaCl). We carry out the titration by adding RDC to 15 bp-long dsDNA. The DNA concentration remains constant whereas RDC concentration is being increased with every single measurement. As a result we measure FRET efficiency as a function of RDC concentration. As mentioned before the efficiency of 15 bp dsDNA is 76%. The efficiency as a function of RDC/DNA ratio for RDC11, RDC34 and RDC44 are shown in graph 2.7:

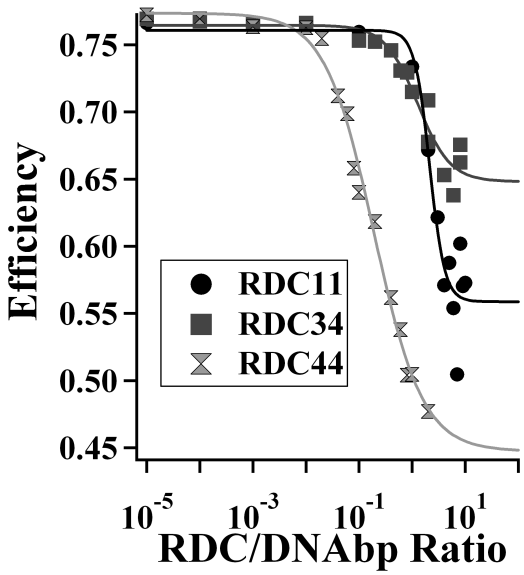

Figure 2.7: FRET efficiency of DNA-RDCxx complex as a function of RDCxx/DNA ratio in low salinity.

The decrease of the FRET efficiency as a function of RDC concentration shows RDC/DNA complexation. It is clearly visible that at a given concentration of RDC the efficiency decreases rapidly. This efficiency drop is simply attributed (according to Equation 2.2) to DNA length increase. Plateau reached at high concentration leads to the saturation of the DNA strands.

To analyze these data we look for a model relating the parameters describing the binding process. We are interested in determining the affinity constant as well as the the number of DNA bp occupied by one single RDC molecule. Although RDC is a very small molecule, around 1 nm in diameter, smaller than most of the proteins, it may

occupy more than one base pair of DNA.

If the number of base pairs bound to RDC molecule is equal to 1, then we can write a mass action law involving the base pairs and RDC concentration. This is a Scatchard's representation [19]. However RDC may bind to $p > 1$ bp. Then the $p - 1$ neighbor base pairs of a complexed RDC molecule possess a lower number of possible complexation configurations than a base pair far away from any complexed RDC molecule. This reduces the total number of configurations and doesn't involve any interaction energy between RDC molecules. This effect is taken into account by McGhee&von Hippel association model (MGVH model). The two models are now briefly described.

At first the Scatchard's model is considered. To quantify interaction equilibrium we thus write:

$$DNA_{bp} + RDC \overset{K_a}{\rightleftharpoons} DNA_{bp}RDC \tag{2.5}$$

where it is implicitly assumed that RDC binds to one DNA base pair at most.

$$K_a = \frac{[DNA_{bp}RDC]}{[DNA_{bp}][RDC]} \tag{2.6}$$

where $[DNA_{bp}]$ denotes the concentration of DNA base pair, and $[RDC]$ the concentration of RDC. Following Scatchard's notation, we call ν the ratio of bound RDC per DNA bp:

$$\nu = \frac{[RDC_b]}{[DNA_{bp}]} \tag{2.7}$$

where $[RDC_b]$ is the molar concentration of RDC bound to dsDNA and $[DNA_{bp}]$ the total concentration of DNA bp. Then, K_a is expressed by equation:

$$K_a = \frac{\nu}{[RDC](1-\nu)} \tag{2.8}$$

Thus, following Scatchard, the equilibrium condition is:

$$\frac{\nu}{[RDC]} = K_a(1-\nu) \tag{2.9}$$

This model assumes that the size of ligand is very tiny and hence one RDC molecule can bind to just one DNA base pair. Therefore, plotting the $\frac{\nu}{[RDC]}(\nu)$, we expect to obtain

the linear plot whose slope would be -1 and intercept with y-axis is K_a. Nevertheless when we plot $\frac{\nu}{[RDC]}$ as a function of ν (Figure 2.10), the slopes occur far different from -1. It means that the number of binding sites is larger than 1 and that slopes and intercepts cannot be interpreted that way. Even the estimation of their linear part results in errors. If one RDC covers two or more binding sites (DNA base pairs), the number of free binding sites left depends not only on the number of free RDC molecules, but also on the distribution the bound RDCs on the DNA [19]. Thus, the adsorption cannot be described by a new chemical equilibrium of unknown stoichiometry.

We must take into account that when the first RDC molecule binds to DNA, it eliminates $p-1$ potential binding sites. But RDC molecules do not bind to DNA adjacently (Figure 2.8). It means that the length g of binding gap can contain $g-p+1$ binding sites when $g \geq p$, or 0 if $g < p$. This implies that the DNA saturation by RDC is impossible in practice [18].

We modify Scatchard's assumption and accept, that one RDC molecule occupies more than one base pair. We call p the number of bp occupied by a molecule of RDC

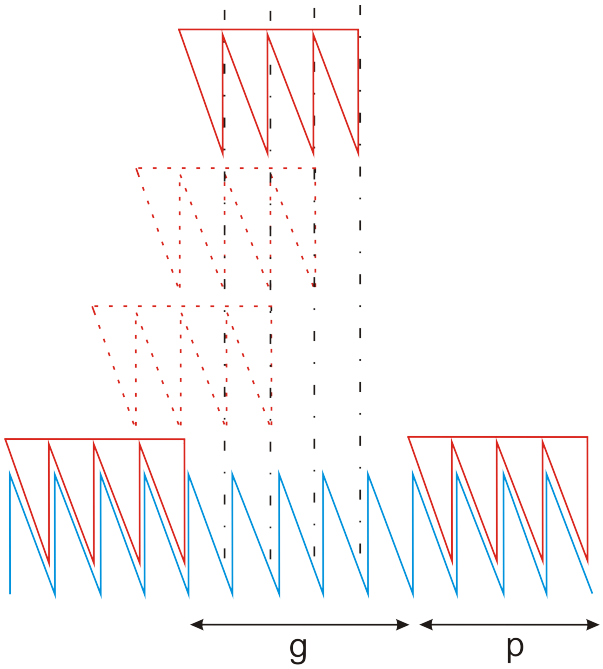

Figure 2.8: Model of McGhee and von Hippel takes into account that if one RDC molecule occupies two or more DNA base pairs, some of the configurations of free binding sides left are forbidden for further binding.

McGhee and von Hippel analyzed exactly this model [18]. They found:

$$\frac{\nu}{[RDC]} = K_a \frac{(1-p\nu)^p}{(1-(p-1)\nu)^{p-1}} \tag{2.10}$$

For $p = 1$, one recovers the equilibrium condition given by Scatchard's standard thermodynamics:

$$\frac{\nu}{[RDC]} = K_a(1-\nu) \tag{2.11}$$

We assumed that the advancement of the reaction, ν, is deduced from the efficiency measurements and DNAs length:

$$\nu = \frac{R_{RDC} - R_{DNA}}{R_{DNA}} \tag{2.12}$$

where R_{RDC} is the length of DNA in each RDC concentration and R_{DNA} is the length of untreated DNA.

From the equilibrium condition (Equation 2.10), we determine the affinity constant K_a, and the number of sites p occupied by an RDC molecule. K_a is given by:

$$K_a = \lim_{\nu \to 0} \frac{\nu}{[RDC]} \tag{2.13}$$

and p is given by:

$$p = \frac{1}{2} - \frac{1}{2K_a} \lim_{\nu \to 0} \frac{\partial}{\partial \nu} \frac{\nu}{[RDC]} \tag{2.14}$$

This allows us to obtain K_a and p from the linear dependance $\frac{\nu}{[RDC]}(\nu)$ used previously in consideration of the first model (Scatchard). However, simple modification of Equation 2.10 gives a function which fits the data shown as $[RDC](\nu)$ and returns K_a and p as the fitting function's coefficients:

$$[RDC] = \frac{\nu}{K_a} \frac{(1-(p-1)\nu)^{p-1}}{(1-p\nu)^p} \tag{2.15}$$

Table 2.1: K_a and p values of RDCxx-DNA in low salinity.

	K_a	ΔK_a	p	Δp	K_a*	ΔK_a*	p*	Δp*
RDC11	3.55E+5	9.9E+4	3.4	0.7	1.24E+5	4.85E+4	2.8	0.5
RDC34	5.18E+4	2.57E+4	3.5	1.4	8.80E+4	6.55E+4	3.7	0.3
RDC44	2.80E+6	3.20E+5	3.1	0.5	2.02E+6	1.74E+5	2.4	0.1

According to this model, we can analyze our data following two different procedures. First we plot $\frac{\nu}{[RDC]}(\nu)$ and fit with a line (Figure 2.10). The results will be called K_a* and p*. Second we plot $[RDC](\nu)$ and fit according to Equation 2.15 (Figure 2.9). The results will be called K_a and p. In order to calculate the uncertainty ΔK_a, Δp, ΔK_a*, Δp* of obtained values we used the total differential method.

Both of the analyzes are presented below.

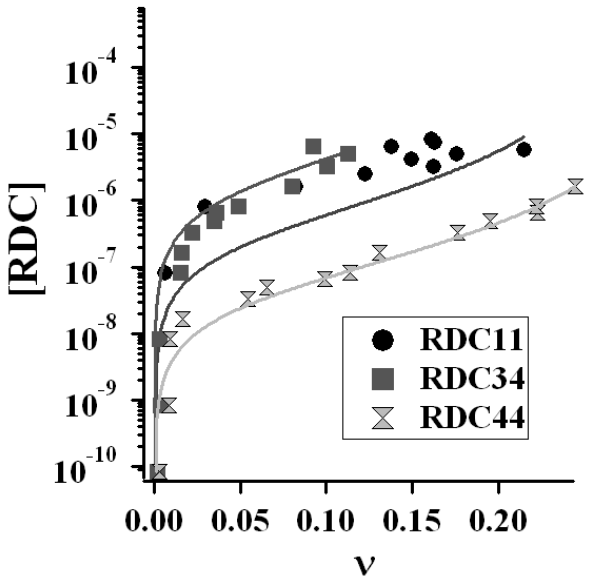

Figure 2.9: McGhee&von Hippel model's fit of unbounded RDC11, RDC34 and RDC44, in low salinity environment

Both analyzes lead to similar values of K_a and p. It is clearly visible that the affinity of these three molecules to DNA differ from each other and $K_{a_{RDC44}} > K_{a_{RDC11}} \geq K_{a_{RDC34}}$ (Table 2.1). As the confirmation of these data the inverse experiment is performed. To already interacted RDC-DNA complex the non-labeled DNA is added. We carry out the titration by increasing the concentration of DNA. On the contrary to previous experi-

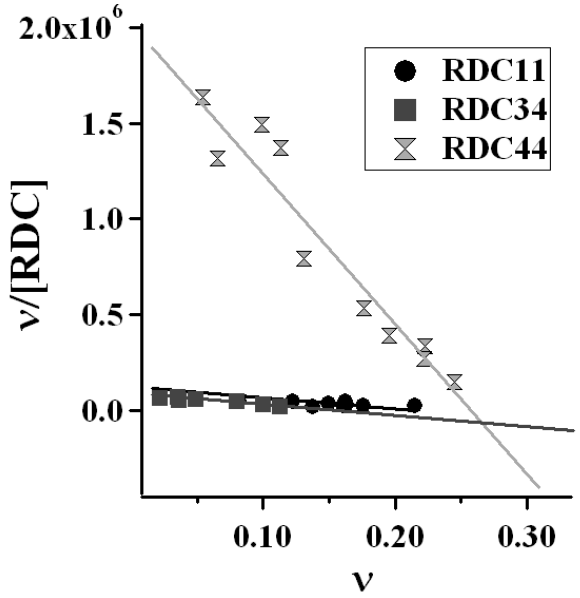

Figure 2.10: McGhee&von Hippel model's linear representation in low salinity environment

Table 2.2: K_a and p values of RDCxx-DNA measured during decomplexation in low salinity

	K_a	ΔK_a	p	Δp	K_a*	ΔK_a*	p*	Δp*
RDC11	2.46E+4	1.35E+5	-2.7	1.2	9.77E+4	9.47E+3	1.5	0.5
RDC34	9.51E+4	5.64E+4	-5.8	8.8	1.17E+5	6.96E+3	4.4	0.7
RDC44	1.30E+6	3.72E+5	-3.3	2.0	1.11E+6	1.41E+6	2.1	0.9

ments, this time we are interested in DNA/RDC ratio. As non-fluorescent DNA has been added, we observe that efficiency of FRET increases as a function of DNA concentration (Figure 2.11), which is in agreement with assumption of equilibrium hypothesis. Using MGVH model we fit the data in two ways to obtain K_a and p (Figures 2.12, and 2.13). The measured values of K_a and p confirm the previous ones (Table 2.2).

These experiments allowed us to measure the affinity of RDC with DNA at 1 mM or 2 mM of salt concentration. They show a strong affinity between DNA and RDC. It may be due to several modes of interactions: Π-stacking, hydrophobic effect, or electrostatic interaction. In order to better understand the salt effect on these interactions we increased the salt concentration.

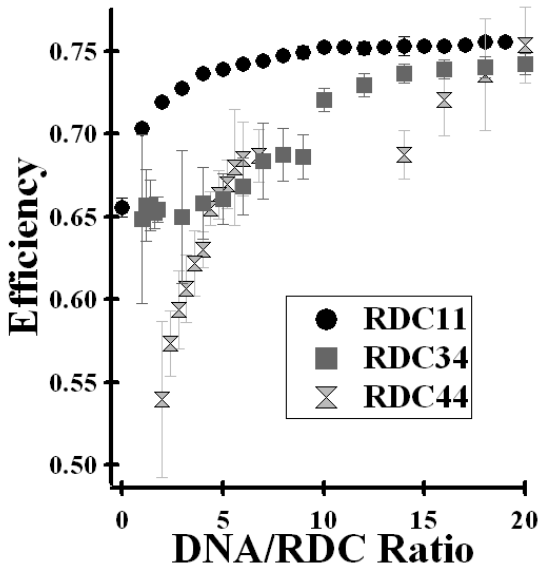

Figure 2.11: FRET efficiency of DNA-RDCxx complex as a function of DNA/RDCxx ratio in low salinity. To prove the equilibrium state, the reversibility of complexation RDC-DNA was performed.

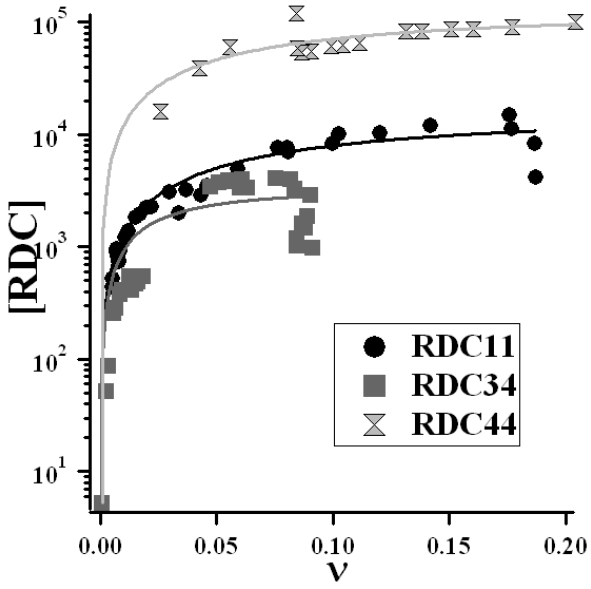

Figure 2.12: McGhee&von Hippel model's fit of unbounded RDC11, RDC34 and RDC44 in decomplexation experiment

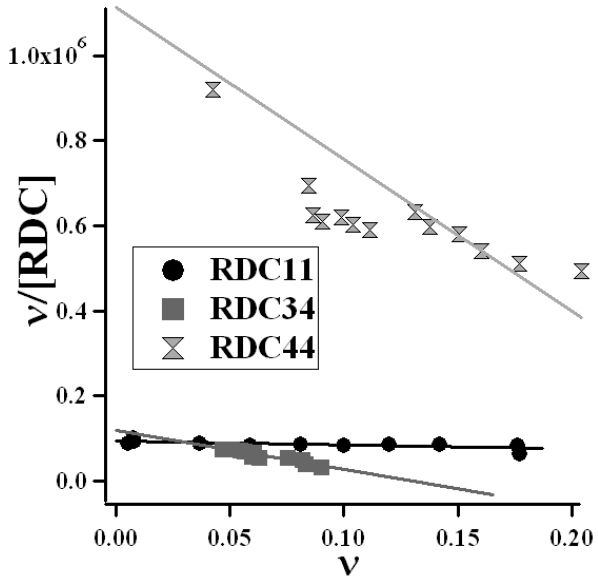

Figure 2.13: McGhee&von Hippel model's linear representation of decomplexation experiment

2.2.2 Salt dependence

We perform again the titration as previously but in environments with different salinity ranging from 2 mM to 200 mM of NaCl.

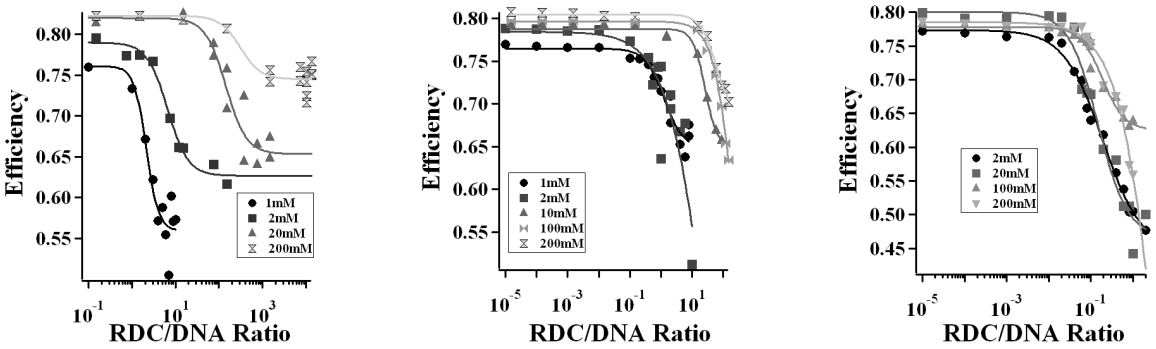

Figure 2.14: RDC-DNA interaction dependance on ionic strength. FRET efficiency of DNA-RDCxx complex as a function of RDCxx/DNA ratio depending on different concentrations of NaCl.

At first glance it is clear that salt occurs to have an impact on the FRET efficiency in different manner depending on the RDC (2.14).

According to MGVH model we calculated affinities in two ways of fitting data (Figures 2.15 and 2.16). We observed a decrease in the affinity of RDC for DNA as a function

of salt concentration (Tables 2.3, 2.4, 2.5).

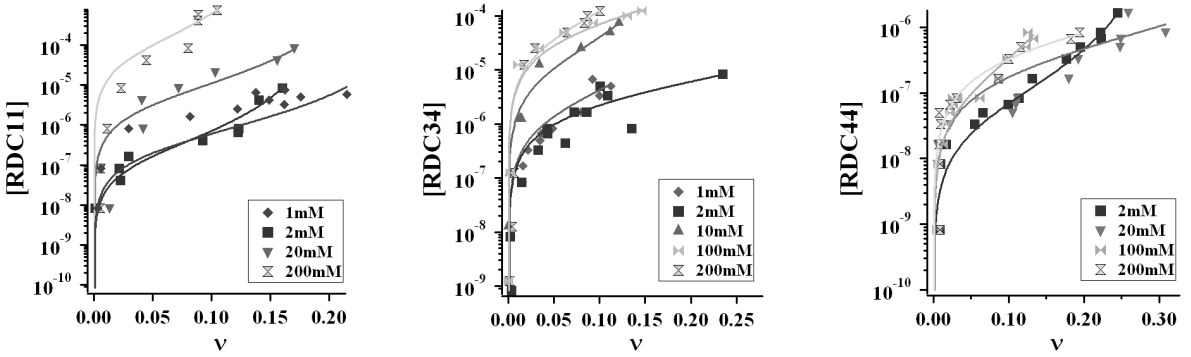

Figure 2.15: McGhee&von Hippel model's fit of unbounded RDC11, RDC34 and RDC44, in different salinity environments.

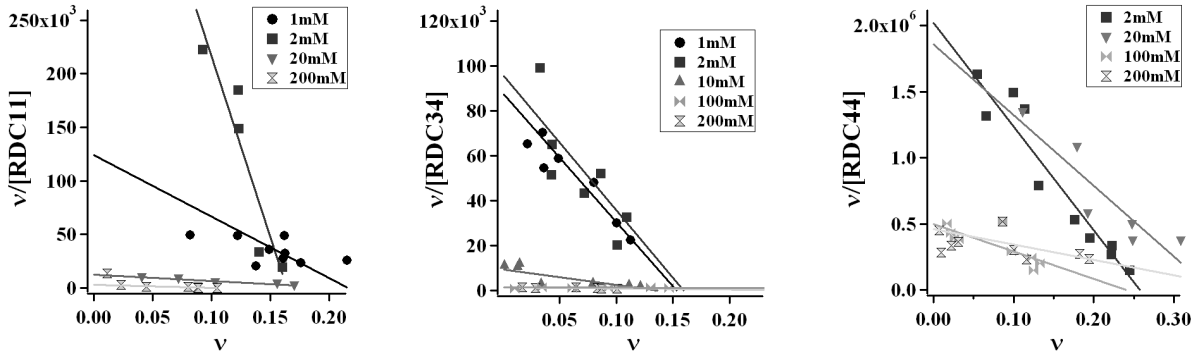

Figure 2.16: McGhee&von Hippel model's linear representation in different salinity environments.

It is known that simple monovalent counterions (like Na^+) interact with polyelectrolyte such as DNA by direct condensation. This reduces the axial charge density of the polyelectrolyte. According to Manning's theory [37, 38] not all of the charges are neutralized, but only a fraction of them, so that, the unneutralized polyelectrolyte charges are screened from each other [33]. ψ is the ratio of neutralized charges along the DNA chain. For dsDNA $\psi = 0.88$ [70].

Let us write the equilibrium between RDC and charged DNA_{bp}:

$$(DNA_{bp}Na^+_\psi) + RDC \overset{\widetilde{K_a}}{\rightleftharpoons} DNA_{bp}RDC + \psi Na^+ \tag{2.16}$$

Table 2.3: K_a and p values of RDC11-DNA complex in different salt concentration

RDC11								
NaCl [M]	K_a	ΔK_a	p	Δp	K_a*	ΔK_a*	p*	Δp*
0.001	3.50E+5	9.9E+4	3.4	0.7	1.20E+5	4.58E+4	2.8	0.5
0.002	5.00E+5	1.55E+5	4.0	0.1	5.50E+5	1.03E+5	3.5	0.1
0.02	2.37E+4	6.97E+3	3.9	0.2	1.22E+4	948	2.9	0.1
0.2	9.71E+2	388	5.6	0.6	3.05E+3	508	5.4	0.3

Table 2.4: K_a and p values of RDC34-DNA complex in different salt concentration

RDC34								
NaCl [M]	K_a	ΔK_a	p	Δp	K_a*	ΔK_a*	p*	Δp*
0.001	5.18E+4	2.57E+4	3.5	1.4	8.79E+4	6.55E+3	3.8	0.3
0.002	5.86E+4	1.62E+4	1.7	0.4	9.59E+4	3.05E+4	3.6	1.3
0.01	7.49E+3	1.3E+3	4.3	0.3	9.23E+3	2.90E+3	4.1	0.7
0.1	2.20E+3	1.18E+2	2.3	0.5	1.36E+3	79	0.9	0.3
0.2	2.06E+3	279	3.8	0.4	1.45E+3	142	2.3	0.5

Table 2.5: K_a and p values of RDC44-DNA complex in different salt concentration

RDC44								
NaCl [M]	K_a	ΔK_a	p	Δp	K_a*	ΔK_a*	p*	Δp*
0.002	2.80E+6	3.2E+5	3.1	0.4	2.02E+6	1.74E+5	2.4	0.1
0.02	7.30E+5	4.29E+5	1.6	0.6	1.80E+6	2.88E+5	1.9	0.1
0.1	7.80E+5	2.28E+5	3.9	0.5	4.99E+5	5.57E+4	1.6	0.4
0.2	3.70E+5	5.89E+4	1.4	0.3	4.59E+5	1.02E+5	1.8	0.9

where $\widetilde{K_a}$ is the thermodynamic constant of this equilibrium. $\widetilde{K_a}$ may be expressed as:

$$\widetilde{K_a} = \frac{[DNA_{bp}RDC][Na^+]^{\psi}}{[DNA_{bp}Na^+_{\psi}][RDC]} \tag{2.17}$$

Our previous analysis of the experimental data leads to an apparent affinity K_a:

$$K_a = \frac{[DNA_{bp}RDC]}{[DNA_{bp}][RDC]} \tag{2.18}$$

so $\widetilde{K_a}$ might be then written as:

$$\widetilde{K_a} = K_a[Na^+]^{-\psi} \tag{2.19}$$

$$K_a = \widetilde{K_a}[Na^+]^{-\psi} \tag{2.20}$$

$$\log K_a = \log \widetilde{K_a} - \psi log[Na^+] \tag{2.21}$$

At constant temperature and pressure, under conditions of excess Na^+, variations of K_a with Na^+ concentration are written:

$$\frac{\partial \log K_a}{\partial \log[Na^+]} = -\psi \tag{2.22}$$

In deriving this relationship we neglected the change of chemical activity of DNA and of RDC due to addition of salt into the solution. A general derivation is given in [70] (Equation 7.16).

It is also shown that, in the case of multivalent is:

$$\frac{\partial \log K_a}{\partial \log[M^{Z+}]} = -Z\psi \tag{2.23}$$

where [M] is a counterions concentration and Z their valency [70].

We fit the measured log K_a (log Na^+) curve with a line of slope -0.88 (Figure 2.17). RDC11 and RDC34 can be estimated well by such a line (the standard deviation of

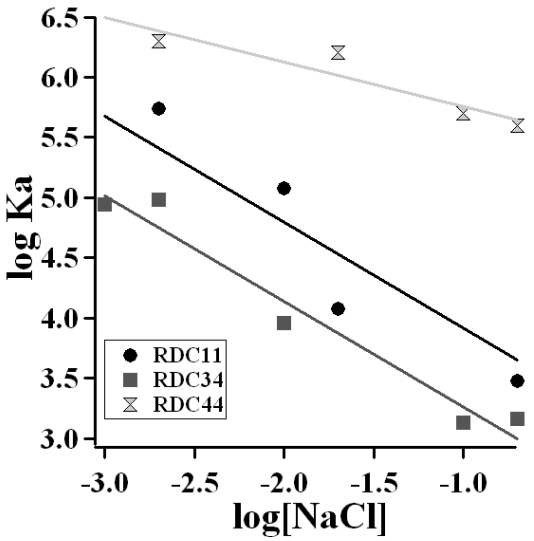

Figure 2.17: Logarithm of K_a values, as a function of logarithm of salt concentration. For RDC11 and RDC34 slope value is equal to the ratio of neutralized charges of DNA, $-\psi = -0.88$. For RDC44 a linear fit of the data is performed leading to a slope equal to -0.37.

Table 2.6: Slopes and standard deviations (sd) of linear fit of LogK_a(Log[NaCl])

	slope	sd
RDC11	-0.88	0.188
RDC34	-0.88	0.081
RDC44	-0.37	0.1

the fits are 0.188 and 0.081, respectively). The evolution of log K_a of RDC44 as a function of log Na^+ is much slower. Linear fit of the data leads to a slope equal to -0.37 (Table 2.6).

2.3 Optical trap experiment

We anchor one end of the double-stranded DNA (dsDNA) molecule onto the glass surface. On the second one we attach the streptavidine bead and trap with IR single laser beam. Using a piezo-electrical device we translate the coverslip and stretch the dsDNA molecule attached between the coverslip and the trapped bead. We then measure the displacement of the bead from the center of the trap and deduce the force exerted by the DNA strand (Figure 2.18).

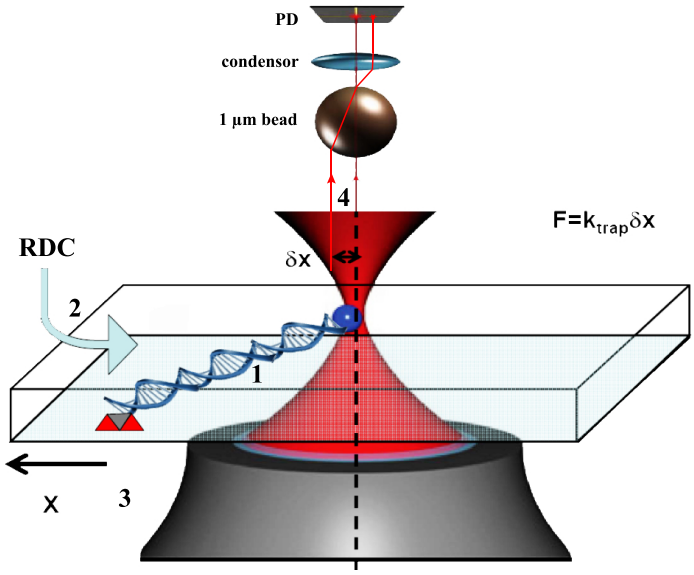

Figure 2.18: Principle of mechanical examination of RDCxx-DNA complex. 1. Attachement of DNA molecule between coverslip and bead, 2. Introduction of RDC to solution, 3. Translattion of the coverslip: stretching of DNA, 4. Measurement of the displacement of bead from the trap center.

Before adding RDC, we first check the force-extension curve of pure, single dsDNA molecules. Then we introduce different concentration of RDC11, RDC34 and RDC44 and obtain force-extension curves as a function of RDC concentration.

The ones corresponding to RDC11 and RDC34 reactions reveal no changes in DNA length at low concentrations added and low forces (below 10 pN) applied. At higher concentrations of RDC11 (40 nM to 4 µM) and RDC34 (40 nM to 400 nM) and higher forces ($F > 10$ pN) we observe that the DNA length increases. We observe a loss of the $B \rightarrow S$ transition (plateau) which is the signature of denaturation due to intercalation [12]. No more plateau is visible around 62 pN in 4 µM and 400 nM concentration of RDC11 and RDC34, respectively (Figures 2.19 and 2.20). Hence, the interaction of RDC11 and RDC34 is typical of intercalation between base pairs.

The analysis of the stretching curves at different ruthenium concentration was performed as follows. In the case of an intercalant, for forces higher than 10 pN the extension of an intercalated DNA is longer than non-intercalated dsDNA. The determination of the fractional number ν of the intercalant per base pairs (that is the chemical advancement of Equation 2.5) was directly related to this change in extension by:

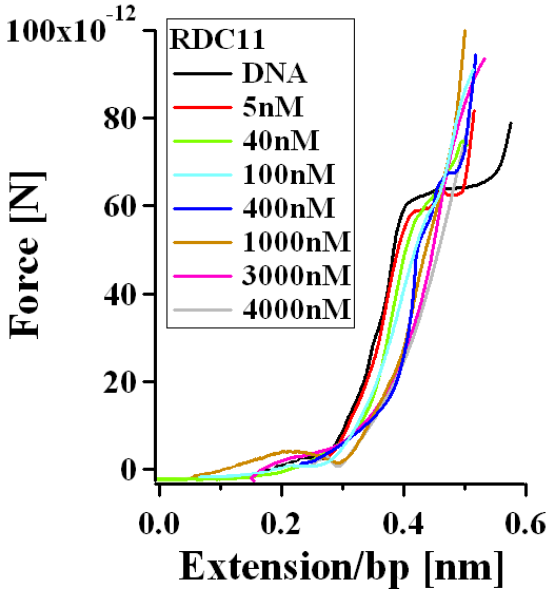

Figure 2.19: Force-extension curve of DNA in different RDC11 concentrations. Untreated DNA is marked in black. Increasing the concentration of RDC11 causes the DNA elongation and loss of the plateau, that is typical intercalator's behavior.

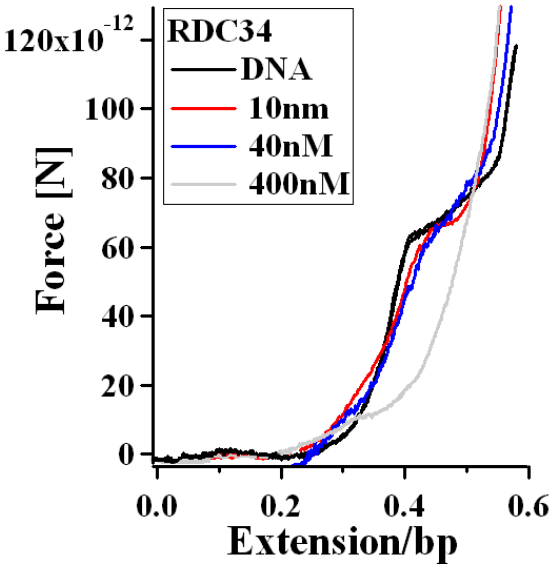

Figure 2.20: Force-extension curve of DNA in different RDC34 concentrations. Untreated DNA is marked in black. Increasing the concentration of RDC34 causes the DNA elongation and loss of the plateau, that is typical intercalator's behavior.

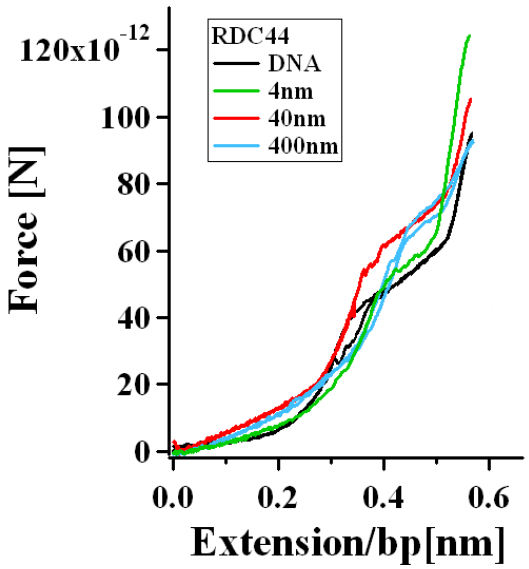

Figure 2.21: Force-extension curve of DNA in different RDC44 concentrations. Untreated DNA is marked in black. Increasing the concentration of RDC44 causes the shift of plateau into higher force and has no significant impact into DNA length which is characteristic for groove-binders.

$$\nu = \frac{x(F,[RDC]) - x_{ds}(F,0)}{x_{ds}(F,0)} \tag{2.24}$$

where $x_{ds}(F,0)$ is the elongation per base pair of the dsDNA in the absence of RDCs at the force F and $x(F,[RDC])$ is the elongation of the dsDNA at the force F in the presence of the RDCs concentration $[RDC]$. Again, we can use the MGVH binding isotherm to fit the curve:

$$[RDC] = \frac{\nu}{K_a}\frac{(1-(p-1)\nu)^{p-1}}{(1-p\nu)^p} \tag{2.25}$$

where K_a is the affinity constant at the given force and p represents the occupancy site in DNA base pairs. The affinity constant depends on the exerted force because once the molecule is lengthened the energy cost to interact is changed.

Using the MGVH model to analyse the curves and measure DNA lengths at forces from 20 (RDC11) or 30 (RDC34) to 50 pN, with step of 10 pN we plot dependence of the DNA relative length as a function of RDC11 concentration at different forces.

Table 2.7: K_a and p values of RDC11-DNA complex dependent on different force applied

RDC11				
Force	K_a	p	K_a (linear fit)	p (linear fit)
20 pN	8.36E+5	4.78	1.03E+6	3.62
30 pN	8.96E+5	4.01	1.40E+6	3.22
40 pN	2.54E+6	3.85	3.05E+6	3.04
50 pN	4.39E+6	3.94	3.14E+6	3.04

The adjustments enable us to obtain the affinity constants at each force and the DNA binding site sizes. Again we carry out two possibilities of fitting: the linear one of dependance $\frac{\nu}{[RDC]}(\nu)$ (Figures 2.24 and 2.25) from which we find K_a and p according to Equations 2.13 and 2.14, respectively, and this one obtained from unbounded RDC ($[RDC](\nu)$) which returns K_a and p directly (Figures 2.22 and 2.23). K_a and p values obtained with both methods are presented in Tables 2.7 and 2.8 and Figures 2.26 and 2.27 .

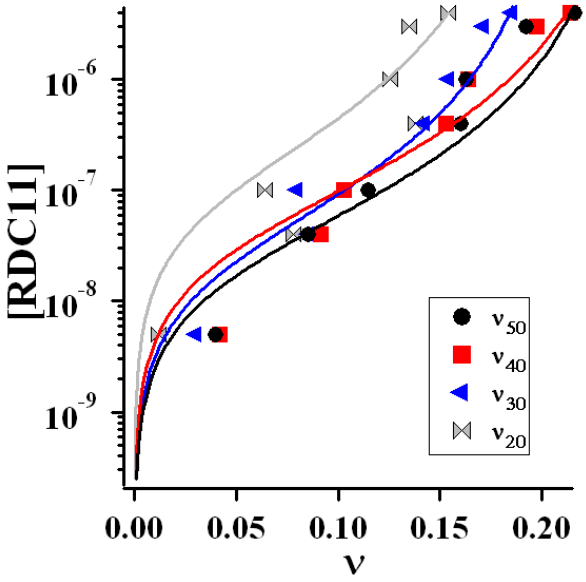

Figure 2.22: McGhee&von Hippel model's fit of unbounded RDC11

In case of RDC44 we observe a different mode of the RDC/DNA interaction. There

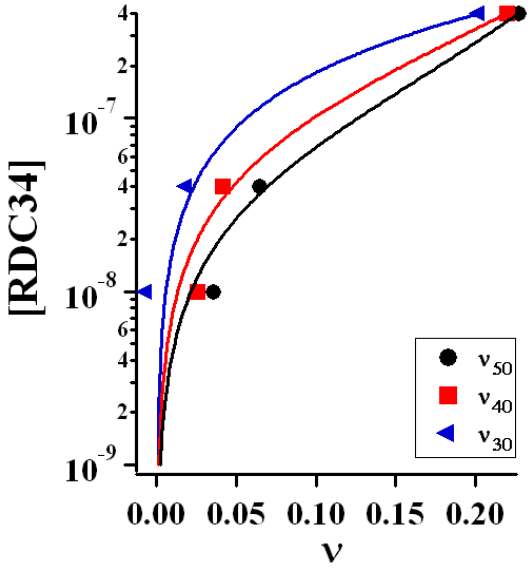

Figure 2.23: McGhee&von Hippel model's fit of unbounded RDC34

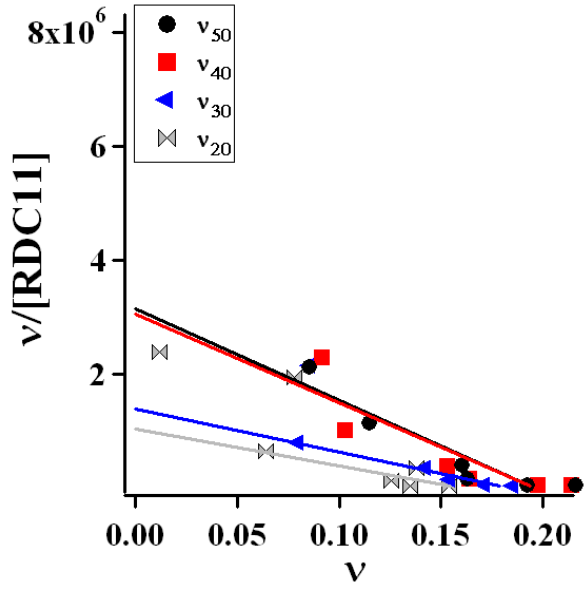

Figure 2.24: McGhee&von Hippel model's linear expression for RDC11

are no visible changes in DNA length in any force. Even at the highest concentration added (400 nM) the plateau does not disappear. Moreover the higher concentration of RDC44 is added, the higher force is required to melt DNA (Figure 2.21). Although it seems like RDC44 binding stabilizes dsDNA structure, it must be, at least partly, disrupted if such effect occurs. These features are very characteristic in groove bind-

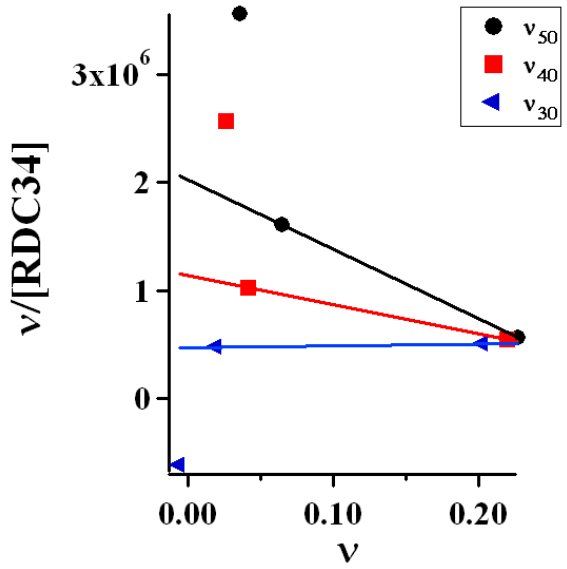

Figure 2.25: McGhee&von Hippel model's linear expression for RDC34

Table 2.8: K_a and p values of RDC34-DNA complex dependent on different force applied

RDC34				
Force	K_a	p	K_a (linear fit)	p (linear fit)
30 pN	5.89E+5	0.83	4.74E+5	0.32
40 pN	1.39E+6	2.02	2.07E+6	2.23
50 pN	2.35E+6	2.46	3.27E+6	2.40

ing [12]. Because the average melting force increases as a function of added compound, the fractional occupancy per base pair ν might be determined by comparing the measured melting force F_m at each RDC44 concentration with the force F_m^0 and F_m^s observed in the RDC44 absence and saturating concentration added respectively. [39]

$$\nu = \frac{F_m - F_m^0}{F_m^s - F_m^0} \tag{2.26}$$

Combination of the equation above with the MGHV model (Equation 2.25) gives the fit determining the affinity constant K_a and p of interaction RDC44-dsDNA, with ν related to F_m, F_m^0 and F_m^s, according to Equation 2.26.

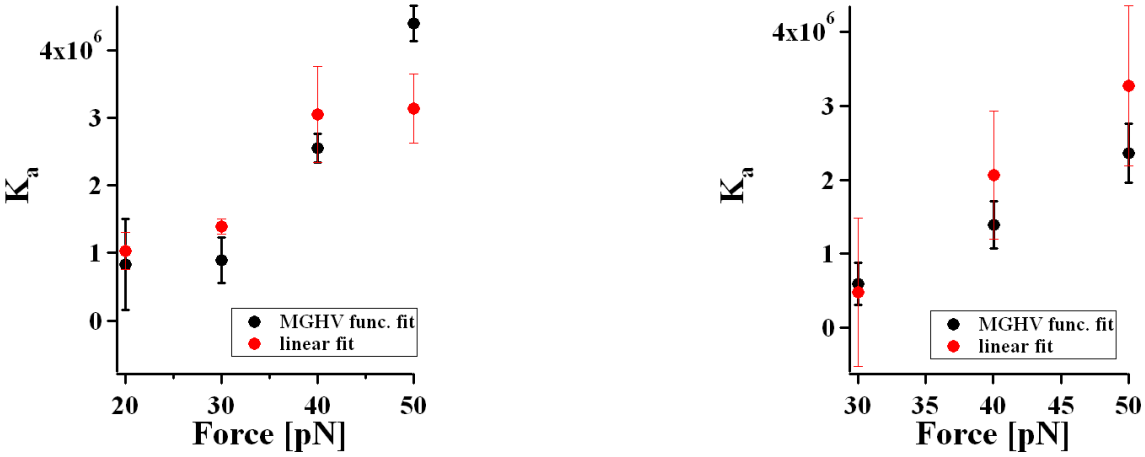

Figure 2.26: Affinity constant K_a of DNA-RDC11 (left) and DNA-RDC34 (right) complexes obtained in two ways of fitting: according to Equation 2.25 (black) and linear 2.13 (red), as a function of force

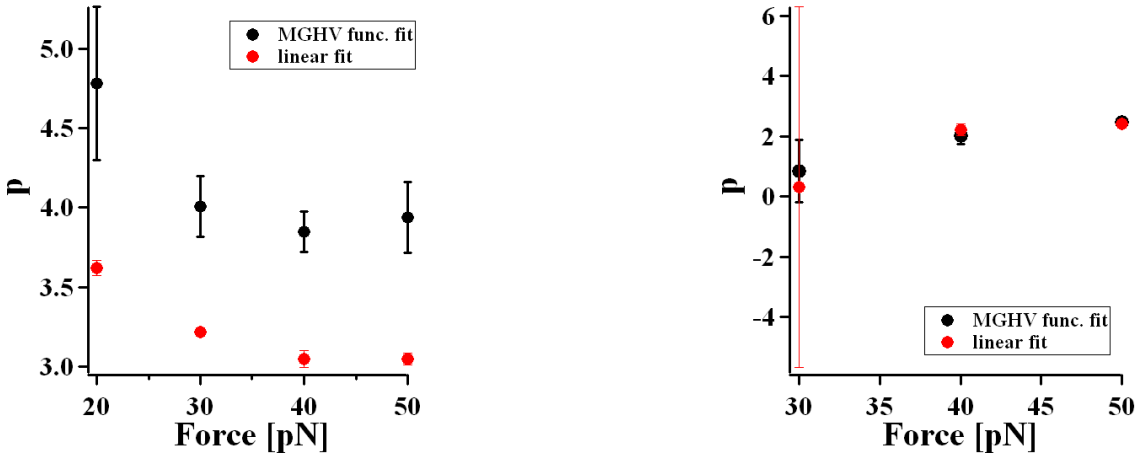

Figure 2.27: Number of binding sites p occupied by one RDC11 (left) or RDC34 (right) molecule obtained in two ways of fitting: according to Equation 2.25 (black) and linear 2.14 (red), as a function of force

But contrary to the previous case, where advancement of the reaction is assumed to be proportional to the extension of DNA, we do not measure experimentally the melting force when DNA is saturated F_m^s. We then keep F_m^s as a fitting parameter. We plot [RDC] as a function of F_m, taking F_m^s, K_a and p as fitting coefficients (Figure 2.28). K_a and p values are given in Table 2.9

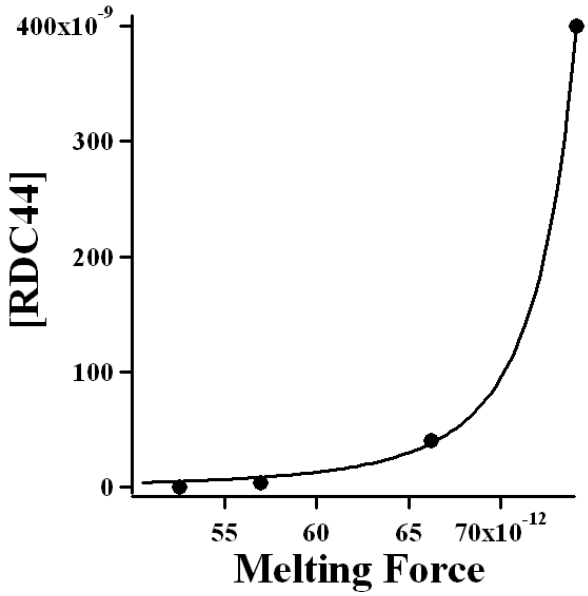

Figure 2.28: McGhee&von Hippel model's fit of unbounded RDC44 leads to obtain the average value of affinity constant K_a and p (independent of force)

Table 2.9: K_a and p values of RDC44-DNA complex

RDC44			
K_a	p	K_a (linear fit)	p (linear fit)
8.34E+6	5.02	-	-

2.4 Discussion

We find that RDC interacts with DNA and this interaction depends on RDC chemical structure. We performed two different experiments in order to answer three complementary questions about the interaction mode of RDC11, RDC34 and RDC44 with DNA.

2.4.1 Determination of the complex conformation

From the force experiments it is observed that RDC11 and RDC34 interact with DNA as intercalators, whereas RDC44 is a groove-binder.

Our main observation is the increase of the DNA contour length from which we must conclude that RDC11 and RDC34 intercalate between DNA base pairs. Intercalation occurs when hydrophobic, planar ligand is inserted between two base pairs. As shown

in Figure 2.1, RDC11 and RDC34 molecules possess a phenanthroline group and C,N-(2-phenyl-pyridine) that have the right dimension to be an intercalator group. Both of them are planar and hydrophobic and play the same geometrical role in the RDCs' chemical structure. However, the hydrophobicity of the phenanthroline group is higher than phenyl-pyridine one. Phenanthroline group is also more planar than methyl groups present in RDC11. Therefore we expect that RDC11 and RDC34 bind to DNA with phenanthroline group in Π-stacking way.

On the opposite we have measured that RDC44 binds to DNA by groove binding process. The spermine tail of RDC44 (Figure 2.1) known to exhibit a strong affinity to DNA groove [42]. Thus it is reasonable to think that RDC44 binds to DNA through groove binding of the attached spermine tail. Our results show that once spermine interacts with groove, there is no more impact of phenenthroline group and intercalation is not observed.

2.4.2 Determination of the thermodynamic parameters of interaction

The measurements allow us to obtain the affinity constant of RDC11, RDC34 and RDC44 with DNA.

We find that K_a values of RDC11 are not significantly higher than of RDC34. Both compounds intercalate by phenanthroline group, hence similar K_a value is not a surprise.

K_a of RDC44/DNA complex is higher than RDC11 and RDC34. RDC44/DNA way of interaction is different than of RDC11 and RDC44, therefore different K_a is expected. The affinity constant of spermine is 2.3E+5 [42], approximately one order of magnitude less than K_a of RDC44. This result is in agreement with the fact that spermine has a higher affinity for the groove binding than phenanthroline for base pairs.

From both methods we obtain values of K_a that are in good agreement with each other. Thus K_a is independent on DNA length (from 15 bp to 8.6 kbp). No cooperativity between ligands is observed.

2.4.3 Description of the molecular mechanism of interaction

The FRET experiments show that the affinity constant decreases with the addition of salt. Slopes of the linear dependence, log K_a as a function of log NaCl, show, that RDC11 and RDC34 are sensitive to salt concentration changes. These results exhibit the counter ions exchange and an electrostatic interaction occurrence between RDC and DNA. Thus, despite intercalation, in which hydrogen bonds and hydrophobic forces play

the most important role in the overall complex stability [44, 45], electrostatic interactions are also of great significance.

On the other hand, mechanical measurements which enable to finely probe the potential energy landscape between DNA and RDC11 and RDC34, show a dependence of the affinity on the applied force—the affinity increases when DNA is pulled. This result is in agreement with previous measurements of the change of affinity under tension. When one pulls DNA, the distance between the base pairs increases and the intercalating group (phenanthroline in our case) has more space to optimize its interactions with the base pairs and state of lower energy may be found [43]. As a consequence K_a increases.

When intercalation implies the replacement of a counterion by charged complexant, of valency Z, then K_a decreases as the Z-th power of the added salt concentration. It was shown that $\frac{\partial \log K_a}{\partial \log[Na^+]} = -Z\psi$ [49]. In our case RDC11 and RDC34 have a valence equal to +1 so that by plotting the logarithm of the variation of the affinity constant K_a as a function of the logarithm of the salt concentration, a linear relationship with a slope of -0.88 is expected. Our results of slope for RDC11 and RDC34 are consistent with this mechanism of interaction. Thus, intercalation of RDC11 and RDC34 is dominated by electrostatic influence, whereas this kind of interaction plays a much weaker role in the groove binding of RDC44. Slope of log K_a as a function of log NaCl reveals very low sensitivity of RDC44 to salt concentration changes, which means that ion exchange does not occur.

Under the external force applied, K_a of RDC44 increases. Number of binding sites p suggests that approximately three adjacent base pairs are forbidden for further binding when RDC44 interacts with DNA.

Chapter 3

RDC uptake and localization inside the cells

3.1 Luminescent features of RDC

RDC34 and RDC44 share a common hydrophobic core containing a phenyl-pyridine and two phenanthroline groups. We hypothesize that phenanthrolines would procure luminescent properties. We test both compounds in a spectro-fluorometer and observe that they display luminescent properties (Figure 3.1) with the emission increasing after 700 nm. As it is shown in chapter 2, RDC interacts with DNA, we hypothesize that upon this interaction, the luminescence of RDC could increase. Luminescent emission from DNA is null over the entire range (Figure 3.1). Once DNA and RDC34 or RDC44 were mixed the luminescent emission of both compounds strongly increases (Figure 3.1). This result indicates that RDC34 and RDC44 display interesting luminescent properties while interacting with macromolecules, such as DNA, confirming that RDC interact with DNA. It also indicates that the luminescent emission of RDC34 and RDC44 present in the extra-cellular compartment versus the intra-cellular compartment may exhibit a good signal/noise ratio allowing to follow the entry and the localization of RDCs molecules into the cells.

We decide to use the intrinsic luminescent properties of RDC34 and RDC44 in order to establish some of the cellular properties of these compounds. To explore the biological properties of RDC34 and RDC44 we investigate their transport and intra-cellular localization using confocal microscopy. Once the drug enters the cell we are interested in the localization of the drug in the cell. Using different labels, we mark different organelles and see if we have co-localization of the drug and the label.

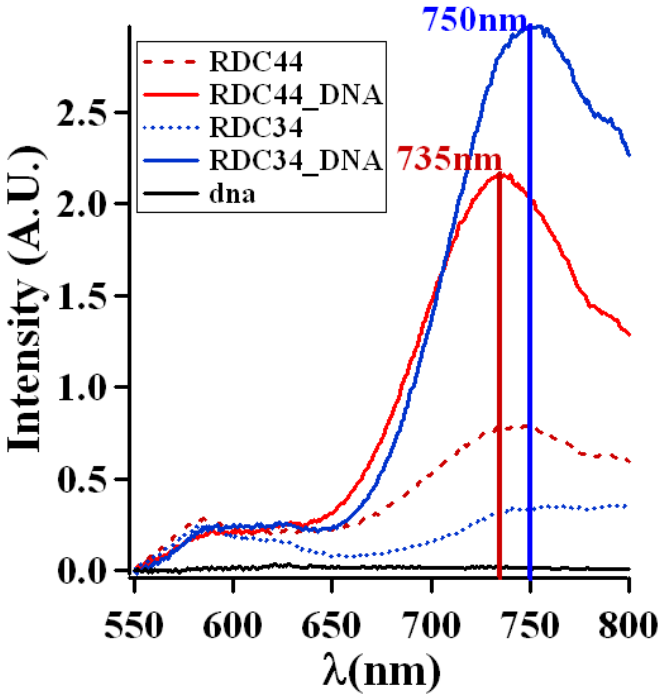

Figure 3.1: Fluorescence properties of RDC34 and RDC44. Fluorescence emission of RDC34 and RDC44 alone or in presence of DNA

Dealing with potentially bio-active compounds implies that the mechanisms of cellular transport and the intra-cellular localizations participate significantly into the biological activity of the compounds. In contrast to the vast variety of the organometallic compounds designed, synthesized and tested on cells or in animals, the data describing the transport and the intra-cellular localization of these organometallic drugs are relatively poor.

3.2 Transport measurements

Molecular transport via cellular membranes is described in biochemical and biophysical books. The reference for description below is chosen from few of them, acknowledged [84–87].

In eucaryotic cells the cellular membrane regulates the transport of molecules into and out of cells. Membranes are dynamic structures in which proteins and lipids diffuse rapidly through the membrane (lateral diffusion), if there are no special interactions restricting it. Although the lateral diffusion of membrane components can be rapid, the spontaneous rotation of lipids from one side of a membrane to the other is a very slow

process. The passage of a molecule from one membrane surface to the other is called transverse diffusion or flip-flop (Figure 3.2).

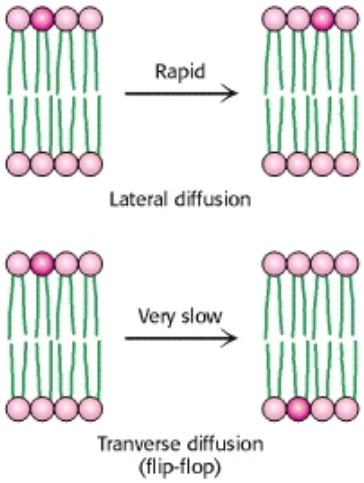

Figure 3.2: Flip-flop is the coordinated transfer of two phospholipid molecules from opposite sides of a lipid bilayer membrane.

Transport across the membrane may be passive, facilitated or active. There are two factors which determine if a molecule crosses a membrane: the permeability of a lipid bilayer and the energy demand.

Most of molecules cannot diffuse across the phospholipid bilayer. The exception are gases (e.g. O_2, CO_2)and small hydrophobic molecules that pass through the membrane by simple diffusion. These small molecules diffuse across a phospholipid bilayer down the concentration or electric potential gradient. The source of energy for the transport proceeding is the gradient itself. No external energy is needed. Higher concentration gradients induce higher diffusion rates, according to Fick's law. If temperature increases, the kinetic energy of system increases and diffusion proceeds faster. Such transport is spontaneous when the positive ΔS value (increase in entropy) overcomes ΔH (the enthalpy change), so that $\Delta G < 0$ (free energy decreases)(Figure 3.3).

In the absence of concentration gradient, molecules are subject to Brownian motion which is the random movement of particles in three dimensions.

On one hand passive ways of transport, such as channels (Figure 3.5), hide the hydrophobic environment of the bilayer to the molecule to be passed through. On the other hand active ways of transport that imply the use of chemical energy exist such as ATP-powered pump or protein transporters(Figure 3.7).

In facilitated diffusion channel proteins (uniporters) support the movement of a specific substrate (some ions, hydrophilic small molecules, hydrophobic larger molecules)

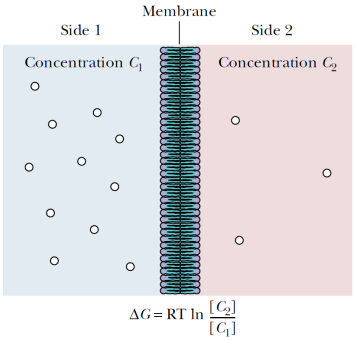

Figure 3.3: Passive kind of transport involves diffusion down the concentration gradient.

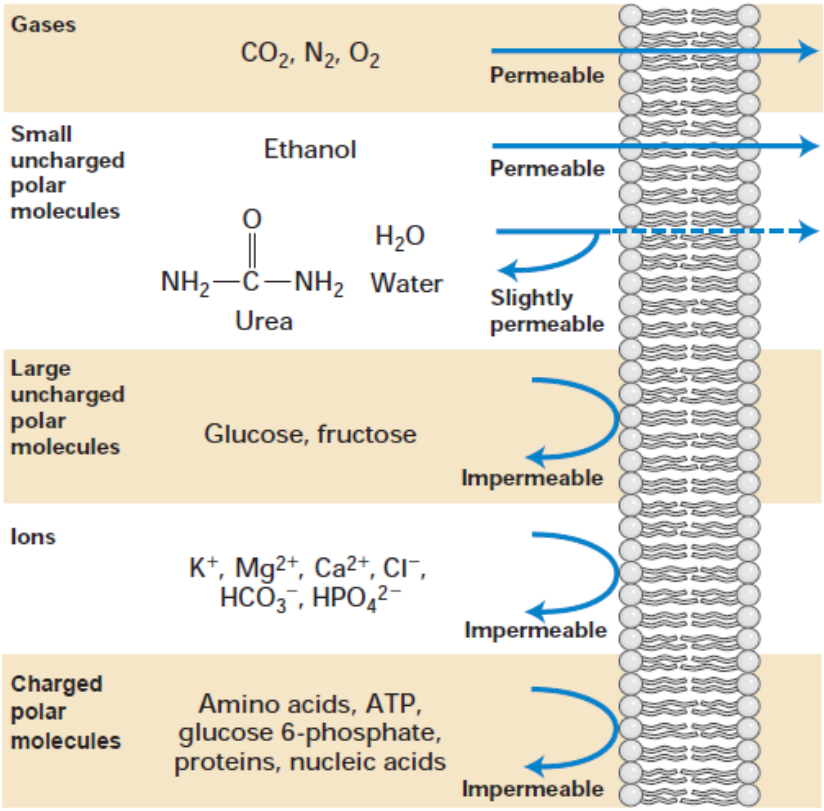

Figure 3.4: In eucaryotic cells the cellular membrane regulates the transport of molecules into and out of cell. Membrane permeability depends on size, hydrophobicity and charge distribution of of molecule.

down its concentration or electric potential gradient. No external energy input is needed. This is a specific kind of transport, uniporters transport only a single species of molecule or a single group of closely related molecules. Transported molecules do not uptake the

cell through the hydrophobic core of the phospholipid bilayer, hence their partition coefficient (hydrophobicity measure) is irrelevant. The rate of facilitated diffusion is higher than of passive diffusion and saturates at high concentration.

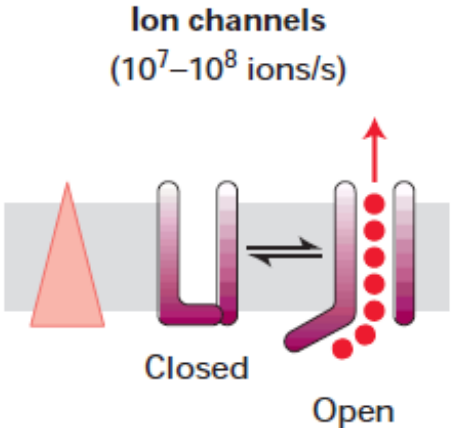

Figure 3.5: Ion channels facilitate diffusion of larger molecules.

Passive diffusion and facilitated diffusion may be distinguished graphically. The plots for facilitated diffusion are similar to plots of enzyme-catalyzed processes (active transport) and they display saturation behavior (Figure 3.6).

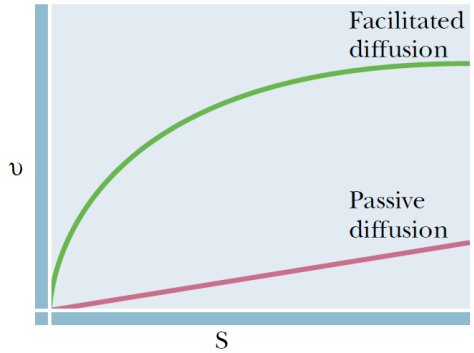

Figure 3.6: Diffusion rate as a function of concentration [87]

In primary active transport, pumps are energy transducers and they convert one form of free energy into another. P-type ATPases and the ATP-binding cassette pumps, two types of ATP-driven pumps, undergo conformational changes on ATP binding and hydrolysis which transports a bound ion across the membrane.

The energy from ATP hydrolysis is used by ATP-powered pumps to move a substrate through the membrane. As facilitated diffusion, it is specific transport with the saturation point of rate which might be inhibited. Most of the enzymes that perform this

type of transport are trans-membrane ATPases. P-type ATPases pump ions against a concentration gradient and become transiently phosphorylated on an aspartic acid residue in the process of transport. P-type ATPases, which include the sarcoplasmic reticulum Ca^{2+} ATPase and the $Na^{+} - K^{+}$ ATPase, are integral membrane proteins with conserved structures and catalytic mechanisms.

The membrane proteins with ATP-Binding Cassette (ABC) domains are complex ATP-dependent pumps. Each pump includes four major domains: two domains span the membrane and two others contain ABC P-loop ATPase structures. For instance these ABC proteins play a role in the rejection of some drugs. Tumor cells in culture often become resistant to drugs that were initially quite toxic to the cells. Remarkably, the development of resistance to one drug also makes the cells less sensitive to a range of other compounds. This phenomenon is known as multi-drug resistance. The multi-drug resistance compounds proteins put the resistance on cancer cells by pumping chemotherapeutic drugs out of a cancer cell before the drugs can take their effects [85].

In a secondary active process a transport proteins (antiporters and symporters) couple the movement of a one type of ion or molecule against its concentration gradient with the movement of one or more different ions down its concentration gradient. These proteins utilize the energy stored in an electrochemical gradient.

Protein-catalyzed transport of a solute across a membrane occurs much faster than passive diffusion, exhibits a maximal velocity V_{max} when the limited number of transporter molecules are saturated with substrate, and is highly specific for substrate.

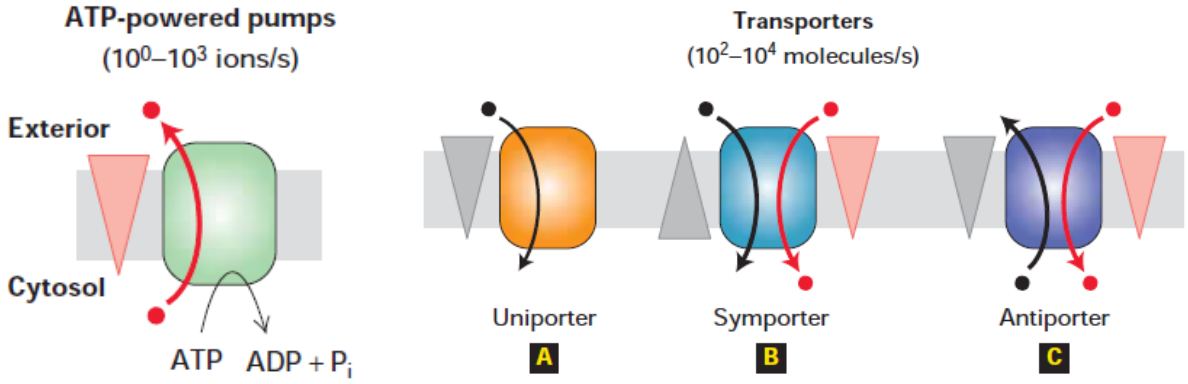

Figure 3.7: In a primary active transport (left) ATP pumps utilize energy from ATP phosphorylation. In secondary active transport (right) different kinds of transporters push molecules across the membrane. They use energy stored in an electrochemical gradient.

If particles are too large to be transported by any of protein ways mentioned above,

endocytosis occurs. In this process cell absorbs molecules from outside by engulfing them with its plasma membrane. In this process, a part of the membrane sinks into a "coated pit," which construction is regulated by a specific set of proteins including clathrin. The pit pinches from the membrane into a small membrane-bounded vesicle containing extra-cellular material and is delivered to an early endosome, a sorting part of membrane-limited vesicles (Figure 3.8). Endocytosis includes three different processes: phagocytosis, pinocytosis and receptor-mediated endocytosis.

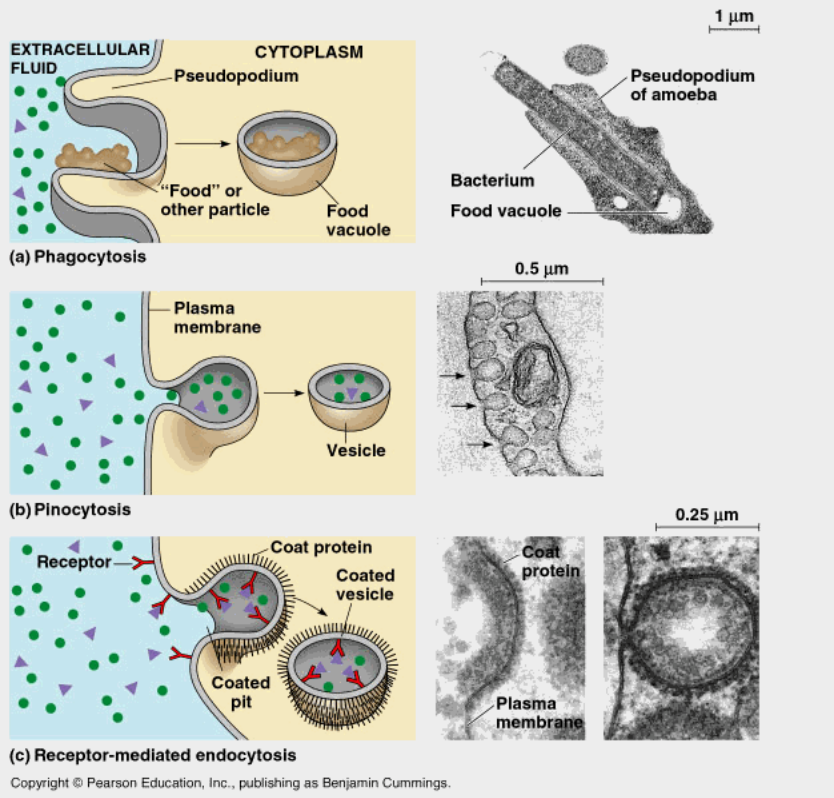

Figure 3.8: If molecules are too large to be transported in primary or secondary active way, cell uptakes them by endocytosis process.

3.2.1 RDC uptake

How are RDCs imported into the cell? And where are they exerting their effect? One of the variant has an overall lipophilic characteristic (RDC34), while the other as a polyamine arm to improve its hydrophilicity (RDC44).

Studies on the transport of these drugs have shown the involvement of multiple mechanisms. Interaction with albumin and transferrin that suggest the use of the iron

transport mechanism transferrin receptor/Ferritin [72]. Other studies performed by Barton's group indicated that passive transport allow ruthenium derived intercalating agent to enter the cells ([73]).

It is reasonable that, thanks to its high lipophilicity, RDC34 may diffuse across the cellular membrane. The hydrophobic character of molecule facilitates passive way of uptake into the cell. Movement of RDC34 down the concentration gradient lets predict passive way of transport.

In case of RDC44, which is more hydrophilic molecule than RDC34, passive way of transport is not so obviously expected. There might be some active mechanisms possibly involved. However its movement down the concentration gradient suggests that diffusion occurs, at least partly.

Bound RDC34 and RDC44 exhibits some changes in fluorescence. We assume that these variations are homogenous across the cellular membrane and do not depend on the possible bindings with some molecules (e.g. proteins) along the way. Therefore the fluorescence intensity variations are expression of RDC concentration changes inside the cell.

Cultivated, alive cancer cells A172 (glioblastoma cells) are placed in PBS buffer. As we checked before, the higher impact of RDCs was registered in PBS than in medium (see Appendix A.4.1). Next cells are imaged with a confocal microscope with an imaging wavelength equal to 488 nm. A two dimensional area of 30x30 μm is being scanned by the confocal microscopy with the 1μm step. The acquisition time of each pixel is 0.05 s. Before any treatment, control image is taken. Then cells are treated with $C_0 = 5$ μM and $C_0 = 10$ μM of RDC34 and RDC44 and being scanned again. Each measurement is performed at room temperature. The signal is collected with a CCD camera that returns the emission spectrum. This spectrum is then divided in ten different parts and integrated over the pixel in ten parts to obtain the fluorescence intensity attributed to a specific wavelength range of 20 nm. We, then, obtain different images from the same cell at different wavelengths. The distribution of fluorescence is obtained for the whole scanned area (inside as well as outside the cell). Obtained image of each full scanning measurement is 30x30 pixels. The color code applied to the images is linearly dependent on the fluorescence intensity. Yellow color is attributed to the highest value of intensity whereas the red one to the lower one. Black color is an expression of the intensity's minimum value which is approximately equal to 2% of the highest one. The same scale of color code was applied to all pictures showing the dependance intensity variations on concentration changes of RDC over time.

Figure 3.9 shows the intensity variation and so that concentration changes in the

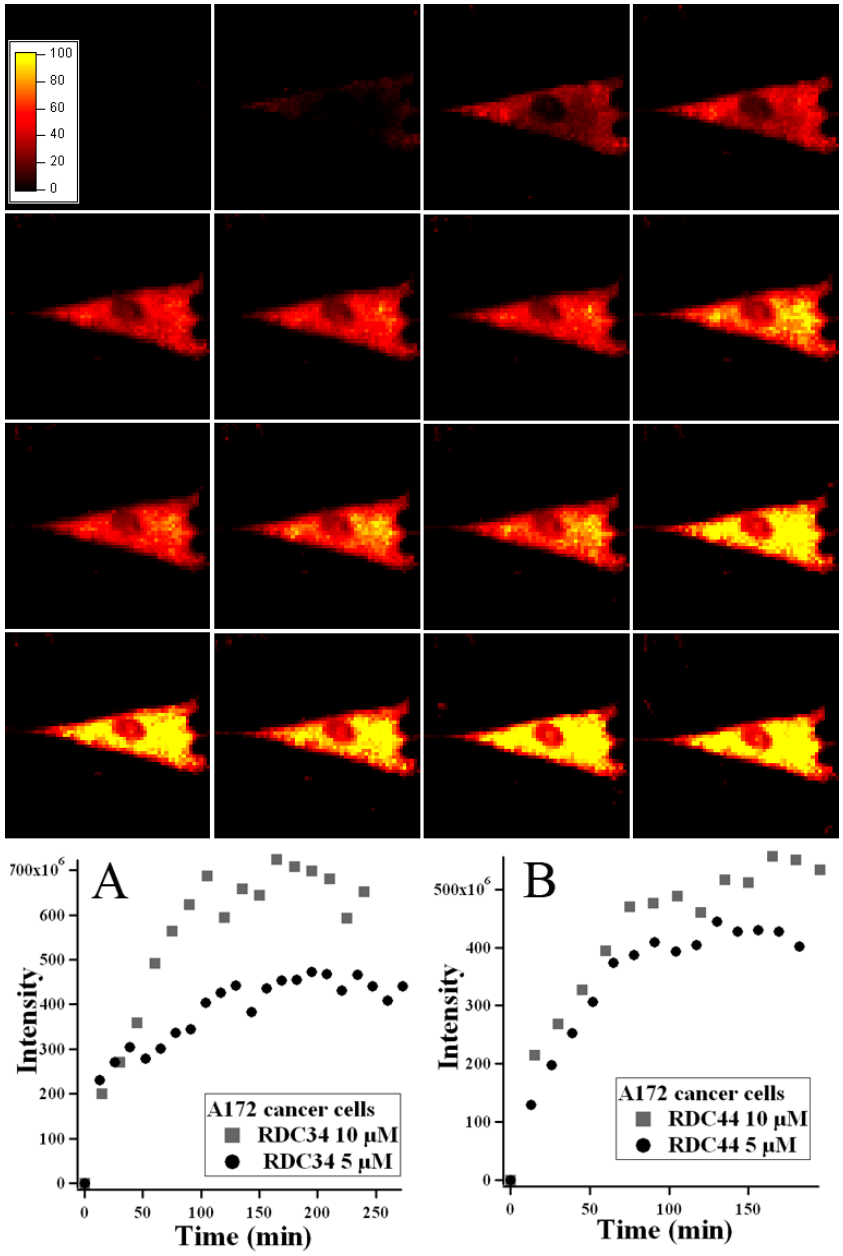

Figure 3.9: Transport identification of RDC34 and RDC44 across the membrane of A172 cancer cell. Two initial concentrations of RDC were introduced to the solution with cells. Then intensity changes over time were measured (Figure A and B).

time course of RDC34 and RDC44 in A172 cells. (A) represents the import of RDC34 at different concentrations, (B) represents the import of RDC44 at different concentrations.

As presented data assumes the shape of exponential function, we decide to fit them with:

$$I = I_0(1 - e^{-(\frac{t}{\tau})}) \tag{3.1}$$

and determine the time constant τ.

Moreover we carry out the same experiment for glial cells and neurons of healthy tissue to perform a comparison between healthy and cancerous cells.

Figure 3.10 shows comparison of different cell lines. A: the normalized intensity of A172 cells in presence of RDC34. B: the normalized intensity of Glial cells in presence of RDC34. C: neuron cells in presence of RDC34. D: A172 cells in presence of RDC44. E: Glial cells in presence of RDC44. The squares represent an outer concentration of product of 10 µM and the circles an outer concentration of 5 µM. The solid lines in all the plots are the fits of the time dependant import adjusted with function of Equation 3.1.

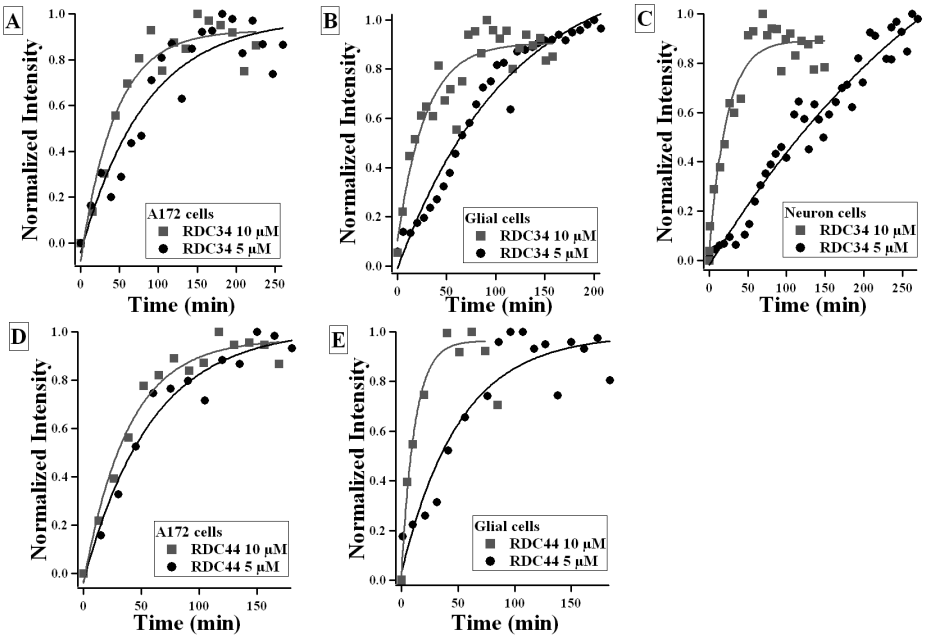

Figure 3.10: Import time course of RDC34 (upper row) and RDC44 (lower row) uptake into different kinds of cells (A172 (left column), glials (central column), neurons (right column)).

Next, time constant τ as a function of $\tau(C_{0_{RDC}})$ of added RDC34 and RDC44 in different cell lines was plotted (Figure 3.11).

The only result we obtain from the fit is value of time constant τ. The value of maximal concentration C_{max} is not found. We can assume that $C_{max} = C_0 = C(eq)$ (concentration in equilibrium) as we have a large reservoir of RDC in comparison to cell

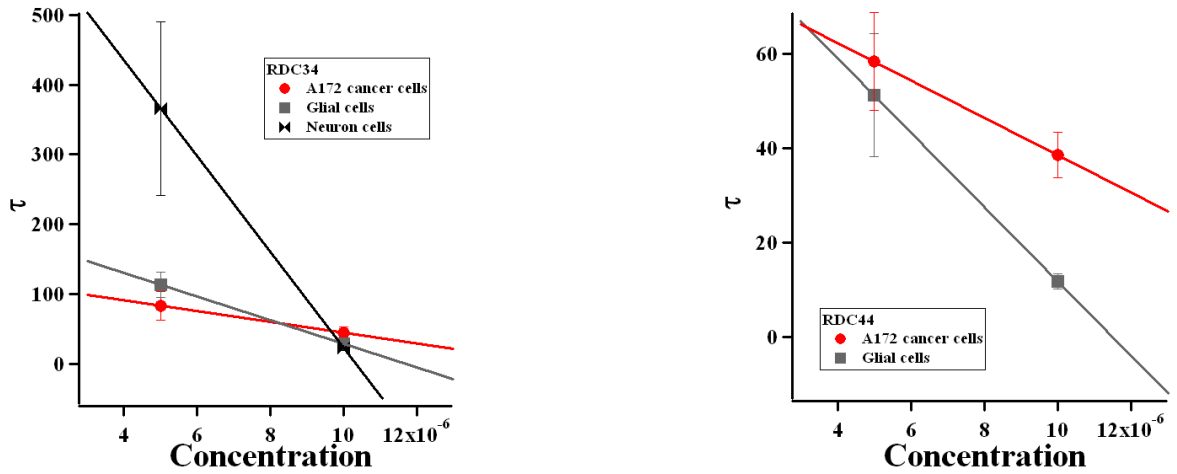

Figure 3.11: Characteristic time of RDC34 (left) and RDC44 (right) uptakes, obtained by fitting experimental data of Figure 3.10 with Equation 3.1.

volume. Results of $\tau(C_{0_{RDC}})$ are shown in Figure 3.11. $\tau(C_{0_{RDC}})$ decreases when C_0 increases. This result is valid for all cell types.

3.2.2 RDC release

For the release, we use the uptake protocol, followed by the replacement of the surrounding environment by fresh PBS, free from RDC.

Figure 3.12 displays release of RDC34 over time in A172 cells (A), in glial cells (B) and in neuron cells (C), and release of RDC44 over time in A172 cells (D) and in glial cells (E). The squares represent a 10 µM concentration, circles represent 5 µM.

The dependence of the characteristic time on initial concentration is shown in the Figure 3.13.

3.2.3 Models of passive RDC uptake

In the first step we find the model of the passive diffusion of RDC across the membrane into the cell and solve the diffusion equation. Second step was to write a chemical equation between inner and outer compartment of the cell separated by membrane.

1. Resolution of the diffusion equation.

If substance moves down its concentration gradient in three dimension in the absence of membrane, the relation between flux and this gradient is linear according to Fick's first law:

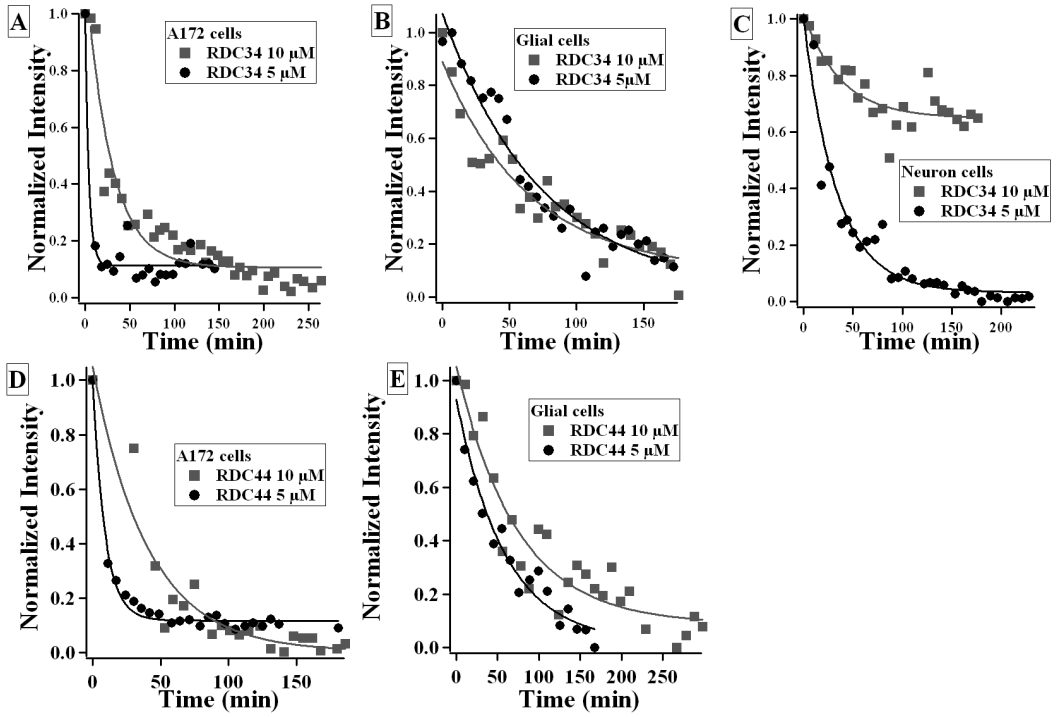

Figure 3.12: Export time course of RDC34 (upper row) and RDC44 (lower row) uptake into different kind of cells (A172 (left column), glials (central column), neurons (right column)).

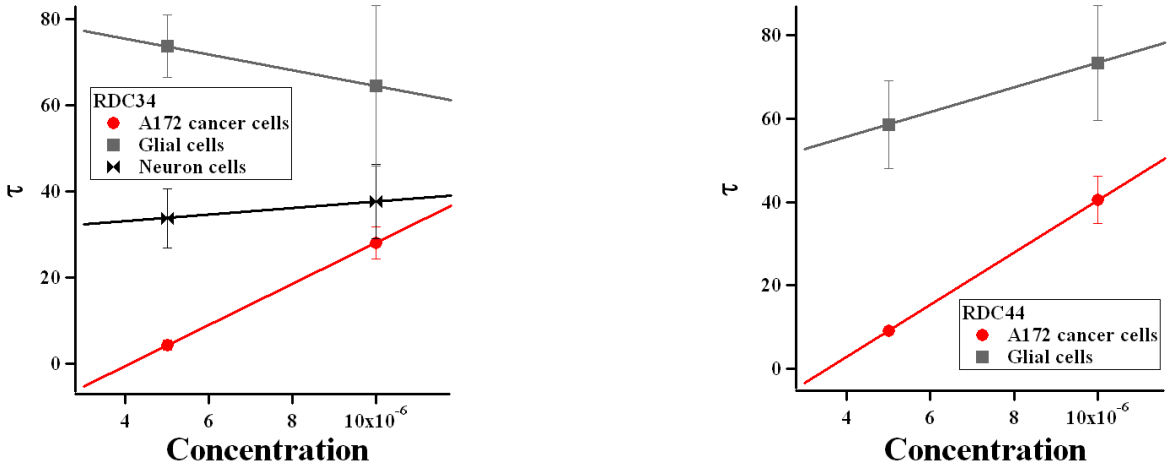

Figure 3.13: Characteristic time of RDC34 (left) and RDC44 (right) releases, obtained by fitting experimental data of Figure 3.10 with Equation 3.1.

$$J = -D\nabla C \tag{3.2}$$

where J is a flux propagated in three dimensions, ∇ is the sum of three spatial derivatives in three dimensions, and C is a substance concentration.

D is a diffusion coefficient and is expressed as:

$$D = \frac{kT}{6\pi\eta r} \tag{3.3}$$

where η is the viscosity of the solvent, r is the radius of the sphere, k is the Boltzman constant, and T is the absolute temperature.

According to the law of conservation of mass:

$$\frac{\partial C}{\partial t} = -\nabla J \tag{3.4}$$

J is eliminated by combining Equations 3.2 and 3.4, so the diffusion equation in three dimensions is:

$$\frac{\partial C}{\partial t} = D\nabla^2 C \tag{3.5}$$

where ∇^2 is Laplacian

$$\nabla^2 = (\frac{\partial^2}{\partial x^2}) + (\frac{\partial^2}{\partial y^2}) + (\frac{\partial^2}{\partial z^2}) \tag{3.6}$$

We need to solve this equation according to some spatial-temporal limits (Figure 3.14).

If we consider the one-dimensional case, for a point like dirac, and initial conditions:

$$C(x, t = 0) = C_0\delta(x) \tag{3.7}$$

the diffusion equation can be solved delivering as a result a Gaussian function:

$$C(x, t) = \frac{1}{\sqrt{2\pi Dt}} e^{-\frac{x^2}{2Dt}} \tag{3.8}$$

In our case solutions with different concentrations are in contact, molecules could diffuse across the cellular membrane. The initial conditions are: $C = 0$ for $x < a$ and $C = C_0$ and for $x > a$. $C_{0_1} = 5$ µM, $C_{0_2} = 10$ µM. Using x' as the center of a point

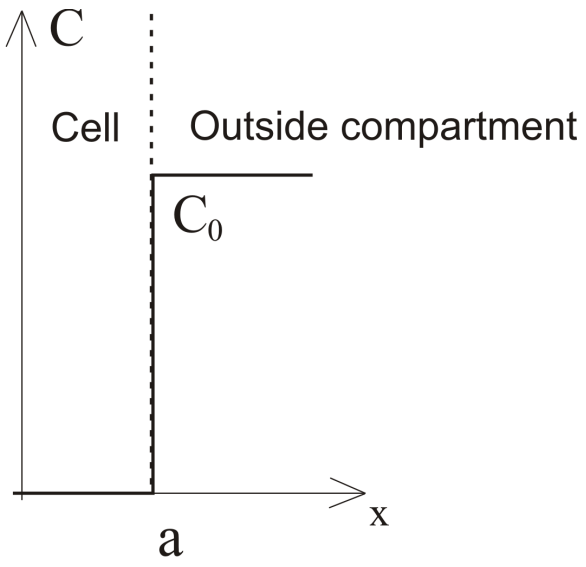

Figure 3.14: Initial state of system

source, and dx' as the distance between adjacent point sources, we obtain $C(x)$ as an integral in the limit of small dx', we can thus write:

$$C(x,t) = \frac{C_0}{\sqrt{2\pi Dt}} \int_a^{\infty} e^{-\frac{(x'-x)^2}{2Dt}} dx' + \int_{\infty}^{-a} e^{-\frac{(x'-x)^2}{2Dt}} dx' \tag{3.9}$$

Let's change the integral into form called the complementary error function:

$$erfc(x) = \frac{2}{\sqrt{\pi}} \int_x^{\infty} e^{-y^2} dy \tag{3.10}$$

and variables expressed as:

$$\frac{(x'-x)}{\sqrt{2Dt}} \tag{3.11}$$

One dirac located at x, integration over the initial conditions gives:

$$C(x,t) = \frac{C_0}{2}(erfc\frac{a-x}{\sqrt{2Dt}} + erfc\frac{a+x}{\sqrt{2Dt}}) \tag{3.12}$$

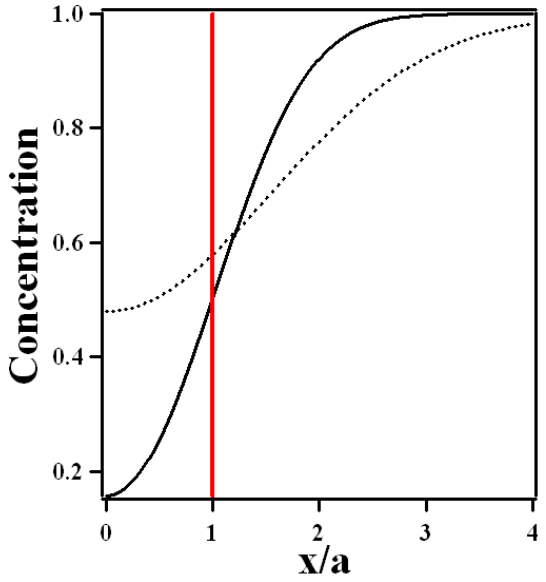

Figure 3.15: Concentration inside ($x < a$) and outside ($x > a$) the cell at times: $\frac{2Dt}{a^2} = 0$ (red), $\frac{2Dt}{a^2} = 1$ (solid curve) and $\frac{2Dt}{a^2} = \frac{1}{2}$ (dotted curve)

whose graphic representation is shown on Figure 3.15.

However we measure the total intensity, not the local one. Therefore:

$$C_{tot}(t) = \int_{-a}^{a} C(x,t)dx \tag{3.13}$$

$$C_{tot}(t) = \frac{C_0}{2a}\left(a + e^{-\frac{2a^2}{Dt}}\left(-1 + e^{\frac{2a^2}{Dt}}\right)\sqrt{\frac{2}{\pi}}\sqrt{Dt} - \frac{a\sqrt{Dt}\mathrm{erfc}\left[\frac{\sqrt{2}a}{\sqrt{D\sqrt{t}}}\right]}{\sqrt{Dt}} + a\mathrm{erfc}\left[\frac{\sqrt{2}a}{\sqrt{Dt}}\right]\right) \tag{3.14}$$

that is plotted on the graph 3.16.

$\frac{C_{tot}(t)}{C_0}$ is a universal function of $\frac{Dt}{a^2}$ but does not depend on C_0. Therefore it is not consistent with our data.

2. Chemical kinetic approach.

We write a chemical equation between RDC concentration inside the cell (A) and outside the cell (B):

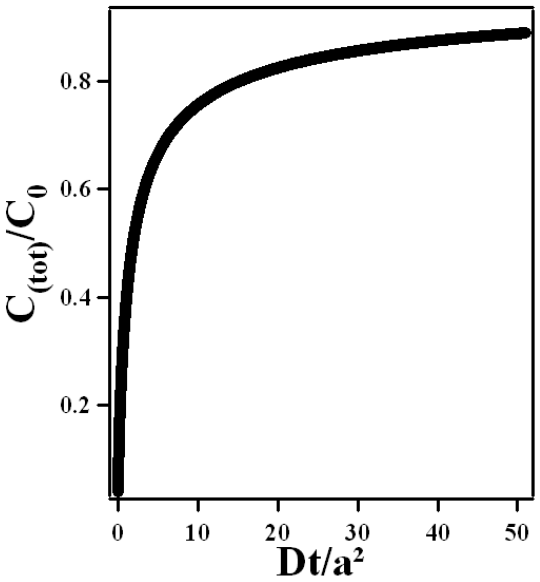

Figure 3.16: Total inner concentration of RDC as a function of reduced time $\frac{Dt}{a^2}$

$$A \underset{k_i}{\overset{k_o}{\rightleftharpoons}} B \tag{3.15}$$

k_o (resp. k_i) is the kinetic constant of RDC leaving the cell (resp. entering the cell). We assume that that the kinetics may be described with:

$$\frac{d(A)}{dt} = k_i(B) - k_o(A) \tag{3.16}$$

$$\frac{d(A)}{dt} = k_i C_o - k_i A - k_o(A) \tag{3.17}$$

which has to be solved with the initial condition $A(t=0) = 0$

$$A(t) = \frac{k_i}{k_i - k_o} C_0 (1 - e^{-(k_i - k_o)t}) \tag{3.18}$$

The representation of Equation 3.18 is plotted in Figure 3.17. k_i and k_o values are chosen and are equal to 1 and 0.5 respectively. Again $\frac{A(t)}{C_0}$ is independent on C_0.

As it is shown, passive models do not work with our data. We need a model which

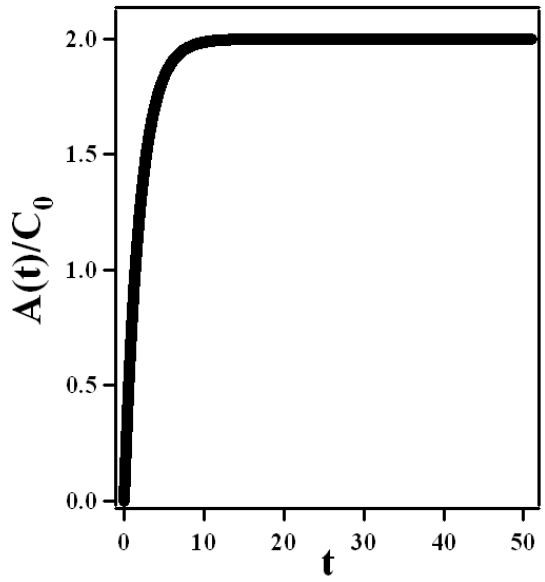

Figure 3.17: Evolution of total inner concentration as a function of time (Equation 3.18) for $k_i = 1$ and $k_o = 0.5$

includes some possible current that do not linearly depend on diffusion coefficient.

When RDC34 or RDC44 enters cells it binds to DNA, RNA or proteins and begins to fluoresce. We have used this property to measure the kinetics of uptake of these RDC inside cells. We observed that of uptake fastens when the outside concentration increases which is contradictory with passive diffusion models. We must assume that active mechanisms are involved in RDC all uptakes. In the next section we examine the role of different compounds that may take part in active cellular transport.

3.2.4 Mechanisms of active transport

As previously said, active transport may utilize ATP-dependent pumps (primary) or variety of transporters (secondary) to push molecules across the cellular membrane in the right direction (down or against their concentration gradient). We decide to examine both kinds of active transport.

1. Blockage of ATP energy source

In order to understand the mechanisms of primary active RDC cellular import, we test inhibitors of ATP synthesis to discriminate between passive and active mechanisms. We treat the cells with oligomycin and 2-deoxy-D-glucose classically used to inhibit ATP synthesis and therefore block active import mechanisms (ATP-dependent pumps).

A172 cells are pre-treated for 1 hour with oligomycin (5 μM) and 2-deoxy-D-glucose

(50 mM) and then treated for 1 hour in room temperature with RDC34 at the four indicated concentration (1, 2.5, 5 and 10 μM). The same concentrations of RDC34 are used to prepare control samples, untreated with ATP-synthesis inhibitors. Cells are fixed by paraformaldehyde and RDC34 intra-cellular luminescence is measured. Next, comparison between treated cells and controls is performed.

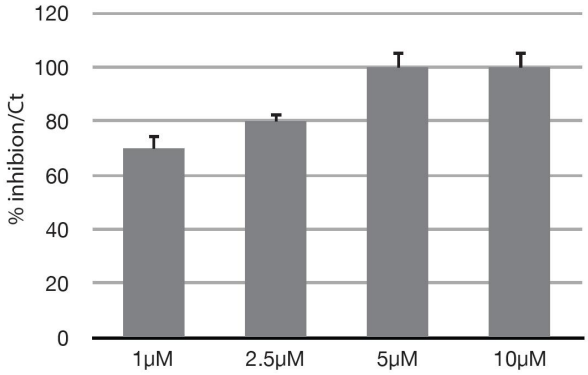

Figure 3.18: RDC34 uses active mechanisms to enter the cells: inhibition of RDC import by oligomicyn and 2-deoxy-D-glucose. import.

Figure 3.18 shows the inhibition of RDC import by oligomycin and 2-deoxy-D-glucose. As shown, the percentage of active import mechanism involved in RDC accumulation increases when the concentration of RDC34 applied to the cells diminished bellow 5μM. At 1μM, 30% of the import is mediated by a mechanism dependent on ATP synthesis.

2. Increase of concentration of iron transporters

To examine the secondary active transport we use the specific transporters supporting a passage through the membrane. Transferrin is a blood plasma protein for iron transport. A documented mechanism of import for ruthenium-derived compound is through the transferrin receptor as ruthenium is of the family of iron and is supposed to be able to mimic it [71, 72]. Therefore we test how deferoxamine, an iron chelator, would affect RDC import.

A172 cells are pre-treated for 1 hour with deferoxamine (200 μM) and then treated for 1 hour with RDC34 at the the same indicated concentrations as previously in ATP-pumps blocking. We again fix the cells by paraformaldehyde and measure luminescence of RDC34 inside the cells. Next we compare intensities of deferoxamine treated samples and controls.

Figure 3.19shows the effect of deferoxamine on RDC import. We observe that de-

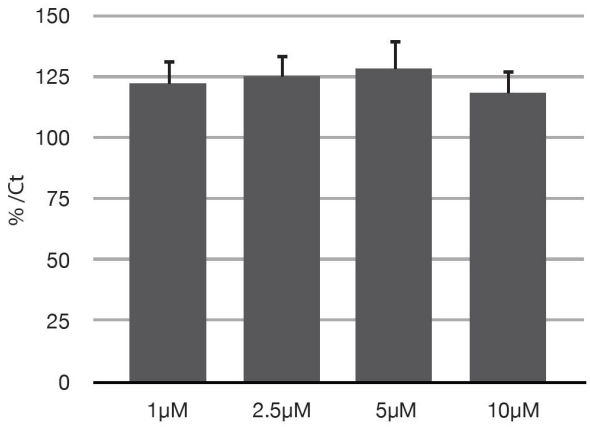

Figure 3.19: RDC34 uses secondary active transport to enter the cells: effect of deoxyferoxamine on RDC import.

feroxamine increases by 25% the accumulation of RDC34 inside the treated cells in comparison to controls, suggesting, that chelation of iron from the medium favored the import of RDC.

3.3 Colocalization observation

As we know that RDC enters the cell we are interested in which organelles it prefers to locate in. As already described in chapter 2, performing FRET and optical trap experiments, RDC interacts with DNA, thus we expect to find RDC in organelles containing DNA: nucleus and mitochondria. Based on previous work showing that one of the RDCs (RDC11) induces an endoplasmic reticulum stress response [3] (ER stress response), we hypothesize that RDC34 and RDC44 could preferentially localize in this organelle and also induce an ER stress response. As the ER contains a concentration of RNA associated to the ribosomes, we check whether RDC34 and RDC44 display increase of luminescence when interacting with RNA. Indeed it does, however the increase of intensity in comparison to non-interacting RDC is $\simeq 44\%$ (Figure 3.20 E), whereas, when interacting with DNA, the increase is much larger ($\simeq 1100\%$, Figure 3.1). Nevertheless, indication, that RDC interacts with RNA, lets us expect some RDC concentration inside the nucleolus where ribosomal RNA is transcribed and assembled.

We then use dyes of specific cellular compartments to localize the sub-cellular concentration of the organometallic compounds. We decide to stain organelles which affinity with RDC is expected: nucleus, mitochondria, ER and nucleolus.

Alive glioblastoma cancer cells A172 are taken out from cullular medium (see section A.4.1) and placed in PBS buffer. The entrance and localization of RDC luminescence is followed by confocal microscopy on single cell treated with 5 μM RDC34 or RDC44. This dose of RDC34 is equal to IC50 (the half maximal inhibitory concentration) allowed maximal cytotoxic effects *in vitro*. All the different labels used in these experiments are purchased from Invitrogen Company and are referenced in the appendix (see section A.5). The cells are prepared following the protocol given by the manufacturer. Then, we wash the cells and fix them using paraformalaldehyde or methanol depending on the label used. Nucleus staining is performed on permeate fixed cells, whereas the rest three are used on alive cells. Next, we attach cells on microscopic basic slip and place them under the microscope.

Samples are being scanned with the same settings as in the case of kinetic studies. The color code of images is applied depending on wavelength of stain emission. White color of any dye is attributed to the highest value of intensity. In the case of mitochondria and ER and nucleolus dyes, green color corresponds to high intensity, whereas blue in nucleus to lower one. RDC concentration is coded by a yellow (high values)-red (low values) color code. Black color is an expression of the intensity's minimum value in all of the pictures.

We observed a strong luminescent emission caused by RDC34 inside the cells (Figures 3.20A and B) and a much weaker emission for RDC44 (Figures 3.20C and D). Interestingly, the highest emission for both compounds gathers around the nucleus. As shown in Figure 3.20, there is a good correlation between the localization of the ER-tracker dye (Figures 3.20A and C) and the luminescence of RDC34 or RDC44 (Figure 3.20B, D). Indeed, the luminescence of both compounds increases upon interaction with RNA, even if it is in a reduced manner. The interaction between RDC and RNA can explain the ER localization. The physical and functional relationship between RDC and ER, are next confirmed by biologists. Performing Western blots, analogous to [3], they show, that RDC34 increases strongly the protein level of the ER stress response protein CHOP (Figure 3.20F). RDC44 does not affect significantly CHOP expression, which could be explained by a poor ability of RDC44 to enter cells (Figure 3.20D). This set of experiments confirm that RDC molecules have a physical and functional relationship with the ER.

To further investigate the sub-cellular localization of RDC34 and RDC44, we perform colocalization experiments with dyes specific for the nucleus, the nucleolus and the mitochondria. Images of RDC44 display again an inability of RDC44 to enter the cell, thus they are not presented. We observe that part of the RDC34 may be local-

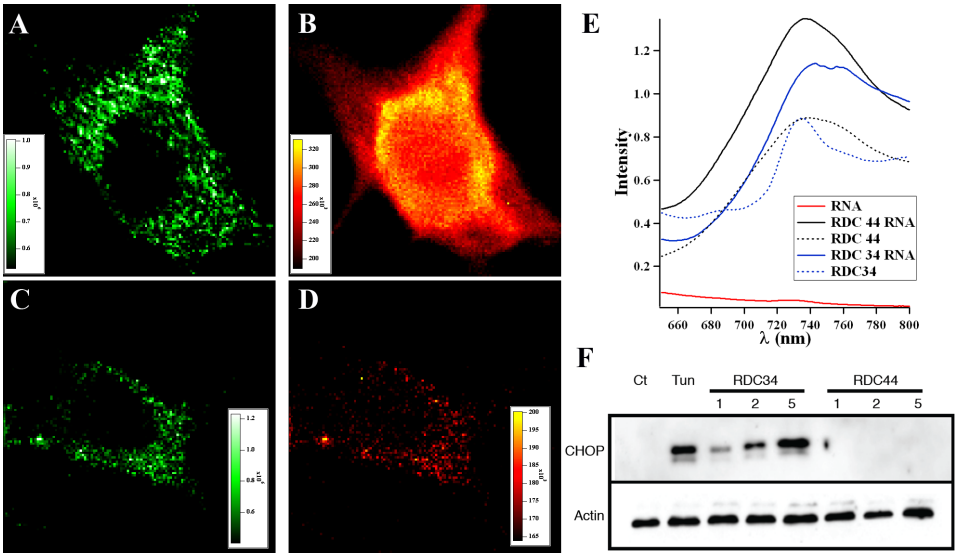

Figure 3.20: Staining of endoplasmic reticulum inside the cell (Figures A and C). Sub-cellular localization of RDC34 and RDC44 in the endoplasmic reticulum (Figures B and D). Luminescent features of RDC34 and RDC44 bounded to RNA (Figure E). Western blots of CHOP protein (Figure F).

ized inside the nucleus as shown on Figures 3.21A and B. The localization of RDC34 in the nucleus is not surprising as it is previously showed that RDC molecules interact with DNA (Figure 3.1), and induce a DNA damage response [3]. It is confirmed that RDC34 (and RDC44 in a lesser extent) induce a DNA damage response as indicated by the phosphorylation of histone pH2AX (Figure 3.21G). However, there is a serious impact of nucleus stain intensity on the measured intensity of RDC. Emission spectrum of Propidium Iodide (PI) partly covers the maximum of RDC emission (in approximately 22% of maximal emission value of PI). As a result of that inside the nucleus where we can expect the highest concentration of dye, its intensity is a part of RDC intensity in around 44%. In the part of cell, where the highest intensity of RDC is measured, that influence is around 17%.

The co-localization studies reveal also that some RDC34 molecules may localize in the mitochondria (Figure 3.21C and D). However these results cannot be interpreted explicitly. As it is shown in Figure 3.21D, mitochondria are everywhere except the nucleus, but they are not the only objects so widely spread inside the cell. Therefore even if we find some RDC intensity in the same area, the correlation cannot be shelled. Again the highest intensity is observed around the nucleus so it is reasonable to think that the highest concentration of RDC is in endoplasmic reticulum. Altogether these studies indicate that RDC34 localizes in various intra-cellular compartments eliciting

diverse cellular responses. We are not able to assess reliably the localization in the nucleolus, as the nucleolus specific dye alters RDC34 luminescence (Figure 3.21E and F). Emission of mitochondria, ER and nucleolus stain do not have any influence on measured RDC fluorescence intensity.

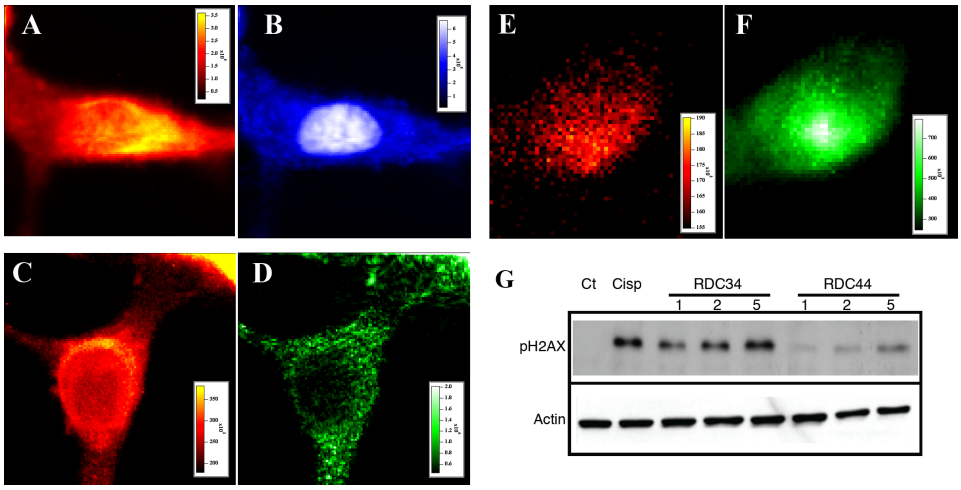

Figure 3.21: B, F, D: images of 3 different A172 cells stained with a nucleus dye (B), a nucleolus dye (F), and a mitochondria dye (D). Corresponding images if RDC34 in the cells are given in A, E and C. Figure G presents Western blots of pH2AX.

Chapter 4

Conclusions and Perspectives

4.1 State of the art

Ruthenium Derived Compounds (RDC) as anti-cancer agents are not a new idea [22, 55, 62]. Many of them have already been created [55]. The main concept was to use ruthenium as a non-toxic transporter of organic ligands, hydrolyzed from ruthenium inside the cell, as interacting groups with biological molecules. Ligands attached to ruthenium atom by metal-nitrogen (chloride, sulfur) coordination bond have been studied and it has been shown that they disrupt easily. As a consequence the local charge of metal increases, which causes it more attractive to negatively charged biomolecule. Electrostatically attracted metal ion may weaken ligands' interaction [4]. Thus RDC compounds with Ru-C bond are now synthesized and studied as anti-cancer agents [4, 63]. Indeed, Ru-C is stronger (covalent) than Ru-N bond and ligands' disruption is not expected.

Before my PhD thesis started it had already been shown that one of the RDC created according to that idea, RDC11, reduces the speed of tumor growth, in comparison to the untreated tumor, as efficiently as cisplatin. That proved anti-cancer features of RDC11. These were very promising results, especially that examination of chronic toxicity (loss of weight) and neurotoxicity (conductivity speed of nerves) came out much better in comparison to cisplatin. However, it revealed the acute toxicity comparable to that one caused by cisplatin. Looking for similarities and differences between cisplatin and RDC, biologists tested *in vitro* RDC11 interacting with DNA, the main target of cisplatin. Results revealed DNA damages caused by RDC11.

4.2 Results of our work

As anti-cancer activity of RDC11 and interaction with DNA were revealed, questions have been raised. Identifying the exact molecular mechanisms involved in RDC action became a main field of interest. DNA was assumed to be the main target of RDC at molecular scale. It was expected that ligands played a key role in the interaction, and as a consequence, that different RDCs' structures possess interaction properties with DNA. Apart from that, the RDC behavior in more physiological environment was interesting to investigate, due to the fact that the potential target of any chemotherapeutic drug is much more complicated that just molecules in saline solvent. Therefore explanation of how RDC enters and penetrates the cellular environment seemed to have a crucial meaning for understanding its mode of action as a biomolecule.

This PhD focused on three structurally different RDCs in these two aspects: molecular and cellular scale. The ligands were modified on purpose in order to modify the structure of the RDC-DNA complex. Optical methods allowed us to measure the affinity of each RDC-DNA complex *in vitro*. It was found that all of the RDC studied, exhibited a strong affinity to DNA, much stronger than to that of cisplatin. Then, using the optical trap I measured the structure of the complex and showed that the ligands linked to ruthenium change the structure of RDC-DNA compound; either groove binding or intercalation between base pairs may be obtained. Research on RDC behavior in cellular environment enabled us to show that an active transport mechanism is involved in the process of RDC uptake by cell. Nevertheless the exact molecular mechanism has not been determined.

Although it was confirmed by localizing RDC inside the cellular nucleus, where most of the DNA is stored, we discovered that the most preferable compartment of cell where RDCs are located is endoplasmic reticulum (ER), from which DNA is absent. However, some amount of RNA is present in endoplasmic reticulum. It is reasonable then to verify the previous assumptions as DNA being the main target of RDC. Obtained results showed that inside the cell RDC prefers to bind to RNA rather than to DNA.

4.3 Perspectives

The chemical structure of RNA is similar to DNA structure with two differences: RNA contains the sugar ribose while DNA contains deoxyribose (a type of ribose that lacks one oxygen atom), and that RNA contains uracil instead of thymine present in DNA (uracil and thymine have similar base-pairing properties). Besides RNA exists mostly in

a single-strand form which causes RNA to be much less stable in comparison to DNA. Despite the fact that structural differences are not large, they change the chemical properties of both molecules significantly [85].

Treatment of RNA with RDC may have an important biological meaning. It has already been referred that the same factors causing damages in DNA, also damage RNA [68]. Moreover it was shown that if the damage to RNA is substantial, apoptosis is induced, which is the desired affect of anti-cancer chemotherapy.

Oxidation damage induced in RNA has a destructive impact on cellular function since the damaged RNA pieces are performing translation (rRNA and tRNA) or coding for proteins (mRNA) [67]. It is notable that studies on some anti-cancer agents show that RNA damage leads to cell-cycle inhibition and cell death, as strongly as DNA does. RNA damage may cause cell's death via pathway involving either p53-dependent mechanism associated with inhibition of protein synthesis or p53-independent mechanism different from inhibition of protein synthesis. Until recently, the knowledge about consequences and cellular handling of the RNA damage has no been sufficient. However, the number of new evidences of detrimental effects of the RNA damage to protein synthesis and the existence of several coping mechanisms including direct repair and avoiding the incorporation of the damaged ribonucleotides into translational machinery, increases. Further investigations toward understanding of the consequences and cellular handling mechanisms of the oxidative RNA damage may provide significant insights into the pathogenesis and therapeutic strategies of cancer.

RNA is not a perfect copy of DNA which it is transcribed on. RNA in cell reveals what genes (DNA) are active in that cell. Not all of the genetic material stored in the DNA has well defined functions. Some of the DNA's segments do not code any specific genes whereas RNA is a "working copy" of DNA's contents indicating the switched on functions. Thus, an agent affecting RNA as effectively as DNA is more probable to cause the significant RNA damage inside the cell. Hence rather than researching the entire DNA sequence, quantifying interactions of RDC with just the operating parts coded in the RNA seems to be more important.

Appendix A

Sample preparation protocols

A.1 Drugs

Ruthenium derived compounds were prepared by the group of chemists following their protocols. Condensation of phenylpyridine on $Ru(phen)_2Cl_2$ leads to $[Ru(phen)_2PhPy](CF_3SO_3)$ RDC34 with a 87% yield. $Ru(phen)_2(Boc_3SperNic)](SO_3CF_3)$ was obtained through coupling reaction between (N1,N4,N9-tri-tert-butoxycarbonyl)-1,12-diamino-4,9-diazadodecane and 6-phenylnicotinic acid (yield 95%), followed by condensation with $Ru(phen)_2Cl_2$ (yield 78%). Deprotection by TMSOTf leads to $[Ru(phen)_2(SperNic)](SO_3CF_3)$ RDC44 with a yield of 80%. The compounds were characterized by ^1H and ^{13}C NMR and HRMS.

RDC34, and RDC44 were synthesized at the Institute of Chemistry, University of Strasbourg in the Laboratory of Metal-Induced Chemistry and were not previously reported. For *in vitro* studies RDC34 was dissolved in dimethyl sulfoxide (DMSO) whereas RDC44 is soluble in water. Both of them are dissolved in the proper solvent to 1 mM final concentration. Water was purified by a water purification system.

A.2 DNA/RDC for FRET

The measurements were performed with 15 base pair double stranded DNA. Number of DNA base pairs is limited by the range over which the energy transfer can take place that is approximately 10 nm (100 Å). Complementary strands were purchased from IBA NAPS(Gmbh) with sequences: GGA GAC CAG AGG CCT and AGG CCT CTG GTC TCC. We chose this sequence because it had been previously used in cisplatin activity studies [11]. The length of 15 base pair DNA equal to 5.1 nm is small enough to stiffen

the DNA structure. Thus any unexpected bends are not supposed to appear.

The first sequence was 5 labeled with Alexa488 and 3 labeled with Alexa568. The distance at which this fluorophores pair undergoes 50% energy transfer, R_0, for these pair of fluorophores is $R_0 = 62$ Å [98].

Two strands were resuspended to a final concentration 8.3μ M in Tris-HCl (pH 8.0 at 25 °C) and KCl of 1 mM each. Next they were annealed by heating the DNA to 94 °C before cooling down the sample to 16 °C for 20 minutes. All of the measurements were performed at 20 °C to ensure the DNA remained fully annealed. To perform experiments of salt dependance, DNA was diluted in NaCl. The salinity have been increasing from 1 mM to 200 mM.

A.3 DNA/RDC for optical trap

An EcoRI linearized pBR322 plasmid is labeled with biotin or digoxigenin. We obtain two differently labeled types of DNA and apply to each of them a HindIII restriction. We purify this restriction product to keep only the 4.3 kb DNA. A final ligation between the two different DNA types leads us to a 50% concentration of a pBR322 dimer co-labeled with biotin and digoxigenin 9.6 kb long. This length is very suitable to single molecule measurements. Is large enough to observe all of the structural changes of dsDNA and small enough to avoid needless artefact. A first incubation with 1 mm streptavidin beads, followed by a second with an anti-digoxigenin coated coverslip results in the assembly of a molecular jokari. Initially coated with aminosilane, the coverslips are additionally treated with glutaraldehyde. It is followed by an anti-digoxigenin incubation. To prevent non-specific binding we finally use Bovine Serum Albumin. All experiments are performed at 20 °C, and the incubation of all the chemicals done in PBS1X. Once the DNA ends are attached to the surface, we perform the required buffer exchanges through a flow chamber.

A.3.1 Labeling of DNA with Biotin and Digoxigenin

Protocols are given by the enzyme's (Fermentas) or particles (Roche) manufacturer.

∝ Perform a restriction by EcoRI on the pBR322:

- ⋆ 10 μl of pBR322 Vector (BioLabs)
- ⋆ 2 μl of 10X FastDigest® Buffer
- ⋆ 5 μl of FastDigest® EcoRI Enzyme (Fermentas)
- ⋆ 3 μl of water

- incubate in 37 °C for 5 min,
- stop the enzyme activity 80 °C for 5 min,
- purify by QIAquick PCR Purification Kit (QIAGEN), receive 60 µl of DNA,
- divide into two tubes, 30 µl each.

∝ Perform labeling by biotin and digoxigenin with Klenow exo enzyme:

⋆ 30 µl of restricted pBR322
⋆ 12 µl biotin (1 tube) and digoxigenin (2 tube) (Roche Applied Science)
⋆ 6 µl of 10X Reaction Buffer
⋆ 3 µl of Klenow Fragment, exo$^-$ (Fermentas)
⋆ 9 µl of dNTP mix:

1 µl of C (BioLabs)
1 µl of A (BioLabs)
1 µl of G (BioLabs)
97 µl of water

- incubate in 37 °C for 15 min,
- incubate in 70 °C for 20 min,
- purify each tube by QIAquick PCR Purification Kit (QIAGEN), receive 30 µl from each tube.

∝ Prepare sharp edges for ligation:

⋆ 30 µl of pBR322 with biotin or digoxigenin
⋆ 4 µl of 10X FastDigest® Buffer
⋆ 2 µl of FastDigest® HindIII Enzyme (Fermentas)
⋆ 4 µl of water

- incubate in 37 °C for 5 min,
- stop the enzyme activity in 70 °C for 10 min,
- purify each tube by QIAquick PCR Purification Kit (QIAGEN), receive 30 µl from each tube,
- mix both tubes together.

∝ Perform ligation:

⋆ 60 µl of pBR322 labeled by biotin and digoxigenin
⋆ 8 µl of 10X T4 DNA Ligase Buffer
⋆ 2 µl of T4 DNA Ligase Enzyme (Fermentas)

- incubate in 16 °C overnight,
- stop the enzyme activity in 70 °C for 10 min,
- purify each tube by QIAquick PCR Purification Kit (QIAGEN).

A.3.2 Treatment of cover slips

∝ Wash the cover slips for 15 min in ultrasonic bath in the solution:

⋆ 27 ml of sulfuric acid (96%)
⋆ 13 ml of hydrogen peroxide

- wash them with water and next with ethanol,
- dry them by nitrogen.

∝ Perform the silanization by incubating the cover slips for 1 h in the solution:

⋆ 1 ml of N-(3-trimethyloxysilylpropyl)diethyl enetriamine (Sigma-Aldrich)
⋆ 45 ml of ethanol
⋆ 4 ml of water

- wash cover slips in chloroform for 15 min in ultrasonic bath,
- dry them by nitrogen.

A.3.3 attachment of DNA onto cover slips and particles

⋆ 10 µl of DNA
⋆ 5 µl of streptavidine coated beads
- mix together and incubate for 2 h in the fridge.

⋆ 225 µl of glutaraldehyde (50% Electron Microscopy Sciences)
⋆ 25 µl of PBS10X
- mix together and suck into the cell by syringe,
- incubate for 30-40 min in a room temperature,
- wash by PBS1.

⋆ 10 µl of Anti-Digoxigenin (50 mg/ml, Roche)
⋆ 190 µl of PBS1

- mix together and suck into the cell by syringe, incubate for 1 h in a room temperature,
- wash by PBS1.

⋆ 2% of Bovine Serum Albumin (in solvent PBS1X)

- suck into the cell by syringe,
- incubate for 1 h in a room temperature,
- wash by PBS1.

⋆ solution of DNA with beads

⋆ 500 µl of PBS1

- mix together and suck into the cell by syringe,
- incubate for 1 h in a room temperature (increasing the incubation time increases the number of beads anchored to the glass surface),
- wash by PBS1,
- wash by water.

A.4 Cellular sample for kinetic measurements with confocal microscopy

A.4.1 Cell culture

A172 human glioblastoma cell line were obtained from ATCC. Cells were maintained in DMEM with 10% FCS and 1% penicillin/streptomycin (called later cellular medium) in incubator (37C; 95% air + 5% CO2), and trypsinized every 3-5 days.

For microscopy observation and measurements cover slips sterilized by ethanol were coated by Poly-L-Ornithine (PO) to adhere cells onto coverslips surface. Coating of each coverslip was performed by 500 µl of the filtered PO solution for 1 h in 37 °C, and further, washing by pure water. A172 cell culture grown for 48 h in Petri Dish with 12 ml of medium in 37 °C with 5% of CO_2 environment saturation were detached from the bottom by 1.5 ml of Trypsin. Trypsin activation was arrested by introduction 2 ml of medium. Around $20 \cdot 10^6$ cells were next suspended in 30 ml of medium containing serum and antibiotic.

Cells were plated in 24 well plates (500 µl of cellular medium in each well) and allowed to recover for 24 h in 37 °C with 5% of CO_2 saturation. 12 ml of culture medium were introduced to the new Petri Dish to keep the cell culture.

A.4.2 RDC uptake

Already recovered, on coverslips, cells were divided for two fractions. In one of them, medium was replaced by 500 µl of filtered and prewarmed to 37 °C PBS1x. Following all of the cells (both in cellular medium and in PBS1x) were treated by 2.5 µl of 1 mM of RDC34 or RDC44. The final concentration of RDC in each well was 5 µM. Cells with RDCs were incubated for 40 min in 37 °C. It occurred that cellular medium prevents RDC from penetrating cellular membrane. Almost no effect is visible in medium environment A.1. Therefore we decide to perform all our experiments in PBS1x.

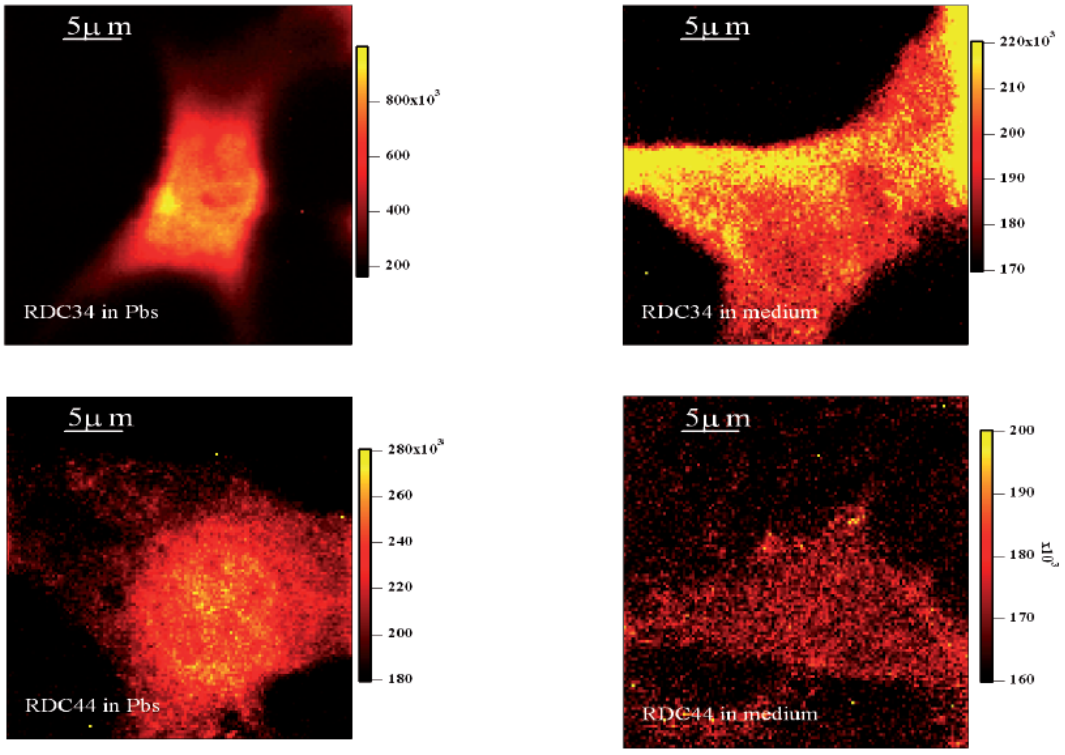

Figure A.1: Difference in intensities of RDC inside the cells incubated in PBS or cellular medium.

Figure A.1 Differences between PBS and medium. Intensity collected from RDC34 and RDC44 incubated in PBS and in culture medium.

A.5 Cellular sample for co-localization examination with confocal microscopy

Endoplasmic reticulum, mitochondria, nucleolus and nucleus dyes were purchased from Invitrogen. Nucleus staining was performed on the impermeant, fixed cells, whereas the rest three were used on alive cells, then fixed. Organella dyes were introduced following the protocols provided by Invitrogen (each dye per 4 wells—2 of cells in Medium and 2 of cells in PBS1x) to already incubated cells with RDC.

A.5.1 Endoplasmatic Reticulum staining (ER-Tracker™ Green dye, cat. no. E34251)

ER-Tracker™ dyes are cell-permeant, live-cell stains that are highly selective for the endoplasmic reticulum (ER)(absorption/emission maxima $\sim$504/511 nm). 1 µl of 0.5 mM stock-solution of ER-Tracker was introduced to wells with cells to receive the final concentration 1 µM.

A.5.2 Mitochondria staining (MitoTracker® Green FM, cat. no. M7514)

The cell-permeant MitoTracker® probes contain a mildly thiol-reactive chloromethyl moiety for labeling mitochondria. 1 µl of 100 µM stock solution of MitoTracker® was added to the wells with cells to receive the final concentration of 200 nM.To label mitochondria, cells are simply incubated with probes, which passively diffuse across the plasma membrane and accumulate in active mitochondria.(absorption/emission maxima $\sim$490/516 nm)

A.5.3 Nucleolus staining (SYTO® RNASelect™ Green Fluorescent Cell Stain, cat. no. S32703)

SYTO® RNASelect™ Green Fluorescent Cell Stain is a cell-permeant nucleic acid stain that is selective for RNA. It exhibits bright green fluorescence when bound to RNA (absorption/emission maxima $\sim$490/530 nm). Maximal fluorescence is observed in the nucleoli, with faint fluorescence throughout the nucleus. Weak fluorescence is also seen throughout the cytoplasm, predominantly associated with mitochondria. 2.5 µl of 100 µM stock-solution of Syto®RNASelect™ was added to wells with cells to receive

the final concentration of 500 nM.

Incubation time with stains was 20 minutes in darkness in 37 °C. Next, cells stained by three dyes mentioned above were washed by BPS1x two times and fixed. Fixation for Reticulum Endoplasmatic and Mitochondria dyed cells were performed by adding 500 µl of 4% PFA and 20 minutes incubation in room temperature whereas for Nucleolus by putting treated coverslip in prechilled methanol for 10 min in -20 °C. Two washings by PBS1x were performed.

A.5.4 Nucleus staining (Propidium Iodide Nucleic Acid Stain, cat. no. P1304MP)

Propidium iodide (PI) binds to DNA by intercalating between the bases with little or no sequence preference and with a stoichiometry of one dye per 45 base pairs of DNA. When bound to nucleic acids, the fluorescence excitation maximum for PI is 535 nm and the emission maximum is 617 nm. Cells destined to be stained in Nucleus had to be fixed before staining. 4% PFA was introduced to 4 wells and incubated for 20 min. in room temperature. Next, washing by PBS1x was performed twice. Following, 2.5 µl of 100 µM stock solution of Propidium Iodide was added to receive the final concentration of 500 nM. Cells were incubated for 5 min in 37 °C, then washed twice by PBS1x.

Final incubation time with RDC was 1 h. There were 2 kinds of control samples prepared: with only RDC treatment and only stains. Coverslips with cells anchored, treated by RDC and stained by organella dyes were next attached onto the microscopic base slide and examine by confocal microscopy.

Appendix B

Optical setups used

B.1 FRET

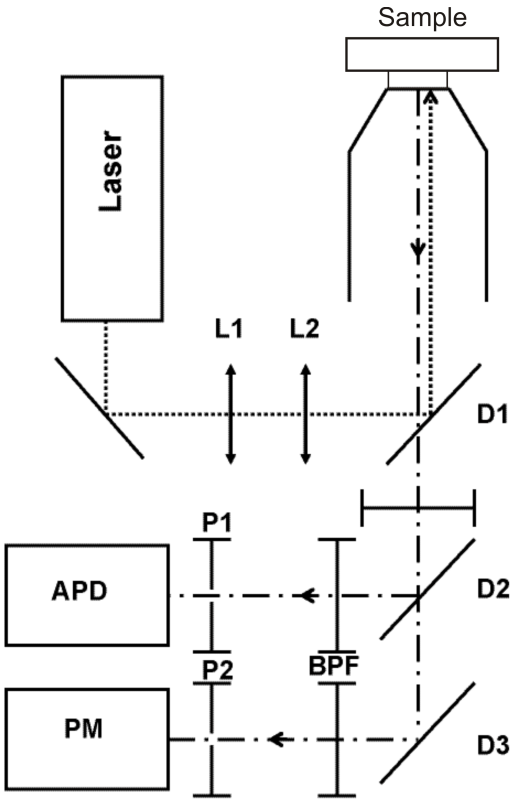

Figure B.1: Scheme of setup. Laser (Sapphire 488 Coherent), BPF, BPF1 and BPF2 bandpass filters, L1L2 telescope, D1, D2 and D3 dichroic mirrors, NF notch filter,P1 and P2 pinholes, APD (avalanche photodiode, Perkin Elmer SPCM-AQR-100), PM (photomultiplier, Hamamatsu H7421).

The beam coming out of the laser (Sapphire 488 Coherent) has wavelength equal to 488 nm. The band-pass filter BPF (FB490-10) allows to pass only a narrow range of wavelengths close to 488 nm (see Figure B.1), then the beam reaches the dichroic mirror D1 (XF2077), by which only some part of the beam is reflected (Figure B.1) and goes further to the objective. Here the sample is illuminated; through the same objective the beam is coming back to notch filter NF (RNF-488.0), which rejects wavelengths around 488 nm (Figure B.1). After that the beam is reflected or passed through dichroic mirror D2 (XF 2017)(Figure B.1)the reflected light comes through band-pass filter BPF1 (XF3105) to the detector; analogous situation takes place with the beam not reflectedit comes through dichroic mirror D3 (2072), band-pass filter BPF2 (XF3083) to another detector. The first detector APD (avalanche photodiode, Perkin Elmer SPCM-AQR-100)counts photons emitted by the donor, the second one PM (photomultiplier, Hamamatsu H7421) by the acceptor.

B.2 Optical trap

As shown in Figure B.2 the polarized infra-red laser (Spectra Physics YAG 1064 nm) beam passes the dichroic mirror and is led to the oil immersion objective (O1, Zeiss 100/1.4). An immersion oil type FF (Electron Microscopy Sciences) is used to match the optical index of the microscope cover slips, of thickness 125 μm. This objective is mounted on a piezoelectric converter (Physics Instruments GmbH) with displacement range from 0 to 100 μm and resolution 0.2 nm. The beam is passing the sample and focused forming the optical trap. The 1m diameter solid-latex bead, bound to the one end of DNA, is held in the trap by focused laser beam which is being scattered, then collected by phase contrast objective (O2, Olympus 40/0.6) and finally detected by the photodiode (PD).

An optical fiber delivers to the setup the white light which is next collimated with the objective O3 (x10, NA 0.3). The sample is visualized by two CCD cameras (C1+C2; Kappa CF8/4, 740x582 pixels) with acquisition frequency 25 Hz, using a lens of 180-mm focal length. C2 is used to visualize the trapped bead, whereas the stuck bead by C1.[64]

B.3 Confocal microscopy

The light coming from the laser (Cyan Scientific 488 nm CW Laser) is enlarged with a telescope in order to fulfill the back aperture plane of the objective. Next the beam is reflected by a dichroic mirror DM (Chroma Q495lp) and focused by a microscope

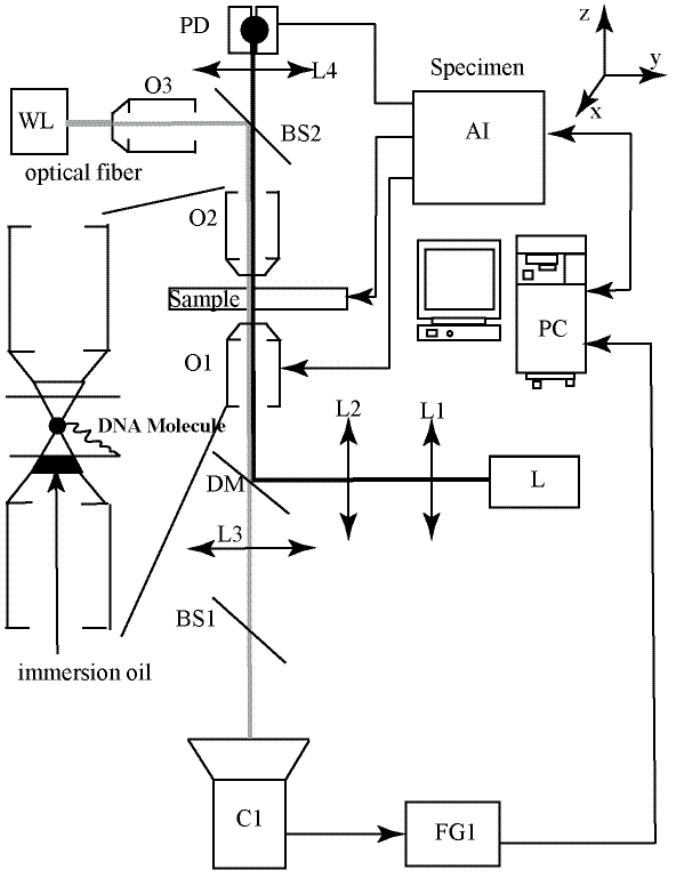

Figure B.2: Optical Tweezers setup. Trapping path: Laser Millenia YAG 1064nm, L1L2 telescope, DM dichroic mirror, O1 objective1 (100X NA 1.3), O2 objective2 (60X NA 0,6), L4 imaging lens, PD position diode. Imaging path: WL white light, O3 objective3(20X NA 0,3), CM cold mirror, C. CCD camera. Signal Acquisition: FG frame grabber, AB acquisition board(NI6135), PC personal computer.

objective O (Olympus 100X N.A. 1.3) to a small spot on the sample. A dichroic mirror reflects one wavelength while transmitting others. When the sample is excited, it starts to emit light in a random direction. A fraction of the emitted photons is collected by the microscope objective and delivered to the detector. Light reflected at the laser wavelength is cut by notch filter NF (CVI).

The confocal microscope collects the fluorescence through an optical fiber (50 μm) coupled to a spectrometer (Andor Shamrock SR 163), which splits the signal in the different wavelength. This signal is delivered to CCD camera (Andor DU971N) that returns the emission spectrum. This spectrum is then divided in ten different parts and we sum the intensity over the pixel in the ten different parts to obtain the fluorescence attributed to a specific range of wavelength 20 nm wide. We then, obtain different

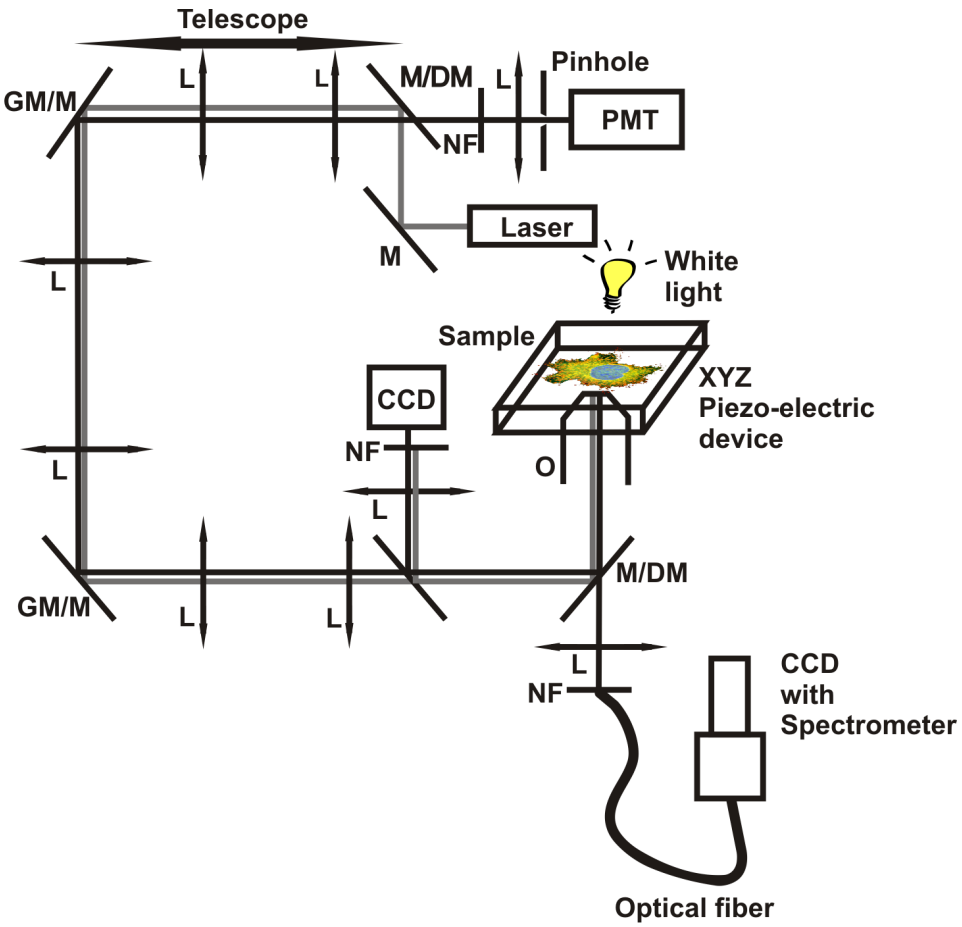

Figure B.3: Confocal microscope setup. L lens, M mirror, DM Dichroic mirror, NF notch filter, PM photomultiplier

images from the same cell at different wavelength. We can compare the fluorescence from the different labels used. The sample is scanned in the xy plane to the propagate of light by a Piezoelectric device (P721), whereas scanning along the optical axis z is performed by a piezo device (P541) onto which the objective is mounted.

With this kind of sample scanning, the beam is kept stationary and the sample is moved. However if sample movement provides some difficulties it is possible to keep the sample fixed and move the laser beam. Then two galvanic mirrors (GM1, GM2) are required to set the laser beam in motion. GM1 is a step motor by which setting of the acquisition time is possible and is conjugated with GM2. GM2 is conjugated with the back aperture plane of the objective and is oscillating with the constant frequency (8 kHz). Reflected from GM1 and GM2 and oscillating laser beam is sliding on the sample. Then light from the excited sample is collected when coming back and focused onto a pinhole (50 μm) and collected by Photomultiplier (PMT).

Nowadays examination with the movement of laser is the preferred way of scanning, because a lot of the variety of biological samples usage. Cells are very flexible objects, so when they move, a lot of blurring occurs. This is also faster method to obtain results. However it is more difficult to utilize, especially in acquisition time settings. Moreover it allows one to scan only in two dimensions-to measure the signal in optical axis z, another solution is required. Therefore we found that the way of scanning with the motionless laser beam is more suitable to our case.

Bibliography

[1] **Alexa dyes, a series of new fluorescent dyes that yield exceptionally bright, photostable conjugates**
N. Panchuk-Voloshina, R. P. Haugland, J. Bishop-Stewart, M. K. Bhalgat, P. J. Millard, F. Mao, W.-Y. Leung, R. P. Haugland
Journal of Histochemistry and Cytochemistry **1999** (47:1179–1188)

[2] **Ruthenium (II)-Derived Organometallic Compounds Induce Cytostatic and Cytotoxic Effects on Mammalian Cancer Cell Lines through p53-Dependent and p53-Independent Mechanisms**
C. Gaiddon, P. Jeannequin, P. Bischoff, M. Pfeffer, C. Sirlin, J. P. Loeffler
Journal of Pharmacology and Experimental Therapeutics **2005** (315(3):1403–1411)
doi:10.1124/jpet.105.089342

[3] **A Ruthenium-Containing Organometallic Compound Reduces Tumor Growth through Induction of the Endoplasmic Reticulum Stress Gene CHOP**
X. Meng, M. L. Leyva, M. Jenny, I. Gross, S. Benosman, B. Fricker, S. Harlepp, P. Hebraud, A. Boos, P. Wlosik, P. Bischoff, C. Sirlin, M. Pfeffer, J. P. Loeffler, C. Gaiddon
Cancer Research **2009** (69(13):5458–5466)
doi:10.1158/0008-5472/CAN-08-4408

[4] **Synthesis of Cycloruthenated Compounds as Potential Anticancer Agents**
L. Leyva, C. Sirlin, L. Rubio, C. Franco, R. Le Lagadec, J. Spencer, P. Bischoff, C. Gaiddon, J. P. Loeffler, M. Pfeffer
European Journal of Inorganic Chemistry **2007** (69(13):3055–3066)
doi:10.1002/ejic.200601149

[5] **The promotion of secondary structures in single-stranded DNA by drugs that bind to duplex DNA: an atomic force microscopy study**
J. Adamcik, F. Valle, G. Witz, K. Rechendorff, G. Dietler
Nanotechnology **2008** (19:384016–384023)
doi:10.1088/0957-4484/19/38/384016

[6] **DNA Condensation Monitoring after Interaction with Hoechst 33258 by Atomic Force Microscopy and Fluorescence Spectroscopy**
M. Saito, M. Kobayashi, S. Iwabuchi, Y. Morita, Y. Takamura, E. Tamiya
Journal of Biochemistry **2004** (136:813–823)
doi:10.1093/jb/mvh191

[7] **A novel assay for drug-DNA binding mode, affinity, and exclusion number: scanning force microscopy**
J. Coury, L. McFailIsom, L. Williams, L. Bottomley
Proceedings of the National Academy of Sciences **1996** (93:12283–12286)

[8] **FRET tells us about proximities, distances, orientations and dynamic properties**
R. M. Clegg
Journal of Biotechnology **2002** (82(3):177–179)
doi:10.1016/S1389-0352(01)00044-7

[9] **Fluorescence resonance energy transfer as a structural tool for nucleic acids**
D. M. J. Lilley, T. J. Wilson
Current Opinion in Chemical Biology **2000** (4:507–517)
doi:10.1016/S1367-5931(00)00124-1

[10] **Orientation dependence in fluorescent energy transfer between Cy3 and Cy5 terminally attached to double-stranded nucleic acids**
A. Iqbal, S. Arslan, B. Okumus, T. J. Wilson, G. Giraud, D. G. Norman, T. Ha, D. M. J. Lilley
Proceedings of the National Academy of Sciences **2008** (105(32):11176–11181)
doi:10.1073/pnas.0801707105

[11] **Structure, Recognition, and Processing of Cisplatin-DNA Adducts**
E. R. Jamieson, S. J. Lippard

Chemical Review **1999** (99(9):2467–2498)
doi:10.1021/cr980421n

[12] **Molecular Mechanisms and Kinetics between DNA and DNA Binding Ligands**
A. Sischka, K. Toensing, R. Eckel, S. D. Wilking, N. Sewald, R. Ros, D. Anselmett
Biophysical Journal **2005** (88(1):404–411)
doi:10.1529/biophysj.103.036293

[13] **Stretching of Single Collapsed DNA Molecules**
C. G. Baumann, V. A. Bloomfield, S. B. Smith, C. Bustamante, M. D. Wang, S. M. Block
Biophysical Journal **2000** (78(4):1965–1978)
doi:10.1016/S0006-3495(00)76744-0

[14] **Stretching DNA with optical tweezers**
M. D. Wang, H. Yin, R. Landick, J. Gelles, S. M. Block
Biophysical Journal **1997** (72(3):1335–1346)
doi:10.1016/S0006-3495(97)78780-0

[15] **Stretching DNA**
J. F. Marko, E. D. Siggia
Macromolecules **1995** (28:8759–8770)
doi:10.1016/S0006-3495(97)78780-0

[16] **Dual Binding Modes for an HMG Domain from Human HMGB2 on DNA**
M. McCauley, P. R. Hardwidge, L. J. Maher III, M. C. Williams
Biophysical Journal **2005** (28:353–364)
doi:10.1529/biophysj.104.052068

[17] **DNA Mechanics Affected by Small DNA Interacting Ligands**
S. Husale, W. Grange, M. Hegner
Single Molecules **2002** (3(2):91–96)
doi:10.1002/1438-5171(200206)3

[18] **Theoretical Aspects of DNA-Protein Interactions : Co-operative and Non-co-operative Binding of Large Ligands to a One-dimensional Homogeneous Lattice**

J. D. McGhee, P. H. von Hippel
Journal of Molecular Biology **1974** (86:469–489)
doi:10.1016/0022-2836(74)90031-X

[19] **The attraction of proteins for small ions and molecules**
G. Scatchard
Annals of the New York Academy of Sciences **1949** (51:660–672)
doi:10.1111/j.1749-6632.1949.tb27297.x

[20] **Equilibrium Dialysis Studies of Polyamine Binding to DNA**
W. H. Braunlin, T. J. Strick, M. T. Record Jr.
Biopolymers **1982** (21(7):1301–1314)
doi:10.1002/bip.360210704

[21] **Study of the interaction between novel ruthenium(II)-polypyridyl complexes and calf thymus DNA**
G. Yang, J. Z. Wu, L. Wang, L. N. Ji, X. Tian
Journal of Inorganic Biochemistry **1997** (66(2):141–144)
doi:10.1016/S0162-0134(96)00194-8

[22] **Synthesis, DNA-binding and DNA-mediated luminescence quenching of Ru(II) polypyridine complexes**
Y. Xiong, L.-N. Ji
Coordination Chemistry Reviews **1999** (185-186:711–733)
doi:10.1016/S0010-8545(99)00019-3

[23] **Modelling the biomechanical properties of DNA using computer simulation**
S. A. Harris
Royal Society Publishing **2006** (364:3319–3334)
doi:10.1098/rsta.2006.1906

[24] **DNA: an extensible molecule**
P. Cluzel, A. Lebrun, C. Heller, R. Lavery, J.-L. Viovy, D. Chatenay, F. Caront
Science **1996** (271(5250):792–794)
doi:10.1126/science.271.5250.792

[25] **Effect of pH on the overstretching transition of double-stranded DNA: evidence for force-induced DNA melting**

M. C. Williams, J. R. Wenner, I. Rouzina, V. A. Bloomfield
Biophysical Journal **2001** (80(2):874–881)
doi:10.1016/S0006-3495(01)76066-3

[26] **Thermodynamics of DNA Interactions from Single Molecule Stretching Experiments**
M. C. Williams, I. Rouzina, V. A. Bloomfield
Accounts of Chemical Research **2002** (35(3):159–166)
doi:10.1021/ar010045k

[27] **Salt dependence of the elasticity and overstretching transition of single DNA molecules**
J. R. Wenner, M. C. Williams, I. Rouzina, V. A. Bloomfield
Biophysical Jornal **2002** (82(6):3160–3169)
doi:10.1016/S0006-3495(02)75658-0

[28] **Mechanisms of DNA Binding Determined in Optical Tweezers Experiments**
M. J. McCauley, M. C. Williams
Wiley InterScience **2006** (85:154–168)
doi:10.1002/bip.20622

[29] **Sequence-dependent mechanics of single DNA molecules**
M. Rief, H. Clausen-Schauman, H. E. Gaub
Nature Structural and Molecular Biology **1999** (6(4):346–349)
doi:10.1038/7582

[30] **A bifurcated hydrogen-bonded conformation in the d(AT) base pairs of the DNA dodecamer d(CGCAAATTTGCG) and its complex with distamycin**
M. Coll, C. A. Frederick, A. H.-J. Wang, A. Rich
Proceedings of the National Academy of Sciences **1987** (84:8385–8389)

[31] **Binding of cationic alpha-helical peptides to plasmid DNA and their gene-transfer abilities into cells**
T. Niidome, N. Ohmori, A. Ichinose, A. Wada, H. Mihara, T. Hirayama, H. Aoyagi
Journal of Biological Chemistry **1996** (272:15307–15312)
doi:10.1074/jbc.272.24.15307

[32] **Identification of binding mechanisms in single molecule-DNA complexes**
R. Eckel, R. Ros, A. Ros, S. D. Wilking, N. Sewald, D. Anselmetti
Biophysical Journal **2003** (85:1968–1973)

[33] **Ion effects on ligand-nucleic acid interactions**
M. T. Record Jr, M. L. Lohman, P. de Haseth
Journal of Molecular Biology **1976** (107(2):145–158)
doi:10.1016/S0022-2836(76)80023-X

[34] **Protein-Nucleic Acid Interactions. II. Oligopeptide-Polyribonucleotide Binding Studies**
S. A. Latt, H. A. Sober
Biochemistry **1967** (6(10):3293–3306)
doi:10.1021/bi00862a040

[35] **Ligand-Target Interactions: What Can We Learn from NMR?**
T. Carlomagno
Annual Review of Biophysics and Biomolecular Structure **2005** (34:245–266)
doi:10.1146/annurev.biophys.34.040204.144419

[36] **NMR approaches to investigate protein-protein and protein-nucleic acid complexes**
M. Yoshimasu, M. Honda, T. Mikawa, T. Shibata, Y. Ito
RIKEN Review **2002** (46:32–35)

[37] **Limiting Laws and Counterion Condensation in Polyelectrolyte Solutions I. Colligative Properties**
G. S. Manning
Journal of Chemical Physics **1969** (51(3):924–933)
doi:10.1063/1.1672157

[38] **On the application of polyelectrolyte "limiting laws" to the helix-coil transition of DNA. Excess univalent cations**
G. S. Manning
Biopolymers **1972** (11(5):937–949)
doi:10.1002/bip.1972.360110502

[39] **Biophysical characterization of DNA binding from single molecule force measurements**

K. R. Chaurasiya, T. Paramanathan, M. J. McCauley, M. C. Williams
Physics of Life Reviews **2010** (7(3):299–341)
doi:10.1016/j.plrev.2010.06.001

[40] **Ligand-dependent interaction of ruthenium(II) polypyridyl complexes with DNA probed by emission spectroscopy**
A. Kirsch-De Mesmaeker, G. Orellana, J. K. Barton, N. J. Turro
Photochemistry and Photobiology **1990** (52(3):461–472)
doi:10.1111/j.1751-1097.1990.tb01787.x

[41] **Aspects of DNA assembly: Extension, lithography and recognition**
G. V. Shivashankar, A. Libchaber
Current Science **1999** (76(6):813–818)

[42] **Structural Analysis of DNA Interactions with Biogenic Polyamines and Cobalt(III)hexamine Studied by Fourier Transform Infrared and Capillary Electrophoresis**
A. A. Ouameur, H.-A. Tajmir-Riahi
Journal of Biological Chemistry **2004** (279(40):42041–42054)
doi:10.1074/jbc.M406053200

[43] **Quantifying force-dependent and zero-force DNA intercalation by single-molecule stretching**
I. D. Vladescu, M. J. McCauley, M. E. Nuñez, I. Rouzina, M. C. Williams
Nature Methods **2007** (4(6):517–522)
doi:10.1038/nmeth1044

[44] **Identification and hydropathic characterization of structural features affecting sequence specificity for doxorubicin intercalation into DNA double-stranded polynucleotides**
G. E. Kellogg, J. N. Scarsdale, F. A. Fornari Jr
Nucleic Acids Research **1998** (26(20):4721–4732)
doi:10.1093/nar/26.20.4721

[45] **Understanding binding interactions of cationic porphyrins with B-form DNA**
D. R. McMillin, A. H. Shelton, S. A. Bejune, P. E. Fanwick, R. K. Wall
Coordination Chemistry Reviews **2005** (249(13-14):1451–1459)
doi:10.1016/j.ccr.2004.11.016

[46] **The polyamine spermine protects against high salt stress in *Arabidopsis thaliana***
K. Yamaguchi, Y. Takahashi, T. Berberich, A. Imai, A. Miyazaki, T. Takahashi, A. Michael, T. Kusano
FEBS Letters **2006** (580(30):6783–6788)
doi:10.1016/j.febslet.2006.10.078

[47] **The natural polyamine spermine functions directly as a free radical scavenger**
H. C. Ha, N. S. Sirisoma, P. Kuppusamy, J. L. Zweier, P. M. Woster, R. A. Casero Jr
Proceedings of the National Academy of Sciences **1998** (95(19):11140–11145)

[48] **Structural Specificity of Polyamines and Polyamine Analogues in the Protection of DNA from Strand Breaks Induced by Reactive Oxygen Species**
H. C. Ha, J. D. Yager, P. A. Woster, R. A. Casero Jr.
Biochemical and Biophysical Research Communications **1998** (244(1):298–303)
doi:10.1006/bbrc.1998.8258

[49] **Interaction of Δ and Λ -[Ru(phen)2DPPZI2+ with DNA: a Calorimetric and Equilibrium Binding Study**
I. Haq, P. Lincoln, D. Suh, B. Norden, B. Z. Chowdhry, J. B. Chaires
Journal of the American Chemical Society **1995** (117:4788–4796)
doi:10.1021/ja00122a008

[50] **Inhibition of Cell Division in *Escherichia coli* by Electrolysis Products from a Platinum Electrode**
B. Rosenberg, L. Van Camp, T. Krigas
Nature **1965** (295:698–699)
doi:10.1038/205698a0

[51] **Platinum Compounds: a New Class of Potent Antitumour Agents**
B. Rosenberg, L. Van Camp, J. E. Trosko, V. H. Mansour
Nature **1969** (222(5191):385–386)
doi:10.1038/222385a0

[52] **X-ray structure of the major adduct of the anticancer drug cisplatin with DNA: cis-[Pt(NH3)2(d(pGpG))]**
S. E. Sherman, D. Gibson, A. H.-J. Wang, S. J. Lippard

Science **1985** (230:412–417)
doi:10.1126/science.4048939

[53] **Why Does Cisplatin Reach Guanine-N7 with Competing S-Donor Ligands Available in the Cell?**
J. Reedijk
Chemical Reviews **1999** (99(9):2499–2510)
doi:10.1021/cr980422f

[54] **Cellular responses to cisplatin. The roles of DNA-binding proteins and DNA repair**
G. Chu
Journal of Biological Chemistry **1994** (269(2):787–790)

[55] **Molecular aspects of resistance to antitumor platinum drugs**
V. Brabec, J. Kasparkova
Drug Resistance Updates **2002** (5(3-4):147–161)
doi:10.1016/S1368-7646(02)00047-X

[56] **Cisplatin nephrotoxicity**
R. Safirstein, J. Winston, M. Goldsein, D. Moel, S. Dikman, G. Guttenplan
American Journal of Kidney Diseases **1986** (8(5):356–367)

[57] **Non-Platinum Chemotherapeutic Metallopharmaceuticals**
M. J. Clarke, F. Zhu, D. R. Frasca
Chemical Reviews **1999** (99:2511–2533)
doi:10.1021/cr9804238

[58] **From bench to bedside – preclinical and early clinical development of the anticancer agent indazolium *trans*-[tetrachlorobis(1*H*-indazole)ruthenate(III)] (KP1019 or FFC14A)**
C. G. Hartinger, S. Zorbas-Seifried, M. A. Jakupec, B. Kynast, H. Zorbas, B. K. Keppler
Journal of Inorganic Biochemistry **2006** (100(5-6):891–904)
doi:10.1016/j.jinorgbio.2006.02.013

[59] **Ruthenium complexes can target determinants of tumour malignancy**
A. Bergamo, G. Sava
Dalton Transactions **2007** (13:1267–1272)
doi:10.1039/B617769G

[60] **Medicinal inorganic chemistry: introduction**
C. Orvig, M. J. Abrams
Chemical Reviews **1999** (99(9):2201–2204)
doi:10.1021/cr980419w

[61] **Development of organometallic (organo-transition metal) pharmaceuticals**
C. S. Allardyce, A. Dorcier, C. Scolaro, P. J. Dyson
Applied Organometallic Chemistry **2005** (19(1):1–10)
doi:10.1002/aoc.725

[62] **Recent Developments in the Field of Tumor-Inhibiting Metal Complexes**
M. Galanski, V. B. Arion, M. A. Jakupec, B. K. Keppler
Current Pharmaceutical Design **2003** (9(25):2078–2089)
doi:10.2174/1381612033454180

[63] **Carbon-carbon and carbon-nitrogen bond formation mediated by ruthenium(II) complexes: synthesis of (1H)-isoquinolinium derivatives**
H. C. L. Abbenhuis, M. Pfeffer, J. P. Sutter, A. de Cian, J. Fischer, L. H. Nelson, H. L. Ji, J. H. Nelson
Organometallics **1993** (12(11):4464–4472)
doi:10.1021/om00035a034

[64] **Design and realization of a high-stability optical tweezers**
S. Drobczynski, P. Hebraud, J.-P. Munch, S. Harlepp
Optical Engineering **2009** (48(11):113601–113605)
doi:10.1117/1.3257269

[65] **Selective cell death mediated by small conditional RNAs**
S. Venkataraman, R. M. Dirks, C. T. Ueda, N. A. Pierce
Proceedings of the National Academy of Sciences **2010** (107(39):16777–16782)
doi:10.1073/pnas.1006377107

[66] **The *let-7* microRNA reduces tumor growth in mouse models of lung cancer**
A. Esquela-Kerscher, P. Trang, J. F. Wiggins, L. Patrawala, A. Cheng, L. Ford, J. B. Weidhaas, D. Brown, A. G. Bader, F. J. Slack
Cell Cycle **2008** (7(6):759–764)
doi:10.4161/cc.7.6.5834

[67] **Oxidative Damage to RNA in Neurodegenerative Diseases**
A. Nunomura, K. Honda, A. Takeda, K. Hirai, X. Zhu, M. A. Smith, G. Perry
Journal of Biomedicine and Biotechnology **2006** (2006:1–6)
doi:10.1155/JBB/2006/82323

[68] **RNA Repair: Damage Control**
A. Bellacosa, E. G. Moss
Current Biology **2003** (13:482–484)
doi:10.1016/S0960-9822(03)00408-1

[69] **Intercalating Residues Determine the Mode of HMG1 Domains A and B Binding to Cisplatin-Modified DNA**
Q. He, U.-M. Ohndorf, S. J. Lippard
Biochemistry **2000** (39(47):14426–14435)
doi:10.1021/bi001700j

[70] **Thermodynamic analysis of ion effects on the binding and conformational equilibria of proteins and nucleic acids: the roles of ion association or release, screening, and ion effects on water activity**
M. T. Record Jr, C. F. Anderson, T. M. Lohman
Quarterly Reviews of Biophysics **1978** (11(2):103–178)
doi:10.1017/S003358350000202X

[71] **Transferrin binding and transferrin-mediated cellular uptake of the ruthenium coordination compound KP1019, studied by means of AAS, ESI-MS and CD spectroscopy**
M. Pongratz, P. Schluga, M. A. Jakupec, V. B. Arion, C. G. Hartinger, G. Allmaier,B. K. Keppler
Journal of Analytical Atomic Spectrometry **2004** (19:46–51)
doi:10.1039/B309160K

[72] **In Vitro Anticancer Activity and Biologically Relevant Metabolization of Organometallic Ruthenium Complexes with Carbohydrate-Based Ligands**
I. Berger, M. Hanif, A. A. Nazarov, C. G. Hartinger, R. O. John, M. L. Kuznetsov, M. Groessl, F. Schmitt, O. Zava, F. Biba, V. B. Arion, M. Galanski, M. A. Jakupec, L. Juillerat-Jeanneret, P. J. Dyson and B. K. Keppler
Chemistry A European Journal **2008** (29(14):9046–9057)
doi:10.1002/chem.200801032

[73] **Methods to Explore Cellular Uptake of Ruthenium Complexes**
C. A. Puckett and J. K. Barton
Journal of American Chemical Society **2007** (129(1):46–47)
doi:10.1021/ja0677564

[74] **Crystal structure analysis of a complete turn of B-DNA**
R. Wing, H. Drew, T. Takano, C. Broka, C. Tanaka, K. Itakura, R. Dickerson
Nature **1980** (287(5784):755–758)
doi:10.1038/287755a0

[75] **Complexes cycloruthenes et activite anticancereuse**
L. M. Leyva
Ecole Doctorale des Sciences Chimiques de Strasbourg, **2007**

[76] **Physics of protein-DNA interaction**
R. F. Bruinsma
Departament of Physics and Astronomy, University of California; Institut-Lorenz for Theoretical Physics, Universiteit Leiden, **2007**

[77] **Optical Trap for Biological Mechanics**
J. Park
Final Report, Optical Spectroscopy Phys598OS Fall 2005, **2005**

[78] **Encyclopedic Reference of Cancer**
M. Schwab
Springer, **2001**, ISBN: 3540665277

[79] **The Gale Encyclopedia of Cancer: A Guide to Cancer and Its Treatments, Second Edition**
J. L. Longe
Thomson Gale, **2005**, ISBN: 1414403623

[80] **Cancer: Principles and Practice of Oncology, sixth edition**
V. T. DeVita Jr, S. Hellman, S. A. Rosenburg
Garland Science, **2001**, ISBN: 0781722292

[81] **Molecular Biology of the Cell, Fourth Edition**
B. Alberts, A. Johnson, J. Lewis, M. Raff, K. Roberts, P. Walter
Lippincott Williams & Wilkins, Philadelphia, PA, **2002**, ISBN: 0815332181

[82] **Multinuclear NMR**
J. Mason
Springer, **1987**, ISBN: 0306421534

[83] **Fundamentals of Crystallography**
C. Giacovazzo, H. L. Monaco, D. Viterbo, F. Scordari, G. Gilli, G. Zanotti, M. Catti
Oxford University Press, **1992**, ISBN: 0198555784

[84] **Molecular and Cellular Biophysics**
M. B. Jackson
Cambridge University Press, **2006**, ISBN: 0521624703

[85] **Biochemistry, Fifth Edition: International Version**
J. M. Berg, J. L. Tymoczko, L. Stryer
W. H. Freeman and Company, **2002**, ISBN: 0716746840

[86] **Molecular Cell Biology, Fifth Edition**
H. Lodish, A. Berk, P. Matsudaira, C. A. Kaiser, M. Krieger, M. P. Scott, L. Zipursky, J. Darnell
W. H. Freeman and Company, **2003**, ISBN: 0716743663

[87] **Biochemistry, Second Edition**
R. H. Garrett
Brooks Cole, **1999**, ISBN: 0030223180

[88] `http://kentsimmons.uwinnipeg.ca/cm1504/membranefunction.htm`

[89] `http://fmrc.pulmcc.washington.edu/fmrc.shtml`

[90] `http://www.kirbyresearch.com/index.cfm/wrap/textbook/microfluidicsnanofluidics.html`

[91] `http://kentsimmons.uwinnipeg.ca/cm1504/membranefunction.htm`

[92] `http://www.arcagy.org/infocancer`

[93] `http://www.oncoprof.net/Generale2000/g01_HistoireGenerale/g01-hg08.html`

[94] `http://www.who.int/cancer/en/index.html`

[95] `http://www.cancer.gov/cancertopics/treatment`

[96] http://www.cancersupportivecare.com/immunotherapy.html

[97] http://www.cisplatin.org/effects.htm

[98] http://www.invitrogen.com/site/us/en/home/References/Molecular-Probes-The-Handbook/tables/R0-values-for-some-Alexa-Fluor-dyes.html

List of Figures

List of Tables